Doctor of Philosophy

Removal of contaminants by biochar-based composite materials

The Graduate School of the University of Ulsan

Department of Civil and Environmental Engineering

Yong Deuk Seo

Removal of contaminants by biochar-based composite materials

Advisor: Seok Young Oh

A Dissertation

Submitted to the Graduate School of the University of Ulsan

In Partial Fulfillment of the Requirements

For the Degree of Doctor of Philosophy

By

Yong Deuk Seo

Department of Civil and Environmental Engineering

University of Ulsan, South Korea

February 2022

Removal of contaminants by biochar-based composite materials

This certifies that the dissertation of

Yong Deuk Seo is approved

Hung-Suck Park
Committee Chair

Seok-Young Oh
Committee Member

Byeong-Kyu Lee
Committee Member

Kwang-Sun Ryu
Committee Member

Jong-Mun Cha
Committee Member

Department of Civil and Environmental Engineering

University of Ulsan, South Korea

February 2022

ACKNOWLEDGMENT

울산대학교에서 박사과정을 밟은 지 7년이라는 시간이 지나며 많은 분들의 도움으로 논문을 완성시킬 수 있었습니다. 그래서 지금 이자리를 빌어 지금까지 저를 지지해 주시고 격려해 주시며 긴 시간동안 포기하지 않도록 도와주신 모든 분들께 감사의 인사를 전합니다.

먼저 부족한 저를 오랜 시간 동안 충고와 격려를 아끼지 않으시고 이끌어 주신 오석영 지도교수님께 감사를 드립니다. 공부에 지쳐 포기하려고 한 저를 몇 번이나 도와주시지 않았다면 이 논문은 불가능했을 것입니다. 그리고 제 부족한 논문에 대해 도움과 평가를 주신 박흥석 교수님, 이병규 교수님, 류광선 교수님과 멀리서 방문해 주신 동아대학교 차종문 교수님께 감사를 드립니다. 여러 교수님들의 도움을 통해 저는 논문의 완성을 마칠 수 있었습니다.

연구실에서 같이 생활하며 도와준 연구실 후배들에게도 감사의 인사를 전합니다. 7년의 시간동안 연구실을 거쳐간 후배 분들의 도움으로 저는 연구실 생활하면서 많은 추억과 도움을 받으며 지낼 수 있었습니다. 그리고 오랜 대학원 생활동안 많은 도움을 주신 건설환경공학부 교수님들과 졸업하시고도 많은 고민 상담을 해 주신 선배님 들에

게도 감사의 인사를 드립니다.

마지막으로 항상 응원과 사랑을 주시며 제가 졸업할 수 있도록 묵묵히 도움을 주신 부모님께 감사드립니다. 오랜 시간 동안 그분들의 헌신이 없었더라면 저는 대학원 생활을 이렇게 끝마치지 못하였을 겁니다. 부모님의 사랑에 진심으로 감사드립니다.

2022년 2월 서용득

ABSTRACT

In this study, We synthesized various types of biochar through pyrolysis and examined their application methods to increase the value of biochar. The feasibility of using biochar as a sorbent to remove nitro explosives and metals from contaminated water was investigated through batch experiments. Biochar, synthesized using biomasses, showed a porous structure and a high surface area and included embedded carbonate minerals. Compared with granular activated carbon (GAC), biochar was competitive as a sorbent for removing Cd, Cu, Pb, and Zn from water according to the maximum sorption capacities of the metals. Some biochars also effectively sorbed nitro explosives from water. Correlation analysis between maximum sorption capacities and properties of biochar showed that the sorption capacity of biochar for cationic toxic metals is related to the cation exchange capacity (CEC) and that the sorption capacity of explosives is proportional to the surface area and carbon content. In addition, results from X-ray photoelectron spectroscopy (XPS), Fourier-transform infrared spectroscopy (FT-IR) analyses, and laboratory experiments suggest that surface functional groups may be responsible for the sorption of cationic metals to the biochar surface. In contrast, carbon contents may account for the sorption of explosives, possibly through π–π electron donor-acceptor interactions.

The feasibility of using biochar as a sorbent to remove nine halogenated phenols (2,4-dichlorophenol, 2,4-dibromophenol, 2,4-difluorophenol, 2-chlorophenol, 4-chlorophenol, 2-bromophenol, 4-bromophenol, 2-fluorophenol, and 4-fluorophenol) and two pharmaceuticals (triclosan and ibuprofen) from the water was examined through a series of batch experiments. Biochar was synthesized using various biomasses, including fallen leaves, rice straw, corn stalks, spent coffee grounds, and biosolid. Compared to GAC, most biochar samples did not

effectively remove halogenated phenols or pharmaceuticals from water. The increase in pH and deprotonation of phenols in biochar systems may be responsible for its inefficiencies at this task. However, when pH is maintained at 4 or 7, the sorption capacity of biochar is markedly increased. Considering the maximum sorption capacity and properties of sorbents and sorbates, the sorption capacity of biochar for halogenated phenols is related to the surface area and carbon content of biochar and hydrophobicity of contaminants. In the cases of triclosan and ibuprofen, the sorptive capacities of GAC, graphite, and biochars were also significantly affected by pH, according to the point of zero charge (PZC) of sorbents and deprotonation of the pharmaceuticals. Pyrolysis temperature did not affect the sorption capacity of halogenated phenols or pharmaceuticals.

The synthesis of zero-valent iron [Fe(0)]-included biochar (Fe(0)-biochar] was applied to remove nitro explosives (2,4,6-trinitrotoluene (TNT) and hexahydro-1,3,5-trinitro-1,3,5-triazine (RDX)) and halogenated-phenols (DBP and DFP) from contaminated waters. Due to the presence of biochar on the outside, the removal of nitro explosives and halogenated phenols was significantly enhanced via sorption. The sorbed contaminants were further transformed into reducing agents, indicating that the inner Fe(0) played the role of a reductant in the Fe(0)-biochar. Compared to direct reduction with Fe(0), the reductive transformation with Fe(0)-biochar was markedly enhanced, suggesting that the biochar in Fe(0)-biochar may act as an electron transfer mediator. Further experiments showed that the surface functional groups of biochar were involved in the catalytic enhancement of electron transfer.

Co-pyrolysis of polymer and biomass wastes was investigated as a novel method for waste treatment and synthesis of enhanced biochar. Co-pyrolysis of RS with polypropylene (PP), polyethylene (PE), or polystyrene (PS) increased the carbon content, CEC, BET surface area, and pH of the biochar. As a result, the sorption of 2,4-dinitrotoluene (DNT) and Pb to

polymer/RS-derived biochar was markedly enhanced. The increased aromaticity and hydrophobicity contents may enhance the DNT sorption to the polymer/RS-derived biochar. In contrast, increasing CEC, higher pH, and the newly developed surface area may account for the enhancement in Pb sorption. The addition of polymer to RS did not significantly change the catalytic role of biochar during DNT reduction by dithiothreitol.

Biochar was synthesized using wood chips (WC), BS, and biomass obtained in large quantities in Korea, and its adsorption capacity was analyzed through a batch experiment. We evaluated the carbon sequestration capacity using biochar–mortar composites according to characteristics for construction and environmental applications. Characterization of biochar–mortar composites showed that 3-5 vt% biochar inclusion did not significantly change the composites' engineering properties, including flowability, compressive strength, and thermal conductivity. Furthermore, as the biochar content increased in the biochar–mortar, the benzene and toluene concentrations in the air were accordingly reduced, suggesting that biochar inclusion may be favorable to remove volatile toxic contaminants. The toxicity characteristics leaching procedure (TCLP) and Micotox®bioassay tests showed that biochar–mortar composites were not toxic. These results confirmed that biochar and biochar-based composite materials are competitive can be effectively used as sorbents, catalysts, or reducing agents for contaminants. The improving value of biochar suggests that biochar production via pyrolysis may be a promising option for carbon sequestration to release CO_2 mitigation.

CONTENTS

LIST OF FIGURES

LIST OF TABLES

Chapter 1. Introduction

1.1. Background

Global warming is also known to many as one of today's most critical environmental issues. Due to global warming, abnormal climate events (e.g., heat waves, heavy snowfalls, floods, sea-level rise due to glacier reduction) occur worldwide. The damage caused by natural disasters is increasing significantly. Dyer (2011) [1] has mentioned that one of the most significant impacts of climate change will be the permanent food supply crisis. Even in the United Nations framework convention on climate change, discussions are taking place to respond to climate change in the agricultural sector [2]. If extreme weather events such as floods and droughts frequently occur, crop production capacity decreases in developing countries, directly damaging livelihoods [3].

Climate change is already threatening human health as an increase in deaths and diseases reported due to natural disasters [4]. As of 2015, Korea's carbon dioxide emissions were the 7th largest globally, and the rate of increase was the highest along with China [324]. In the case of Korea, to solve this problem, it has announced that it will reduce greenhouse gas by 37% compared to BAU by 2030 [5]. Negative emissions based on carbon storage and account refer to measures to mitigate climate change by absorbing and fixing carbon, a greenhouse gas in the atmosphere, and isolating it directly in forests and soils [6].

Professor Lehman suggested that adding biochar to the soil was a better carbon-negative method than growing existing plants to recover bioenergy [7]. To this end, various strategies are being discussed in the literature, ranging from extensive afforestation of terrestrial ecosystems to pumping CO_2 into deep seas and geological structures [8]-[10]. In the case of terrestrial ecosystems, it suggested that carbon sequestration could increase by increasing the

carbon stock in the soil [11]-[13]. According to a recent analysis, or the effort to isolate the C soil is often offset by other greenhouse gas emissions in the usual way has urged caution, stressing the possibility is low to accumulate C [14]-[17].

Biochar is a compound word of biomass and charcoal, and it is a solid material with high carbon content made by pyrolyzing biomass in an oxygen-free environment. Biochar has an aromatic structure through thermal decomposition, so it maintains a stable state and is not easily decomposed by soil microorganisms. Furthermore, by adding it to the soil, we can sequester carbon semi-permanently [7], [18].

The pyrolysis gas is a non-condensable gas with relatively small molecules. The calorific value of the pyrolysis gas is about 11-20 MJ/Nm^3, which can sufficiently be used as a fuel for biochar production [19]. Bio-oil has a higher energy density than dried biomass and is easily transported and stored, advantageous for various purposes. However, bio-oil produced by pyrolysis has high water content and acidity and has less calorific value than fossil fuels. It can use with existing fossil fuels or another renewable energy source [20].

When biochar adds to the soil, it can improve crop productivity by improving the quality of carbon sequestration, CEC enhancement, acidity control, water holding capacity, and retention capacity improvement, and soil microbial activity [21]. When biomass is synthesizing into biochar, C is immobilized in charcoal, slowing the carbon cycle rate, and suppressing CO_2 emission for a long time [22]. Biochar can also be synthesized using organic waste biomass such as agricultural waste and sewage sludge, which helps in waste management and treatment. It reported that the physicochemical properties of biochar have a practical effect on heavy metal adsorption [23]-[25]. There is much room for improvement in that biochar is produced through thermal decomposition, so energy consumption is high. The performance varies depending on the environment, such as the manufacturing conditions [26].

Biochar performance is inconsistent, and it is not easy to match an application method suitable for the characteristics of biochar, so only some industries are using biochar [20]. Biochar is effective for soil structure improvement and soil quality improvement [27]. Recently, trichloroethene (TCE) adsorption removal [28], heavy metal adsorption removal, Pollution reduction studies using biochar [29], [30], such as and removal of phenolic compounds in water [31], have been actively reported. The contaminant adsorption mechanism of biochar mainly includes partitioning, surface adsorption, pore maintenance, and micro-adsorption, but the adsorption process proceeds by a combination of several mechanisms [32], [33]. In general, adsorption using activated carbon apply as a method of removing contaminants from water quality. Activated carbon is produced by thermal decomposition at a temperature of 700 ℃, so energy consumption is large, and the production cost is also high due to the physical and chemical activation process [18], [28]. Biochar has a large surface area, a porous structure, and many surfaces functional groups, thus showing potential catalysts in various applications [34], [35].

Biochar is used as a sustainable electron donor, acceptor, or mediator, and biochar can be tuned properties through pyrolysis and post-treatment [36]. Biochar is synthesized using less energy than activated carbon. However, the performance of the produced biochar is not constant, so the merit of a product tends to decrease. The current price of carbon credits has risen more than tenfold in Europe from 4 euros/ton in 2017 to 44 euros/ton in 2021 and has significantly increased from 8,000 won/ton in Korea in 2015 to 40,000 won/ton in 2019. Furthermore, as of 2021, it is maintained at 19,000 won/ton. Although the price of carbon credits continues to fluctuate, overall, the price of carbon credits is on the rise. The typical selling price of biochar is sold colorfully within approximately 9.99 US dollars to 100 US dollars from overseas. The price varies greatly depending on the type of biomass, and most are

used as soil conditioners.

Studies have shown that the price per ton must be at least $83 for sellers to profit [37]. Biochar has a low-cost value compared to the cost of production and sale, so its use for carbon reduction is not profitable, so it is not widely used. If the performance of biochar is improved, biochar will use in various fields such as a catalyst, a reducing agent, and an adsorbent as well as a soil reducing material and improving agent, thereby improving the global environment and creating new added value commercially.

1.2. Objectives

The increase in carbon dioxide (CO_2) has accelerated global warming and has caused climate change, leading to various problems globally. As such, research on methods to respond to climate change has been conducted worldwide, with associated policies introduced to solve these problems. Many national policies in this vein have focused on regulating the sources of greenhouse gas emissions, such as establishing management systems for greenhouse gas targets and setting up emission trading systems. However, these policies may not be embraced by developing countries and, because they are not perfect solutions, alternative measures for the reduction of CO_2 are required.

Various CO_2 reduction measures have been proposed and investigated, including eco-friendly fuels (e.g., biodiesel), tree planting, algae farming, space mirrors, and seafloor carbon dioxide reclamation. However, many of these methods are difficult to commercialize or operate on an industrial scale because they are expensive or damaging to local ecosystems. One proposed strategy that has received significant attention due to its low cost and excellent environmental remediation ability is biochar. Biochar has previously been used as an adsorbent to remove various contaminants and to improve soil quality, and many studies have highlighted its ability to sequester CO_2. For example, according to Cornell University researchers in the US, biochar effectively improves soil fertility and can efficiently fix CO_2 from the atmosphere, meaning that it can play an essential role in reducing global warming [330].

Biochar also has significant potential as a means to combat climate change because it can be manufactured using various organic materials. However, this also means that it is sensitive to changes in conditions, leading to inconsistent performance. In addition, although biochar can reduce pollutant levels, it is not a perfect substitute for activated carbon because it does not reach the same level of performance. In addition, when comparing the CO_2 reduction

capacity of biochar and current carbon emission permits, the price of these permits is low, so biochar does not have significant commercial advantages yet. Due to these problems, the practical use of biochar in carbon reduction measures has been delayed. Even so, for the future, biochar has the potential to develop into a useful alternative if its performance is incrementally improved and new applications are discovered.

In this study, to increase the added value of biochar, the basic characteristics of biochar are described, and its ability to reduce contaminants is identified, while biochar performance is improved by synthesizing high molecular compounds or iron-containing materials using biomass. In particular, this study attempts to identify various application methods such as biochar mortar, adsorbents, and catalysts. The results can thus be used to improve the commercial capacity of biochar as a new value-added resource for use in carbon reduction measures that improve the environment.

Chapter 2. Literature review

2.1. Biochar

Many researchers have recently conducted biochar research as interest in environmental pollution and the understanding of biochar increased. Biochar is a carbon-rich solid material produced through thermochemical transformation and synthesized by biomass pyrolysis in an anaerobic environment (Fig 2.1), with synthesis gas (H_2 + CO), pyrolysis oil, methane (CH_4), and heat as the generated by-products. After Herbert Smith, who explored the Amazon in 1879, attributed the phenomenal growth rate of sugarcane grown by indigenous people to the black soil (*terra preta*), biochar research began to be conducted extensively. In 1966, Dr. Sombrek and Glaser discovered that the indigenous people of the Amazon had artificially made the soil using charcoal in the past (Fig 2.2) [38], [332]. Thereafter, the World Congress of Soil Science in 2006 discussed that *terra preta* must be understood from the perspective of carbon sequestration and biofuel [39]. Since then, the term biochar started to appear in the literature, and numerous research papers related to climate change began to be published. According to Transparency Market Research (2017) [40], the global biochar market is estimated to be worth USD 3.2 billion in 2026, and the average growth rate is expected to be 14.5% per year.

Biochar is synthesized through the pyrolysis of various organic wastes at about 300°C–1000°C under anaerobic conditions. The slower the heating rate, the greater the amount of biochar produced [41]. Generally, low-speed pyrolysis is used to manufacture biochar. This process is ideal for the production of biochar in an inert atmosphere (hypoxia or anoxic) with a slow heating rate (~10°C/min) [42]. Biochar derived from biomass typically weighs 20–40 wt% of the weight of the biomass [43]-[44]. However, the yield and properties of the biochar produced depend on the biochar synthesis conditions (e.g., temperature, heating rate, pressure,

purge gas, and particle size) and feedstock [45]-[47]. The advantage of slow pyrolysis is that biomass of various molecular sizes can be used through a stationary reactor, so no additional energy is required for preconditioning. Furthermore, fixed beds are the most efficient for biochar production because they can do smaller operations than those using fluid beds. Fig 2.3 shows the fixed bed reactor “packed bed reactor” and the continuous manufacturing process “rotary kiln reactor process” and “screw pyrolysis reactor” [48]-[50].

Figure 2.1. Various types of biochar [331].

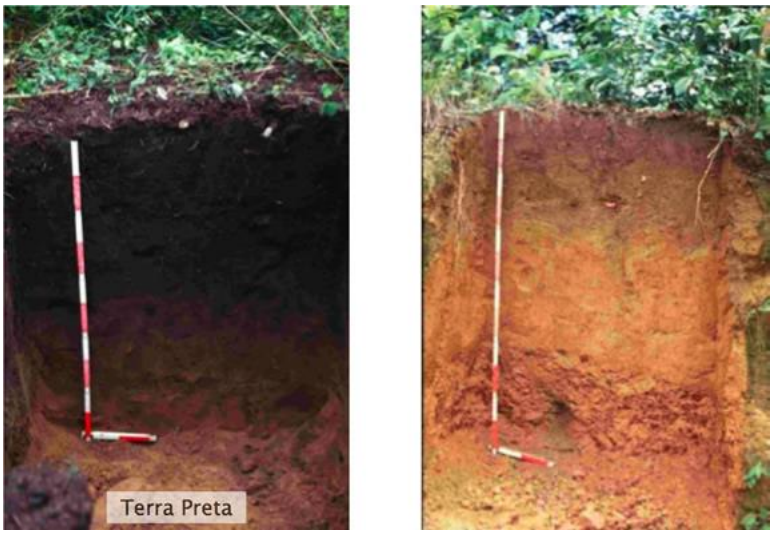

Figure 2.2. Terra preta and soil comparison [334].

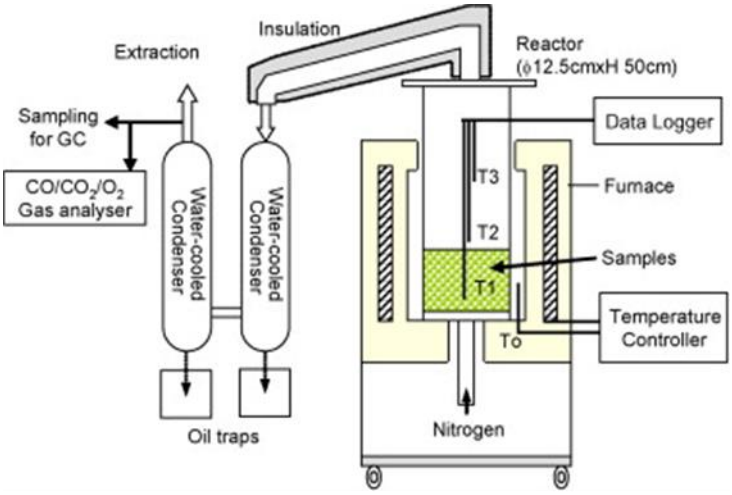

Packed bed reactor [48]

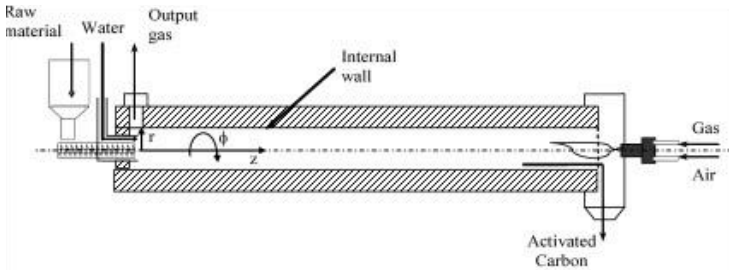

Rotary Kiln reactor [49]

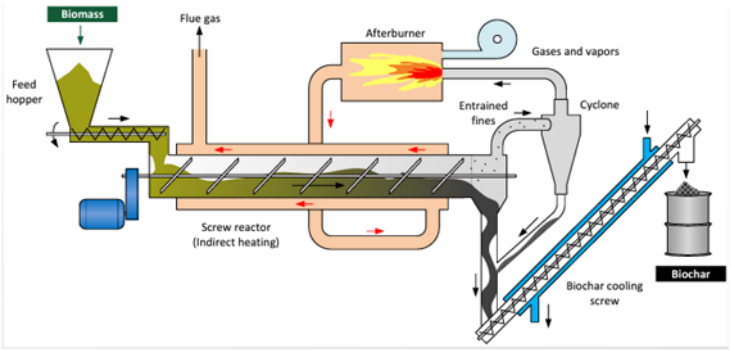

Commercial screw-type pyrolysis reactor [50]

Figure 2.3. Schematic of fixed bed.

2.2. Properties of biochar

As mentioned above, biochar is a very carbon-rich substance. Because of its high carbon content, it is used as a soil additive to improve soil quality and as renewable fuel [18]. This is because volatile substances are volatilized in the vapor phase during pyrolysis, and the remaining part, carbon, forms part of the aromatic structure of biochar. Thus, the aromatic structure of biochar is very stable and not easily decomposed. Furthermore, biochar has a high calorific value because of this structure [20].

The internal structure of biochar depends on the shape and inclusions of the biomass [51]. Carbonization temperature is also a factor influencing the biochar structure. The aromatic carbon structure and nanopore size of biochar are known to increase with increasing temperature. However, pyrolysis temperatures exceeding 700°C may partially destroy the microporous structure of the biochar surface during biochar synthesis [52], [53].

Biochar is usually composed of elements such as C, H, O, N, S, P, K, Ca, Mg, Na, and Si. Among them, the C content is the highest (generally 60%), followed by those of H and O, and the mineral components are mainly present in the ash [54]. Biochar C deposits in irregular stacks of aromatic rings stabilized by aromatic carbon [55]. The types of carbon compounds include fatty acids, alcohols, phenols, esters, and fulvic and humic acid components. [56]. Nitrogen is mainly present in the C–N heterocyclic structure on the biochar surface, and the N content is less than the C, H, and O contents in the biochar [9]. The P, K, Ca, Mg, and Na contents appear differently depending on the various types of biochar. The elemental composition and activity of biochar are closely related to the raw material, carbonization process conditions, and pH [57], [58].

The pH of biochar is made alkaline by ash and inorganic minerals such as carbonates and phosphates [54]. Biomass type and pyrolysis carbonization temperature also affect the pH of

biochar [51]. For example, the pH of leguminous biochar is higher than that of nonlegume biochar. Under the same pyrolysis and carbonization conditions, poultry manure biochar has the highest pH, followed by herbaceous and woody plant biochar [7], [54]. As the pyrolysis temperature increases, acidic functional groups such as carboxyl and phenol hydroxyl groups decompose and organic acids volatilize, thereby changing the pH value [59], [54], [60].

The specific surface area of biochar generally ranges from 1.5 to 500 m^2/g [61], [62]. Pyrolysis at very low temperatures causes volatiles or tar and other substances to fill the internal pore structure of biochar, reducing its specific surface area. As the temperature rises, these volatile substances decompose into volatile gases and escape, creating microporous structures in biochar and thus causing larger specific surface areas [63]. As such, the specific surface area of biochar increases with increasing pyrolysis temperature within a certain temperature range [64]. When the pyrolysis temperature exceeds the critical value, cracks occur in the micropore structure of the biochar surface, reducing the surface area [65].

Biochar has many functional groups such as carboxyl, carbonyl, and hydroxyl. Therefore, it has excellent adsorption capacity, hydrophilic/hydrophobicity, buffering capacity, and ion exchange properties [66]. The number of functional groups on the biochar surface is closely related to the carbonization temperature. As the carbonization temperature increases, the C–O, C–H, and O–H bonds of biochar decrease. The number of functional groups containing oxygen, such as hydroxyl, carboxyl, and acid, decreases with increasing temperature, whereas the number of alkali groups increases [67], [68].

Cation exchange capacity (CEC) is strongly related to biomass and pyrolysis temperature [61]. Functional groups such as hydroxyl, carboxyl, and carbonyl are generated during carbonization because of the incomplete decomposition of cellulose, which increases the CEC of biochar. [69]. In addition, some functional groups on the biochar surface are oxidized over

time to produce more oxygen-containing functional groups. This increases the O/C ratio and CEC of biochar through many processes [21], [70]. However, the CEC of biochar may reduce in some cases [71]. The biochar surface's negative charge and O/C ratio decrease as the biochar pyrolysis temperature increases [69], [72]. If the alkali metal content in biochar such as K, Ca, and Mg increases, the CEC value may increase as the temperature rises [24], [71]. Also, as the pyrolysis temperature increases, the hydrophobicity of biochar increases and the number of functional groups with O and H decreases; thus, the water holding capacity of biochar also decreases [73]-[75].

Biochar has very low solubility, a high boiling point, high stability, and high resistance to physical, chemical, and biological degradation [76], [77]. These properties allow biochar to exist in soil for thousands of years under natural environmental conditions (Fig 2.4) [78]. Biochar has such excellent physical and chemical properties that it is used in various fields and has already been reported for more than 50 [79].

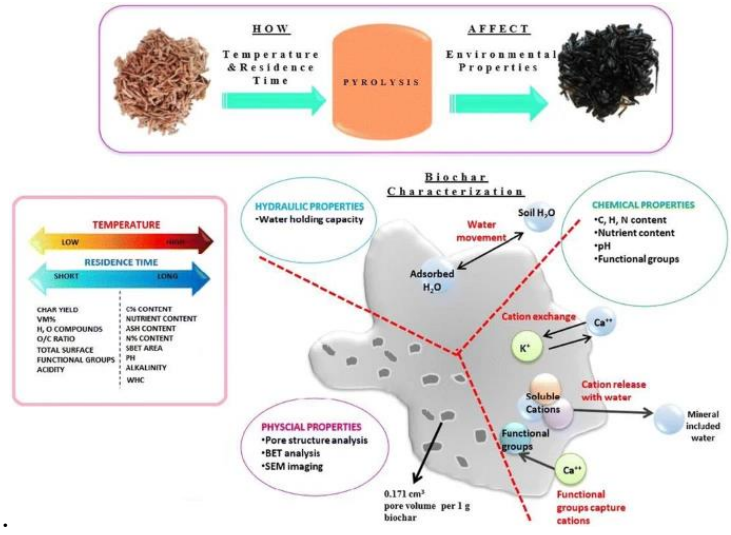

Figure 2.4. Basic physical properties of biochar [332].

2.3. Biochar application

Research on climate change response, energy production, soil improvement, waste management, and pollutant reduction is necessary for biochar utilization. As a soil conditioner, biochar contains abundant organic carbon and minerals, which helps increase the soil's organic carbon and mineral content [80], [81]. The porous structure of biochar dramatically improves the water holding capacity of the ground [82], [83]. Biochar can also be used as a neutralizing agent for acidic soils because of its alkalinity [59], [84], [85]. It also promotes the growth of crops and plants, inhibits pathogen invasion, and reduces the absorption of harmful substances such as heavy metals and pesticides [86]. It improves the efficiency of fertilizer utilization by reducing soil nutrient leaching and fixation losses [87].

Biochar gradually decreases in size as it is weathered and broken by nature over time within the soil. Although it remains for a long time in the environment, it is not entirely stable. Even in the *terra preta* of the Amazon, biochar is hardly seen in particle size. It is usually observed microscopically, wholly mixed with the surrounding soil. In addition, the organic matter in the soil blocks the surface of the biochar, reducing its adsorption capacity. Moreover, the functional group increases as the remaining organic fragrance is oxidized, which increases the CEC of the soils [88].

On another note, biochar helps plants grow. However, it is not very rich in nutrient content, which depends on the biomass composition used during pyrolysis. When biochar is added to arable land, it can help create an environment suitable for crop cultivation by maintaining an environment where bacteria can live and lowering the mobility of substances that negatively affect crop growth, such as herbicides and heavy metals [20]. When biochar is injected, the pH of the soil generally increases, thus promoting the absorption and movement of trace elements (e.g., Mg and Mo) required for plant growth.

The micropores of biochar can be used as passageways for supplying oxygen in the soil. Moreover, biochar can promote nitrification during nitrogen fixation and induce a smooth nitrogen supply to soils and plants [89]. It can significantly improve the environment, such as by slowing the carbon cycle or reducing greenhouse gas emissions [87]. The carbon structure of biochar is so stable that it is hard to decompose, thus fixing it in the soil [90]. Landfilling biochar into soils slows the carbon cycle, reducing soil CO_2 emissions [60], [91] and potentially minimizing N_2O generation through biological nitrogen fixation [92], [93].

Pollution control using biochar has been studied for a long time [94]. Biochar is used as an adsorbent and impacts the removal of contaminants such as heavy metals from soil and water systems because of its high aromaticity and porous structure [95]. It removes heavy metals through chemical adsorption under the influence of functional groups on the char surface [96]. Moreover, its alkaline nature can increase the soil pH or indirectly decrease the bioavailability of heavy metals [32], [33]. Further, it can change the soil moisture and internal air conditions, which can affect the redox potential of the soil and change the toxicity of some heavy metals, such as cadmium [97]. It can adsorb and remove various organic pollutants (e.g., polycyclic aromatics and hydrocarbons) [98].

The adsorption mechanism of biochar for organic pollutants is as follows: 1) splitting, 2) surface adsorption, 3) pore sharing, and 4) micro-adsorption. These mechanisms are combined to remove organic contaminants [32], [33]. In biochar production, various conditions (degree of carbonization, elemental composition, pH, pore structure, and surface chemistry) play essential roles in the adsorption of contaminants [99]. Thus, biochar can be used to reduce the practical harm of pollution to humans and the ecosystem by removing pollutants from water and suppressing the movement of pollutants in the soil.

Biochar can also help a lot in waste management. It can be manufactured using plant-

based biomass and organic waste (e.g., livestock manure and sewage sludge) and various waste biomass (e.g., food waste and coffee grounds) generated in daily life. Moreover, its production also generates gas (syngas) and liquid (pyrolysis oil) energy sources. Char itself is also often used as a fuel [19]. Pyrolysis oil has a higher energy density than that of dried biomass, making it easier to transport and store. This is why it can be used with fossil fuels or used as another renewable energy source [20]. Primary data for pyrolysis bio-oil and conventional petroleum fuel are summarized in Table 2.1 [100]. On another note, syngas produced during pyrolysis appears differently depending on the pyrolysis temperature. The calorific value of the pyrolysis gas is generally low and ranges from 11 to 20 MJ/Nm^3. However, it is sufficiently usable as a fuel for biochar production (about 500°C) [19], [20]. Char has H/C and O/C ratios and a calorific value similar to those of coal [101]. The combustion characteristics of biochar mainly depend on the biomass supplied and the carbonization process. Several studies have shown that biochar can achieve a higher calorific value if the pyrolysis is optimized to increase the specific surface area (Fig. 2.5) [102], [103].

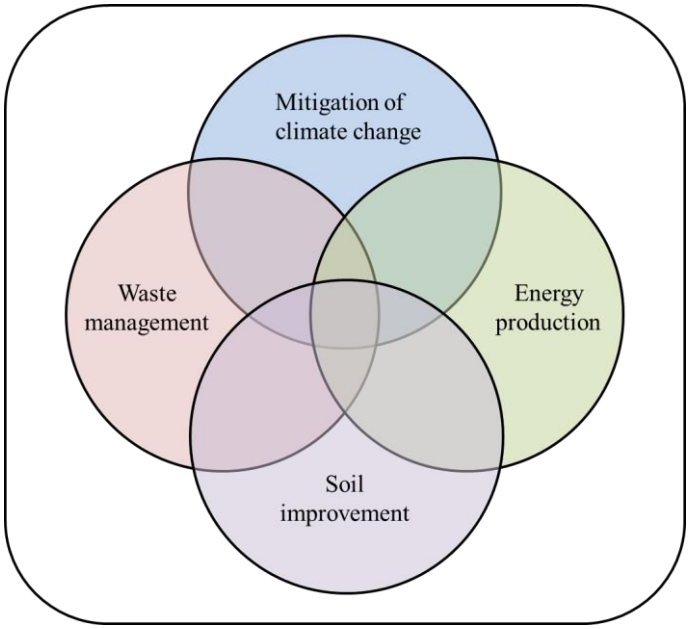

Figure 2.5. Motivation for applying biochar technology [55].

Table 2.1. Typical properties of wood pyrolysis bio-oil and heavy fuel oil [100].

Physical property	Bio-oil	Heavy fuel oil
Moisture content, wt.%	15-30	0.1
pH	2.5	-
Specific gravity	1.2	0.94
Elemental composition, wt.%		
C	54-58	85
H	5.5-7.0	11
O	35-40	1.0
N	0-0.2	0.3
Ash	0-0.2	0.1
HHV, MJ/kg	16-19	40
Viscosity (at 50 °C), cP	40-100	180
Solids, wt.%	0.2-1	1
Distillation residue, wt.%	up to 50	1

2.3.1. Biochar as an adsorbent

Adsorption refers to the phenomenon where a substance is in fluid contact and adheres to a solid surface. Contaminant removal through adsorption involves the binding of contaminants to the surface of the adsorbent until the adsorbent reaches equilibrium. Adsorption includes the

following steps: 1) physical adsorption, in which the adsorbate is a deposit on the adsorbent surface; 2) precipitation and complexation, where the adsorbate is a deposit on the adsorbent surface; and 3) pore filling, where the adsorbate condenses into the pores of the adsorbent [104]. This process occurs in three points. The first is called the clean zone, where adsorption does not occur. The second is the mass transfer region, where adsorption proceeds. The last stage is the breakthrough point, where the adsorption stops when equilibrium is reached. As adsorption proceeds, the saturation or exhaustion area increases and the clean area decreases. As the adsorbate concentration increases, the mass transfer zone is affected, and this trend continues until the breakthrough point at which the adsorbent is saturated [74].

Various mechanisms (surface adsorption, ion exchange, electrostatic interaction, precipitation, and complexation) for toxic metals during biochar adsorption are shown. Surface adsorption is a physical process that forms chemical bonds through the diffusion of metal ions in the pores of the adsorbent. The volume and surface area of the pores in biochar depend on the carbonization temperature during manufacturing. Kumar et al. (2017) [105] studied uranium adsorption using biochar prepared by thermally decomposing pine trees at 300°C to 700°C. They found that biochar prepared at high temperatures showed higher uranium removal ability than those of biochar prepared at low temperatures. They also showed that the high carbonization temperature increases the surface area and pore volume of biochar.

Electrostatic interactions with metals occur in biochar to control the toxic metals adsorbed on its surface [326]. For example, Qiu et al. (2009) [106] showed a high lead removal rate due to the attractive force between positively charged lead and negatively charged biochar. Lead was removed from a lead-contaminated aqueous solution using biochar made from rice and wheat. In addition, this ability to adsorb pollutants reportedly can increase by increasing the electrostatic interaction of biochar, and this electrostatic interaction is one of the primary

mechanisms for removing potentially toxic metal ions [107]-[110]. However, this adsorption process depends on the pH of the solution and the point of zero charge of the biochar [111]. Contaminants are adsorbed on and removed from the surface of biochar through proton and cation exchange with dissolved salt [112]. Ali et al. (2017) [113] reported that the higher the biochar CEC, the higher the metal adsorption capacity. Trakal et al. (2016) [114] studied biochar's ability to remove Cd and Pb using various organic materials such as straw, grape stems, and grape skins. The ion exchangeability of biochar was improved when biochar and iron oxide were used together. In addition, metal ions precipitated on the surface of the adsorbed material to form mineral deposits and were removed.

The above phenomenon occurs in biochar because biomass materials such as cellulose and hemicellulose are pyrolyzed at 300°C or higher temperatures, and biochar has alkaline properties. Puga et al. (2016) [115] reported that biochar made from sugar cane and straw dust could enhance the precipitation of Cd and Zn. Biochar forms complexes by mixing metals with the adsorbates. Metal complexation consists of complexes containing multiple atom-forming arrangements through the interaction of specific metal ligands. Biochar binds to heavy metals through functional groups containing oxygen (such as hydroxyl and carboxyl groups). When the numbers of these functional groups increase, the surface oxidation of biochar can be increased, thereby improving its ability to remove heavy metals through metal complexation [116], [117]. In this regard, the results of Cao et al. (2009) [118] and Zhang et al. (2017) [119] were confirmed in the paper. Biochar prepared from vegetable biomass shows high efficiency in forming complexes with metals such as Cu, Cd, Ni, and Pb and functional groups through metal bonds.

The adsorption mechanisms for organic pollutants are pore filling, hydrophobic interaction, partitioning, electrostatic interaction, and electron donor–acceptor complex

formation. Organic contaminants diffuse into the pores of the uncharred portion of the biochar, causing adsorption in the process [111]. Zhang et al. (2013a, b) [120], [121] showed that biochar prepared through pyrolysis at 200°C and 350°C has high sorbate partitioning of atrazine contaminants using its organic carbon fraction [120], [121]. Sun et al. (2011) [122] showed a similar case. The organic fraction of biochar made from wood and grass can enhance the adsorption of norflurazone and fluridone through cleavage. Moreover, the splitting mechanism is more visible and effective when the volatile content of biochar is high or the concentration of organic pollutants is high [107]. On the same note, the pores of biochar determine its adsorption capacity. The mechanisms of pore filling by mesopores (2–50 nm) and micropores (<2 nm) acting on the biochar surface depend on the biochar type and the polarity of organic contaminants.

Electrostatic interaction is the most critical mechanism aiding the adsorption of ionizable organic compounds on positively charged biochar surfaces. The efficiency of contaminant attraction or repulsion depends on the pH or ionic strength of the aqueous solution [123], [124]. Mukherjee et al. (2011) [326] investigated the effect of pH on the electrostatic interaction between organic contaminants and the biochar surface. The reflection that showed a positive charge at a low pH value maintained a negative charge when the pH was high. This shows that the electrostatic interaction between organic pollutants and biochar is also affected by the ionic strength in aqueous solutions. Further, interactions between electron donors and acceptors have been noted in biochar with graphene structures and are applied to the adsorption of aromatic chemicals.

Complete graphitization requires thermal decomposition at temperatures above 1100°C [125]. However, the electron density of biochar producing π-electrons depends on its pyrolysis temperature. When the biochar production temperature is below 500°C, the biochar π aromatic

system acts as a transcription acceptor. When the manufacturing temperature exceeds 500°C, biochar acts as a donor [126], [124]. Zheng et al. (2013) [124] conducted an adsorption experiment for sulfamethoxazole by preparing biochar using a reed. High sorption was observed between the aniline-protonated ring of sulfamethoxazole and the graphene surface of biochar. They argued that the π-electron donor–acceptor interaction between the chlorine on the biochar surface and the electron-withdrawing substituent of the aromatic carbon enhanced the compound adsorption capacity.

Hydrophobic interactions are used for the adsorption of hydrophobic and neutral organic compounds. For instance, organic contaminants are primarily adsorbed on the surfaces of graphene structures through hydrophobic interactions [325]. Li et al. (2018) [128] reported similar results. Moreover, related studies have shown that hydrophobic interactions are the primary mechanisms involved in the adsorption of ionizable organic contaminants (e.g., benzoic acid, O-chlorobenzene acid, and p-chlorobenzene acid). Chen et al. (2011a; 2011b) [24], [129] also reported the removal of organic pollutants through hydrophobic interactions. The number of functional groups on the biochar surface decreased as the pyrolysis temperature increased. The organic and inorganic adsorbent removal mechanisms, including biochar adsorption, are shown in Figure 2.6. The metal adsorption mechanism of biochar mainly proceeds by precipitation on the adsorbent surface, ion exchange, and electrostatic attraction. The adsorption of organic contaminants is through van der Waals forces, hydrogen bonding, and hydrophobic interactions. Also, functional groups (hydroxyl, carboxyl, carbonyl, and amine) favor the affinity of organic molecules and adsorption on the biochar surface. This adsorption mechanism involves a π-electron donor–acceptor based on the uneven electron distribution between the organic compound and the adsorbent functional group [111].

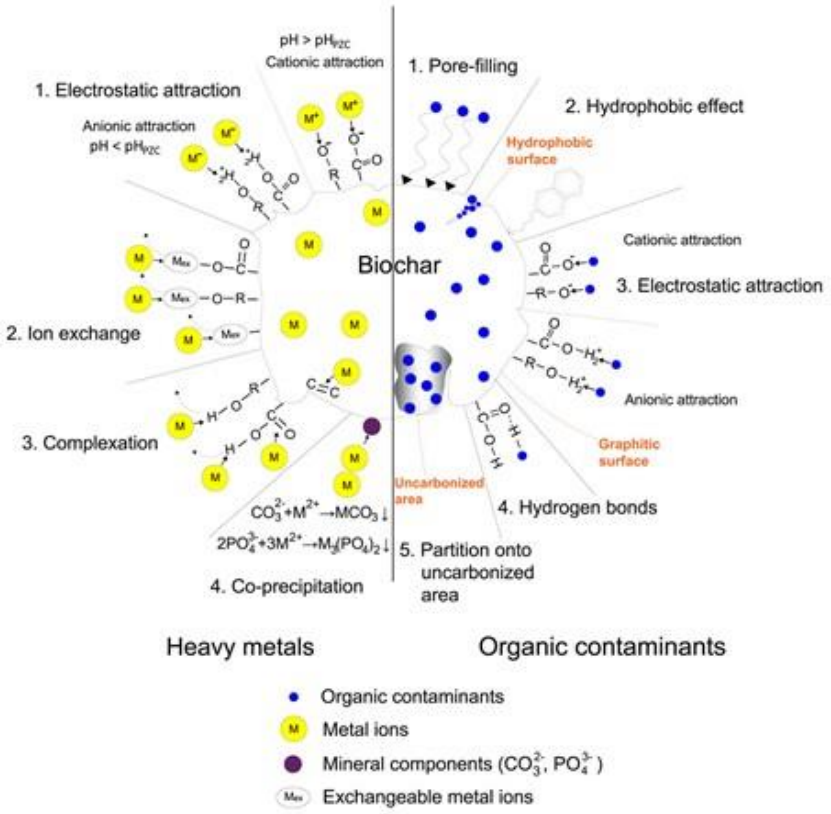

Figure 2.6. Different biochar adsorption mechanisms for organic and inorganic contaminants [130].

2.3.2. Biochar as a catalyst

Although biochar has relatively low porosity and surface area, it is rich in surface functional groups. It contains minerals such as N, P, S, Ca, Mg, and K. [131]. Because of these properties, biochar can be used as a catalyst and catalyst support [9], [132]. However, biochar has disadvantages such as unstable porosity and limited surface functional groups, making its commercialization as a catalyst and catalyst support difficult [35]. Fortunately, biochar activation and functionalization can easily remedy these issues [133], [134]. This biochar utilization method is confirmed in Figure 2.7.

Carbon-based materials have been used as direct catalysts in many industries. In this regard, biochar shows high potential as an alternative to existing solid carbon catalysts (which are expensive and not environmentally friendly) in that it can modify its physicochemical properties through activation [135]. The mass transport phenomenon of heterogeneous catalysts can be classified as follows (Figure. 2.8): 1) diffusion of reactants from a gas or liquid to the outer surface of the catalyst; 2) diffusion of reactants through the catalyst pores to the inner surface; 3) adsorption of reactants on the catalyst surface; 4) a reaction that occurs at the catalytically active site on the catalyst surface; 5) desorption of the product from the catalyst surface; 6) product diffusion from the interior surface through the catalyst pores; and 7) product diffusion from the external catalyst surface into the gas or liquid phase [136], [137].

Easily scalable biochar can produce various carbon and nanohybrid structures. Biochar has catalytic properties because of the O-, N-, and S-type functional groups on its surface. Su et al. (2013) [138] found that carbon-based metal-free heterogeneous catalysts and carbon nitrides may be used as alternatives to some metal-based catalysts and can be considered a new class of catalysts. In addition, biochar is studied as support for stabilizing metal nanoparticles (NPs) in various catalytic applications. Johnson et al. (2011) [139] reported the synthesis of

cellulose-derived carbon-supported Pt NPs and investigated the application of oxygen redox reaction (ORR) to catalysis. The synthesized Pt NPs have a metal core and oxide shell with a narrow particle size distribution. Furthermore, the cyclic voltammetry curve of ORR confirmed that the synthesized material had a catalytic activity comparable with that of the state-of-the-art Johnson Matthey Pt/Cd for O_2 electric reduction. Ma et al. (2014) [140] found that Fe_3O_4 NPs/partly graphitized carbon composites (derived from cornstalk and pomelo skin biomass) performed well when used as cathode electrode catalysts for microbial fuel cells. Chen et al. (2015) [141] found that Pd nanoalloys such as Pd-b and Pd-Ni-B using coconut-shell-derived carbon are highly selective catalysts for a wide range of reactions related to hydrogenation nitro-aromatic derivatives. As such, biochar can provide more active sites for catalysis through the stabilization and dispersion of metal nanoparticles. In addition, biochar itself can act as a catalyst because of inorganic compounds. Klinghofer et al. (2015) [142] demonstrated that inorganic substances such as Ca, K, Na, P, Si, and Mg, which constitute about 2% of poplar tree biochars, play an essential role in the catalytic activity of the methane decomposition reaction. A similar case was reported by Perander et al. (2015) [143]. In these various studies, biochar-based functional materials have shown good catalytic performance.

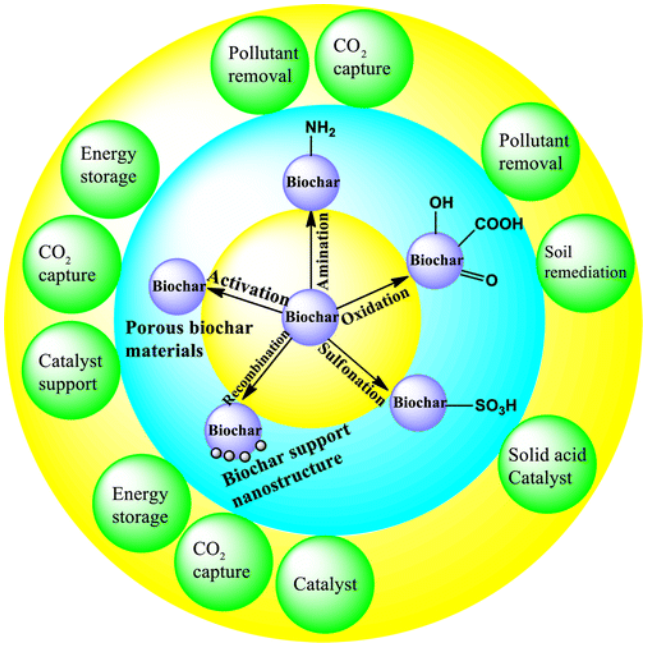

Figure 2.7. Biochar is a carbon material synthesizing various functional materials and their potential application [144].

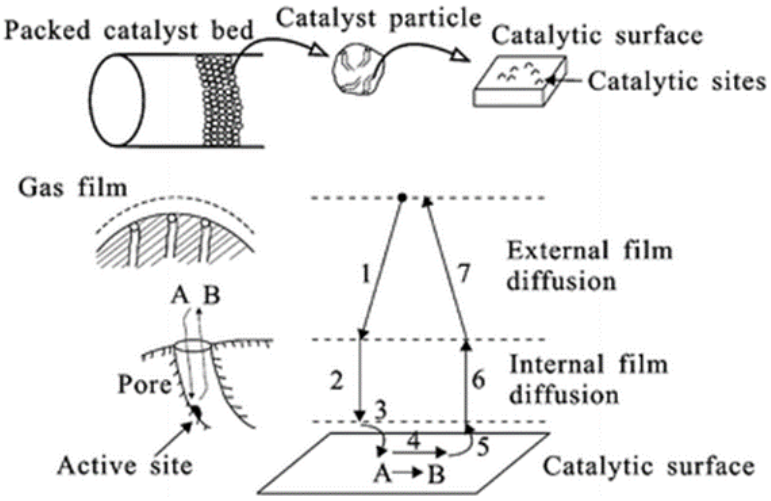

Figure 2.8. Schematic of the seven steps involved in heterogeneous catalysis on a porous material [137].

2.3.3. Biochar as a soil conditioner

Biochar can store carbon in the soil for a much more extended period than can nonpyrolyzed biomass [145]. Biochar application affects several soil properties, including electrical conductivity, pH, CEC, nutrient levels, porosity, bulk density, and microbial community structure [146]-[150]. Also, changes in these soil properties can alter soil fertility. By improving the soil's nutrient level, the leaching of nitrogen can be reduced, thereby improving the productivity of crops [151]. Biochar also influences the availability of nutrients to plants by providing additional habitat for microbial populations in the soil [145]. In addition, it can reduce the risk of soil pollution by removing organic toxic substances such as herbicides through adsorption [123], [152], [153]. Biochar applications in soil are summarized in Table 2.2. Directly, increasing the average residence time of the soil organic carbon (SOC) of biochar improves the stabilization process of SOC and thus can contribute to SOC sequestration (while SOC-C is in the soil) [154]. Indirectly, biochar affects the net primary yield (NPP) and affects the amount of biomass remaining in agricultural ecosystems, thus affecting the carbon input in the soil.

The increased content of root-derived carbon after high subsurface NPP and biochar application increases SOC [155]. The amount of plant biomass or carbon transport to roots and root symbionts is a significant determinant of carbon influx in soils in agricultural ecosystems [156]. The soil applications of biochar can increase carbon fixation through photosynthesis by increasing the amount of CO_2 stored as SOC through soil carbon influx into plants and root symbionts. Oguntunde et al. (2004) [157] reported that the grain yield in charcoal-sown soil was higher when comparing the grain yield of corn grown in nonfertile soil with that of corn grown in charcoal-sown soil.

Biochar crop productivity depends on biochar's biological, chemical, and physical

transformation in soil. Improving soil acidity, nutrient availability, CEC, soil field capacity, and soil microbial habitat ("lime effect") due to increased soil pH are major contributors to productivity gains [154]. pH control using biochar can improve the productivity of acidic soils with low biochar application [158]. To date, the primary use of biochar is neutralizing acidic soils [89], [159]. Yamato et al. (2006) [160] reported increased crop yields and neutralization of acid soil when Supitan produced from wild *Acacia mangeum* was used.

On another note, biochar has a high CEC value and is known to improve soil CEC but purportedly does not necessarily increase it [161]. Depending on its persistence, biochar modifies soil nutrient dynamics or provides a chemically active surface that promotes good reactions and affects crop productivity in the long run by modifying soil physics to aid in nutrient retention and acquisition. Moreover, improved phytonutrient availability by increased CEC may contribute to plant growth. However, the temporal change in crop viability through chemical changes in the soil is variable [155]. It depends on the mineral nutrient content of fresh biochar and the complex physicochemical reaction between soil particles and biochar due to weathering and changes in CEC over time [162]. CEC represents the ability of plants to maintain nutrient cations in usable form and minimize losses due to leaching. An increase in CEC is considered a key factor in improving crop productivity. However, this has not been unconditionally observed to increase productivity. For instance, Novaket et al. (2009) [59] showed improved soil fertility when pecan shell-based biochar was applied, but the CEC results were not significantly different.

The addition of charcoal to improve crop productivity had a beneficial effect on tropical soil because of the increase in Ca, Cu, K, P, and Zn [163]. However, small amounts of N and Mg absorption were observed when charcoal was added, which could reduce crop growth. Thus, controlling the amount of charcoal used was necessary. Excluding this, the addition of biochar

is expected to correspond positively to crop yields. [82]. This is because the reduced leaching and loss due to the increased phosphorus and potassium retention on the porous surface of biochar can contribute to the increase in phosphorus and crop yields in the soil [164].

The effect of biochar addition varies according to its characteristics. For example, the addition of pulverized pecan shell biochar pyrolyzed at 700°C to Norfolk sandy loam with poor physical properties reduced the soil strength and improved the soil moisture content during free drainage. However, no improvements in soil coagulation or water penetration were observed [165]. Novak et al. (2009) [59] showed different results for the soil water holding capacity when biochar produced through the pyrolysis of various biomass (e.g., peanut husk, pecan husk, poultry litter, and switchgrass) at 250°C–700°C was applied to the soil.

The primary impact of biochar on soil fertility improvement is its effect on soil microbes. Many studies have shown that the addition of biochar increases the microbial biomass in the soil [164]. Significant changes in microbial community composition and enzymatic activity have been noted, and pore structure, surface area, mineral material, biochar adsorption, pH, and several physical properties play an important role in determining the effect of biochar on soil biota [166], [167]. Biochar has multiple effects on the soil and can cause biological, chemical, and physical changes that affect crop yield. In addition, biochar's promotion of beneficial soil microbes also contributes to fertilizer use efficiency (Fig 2.9) [168].

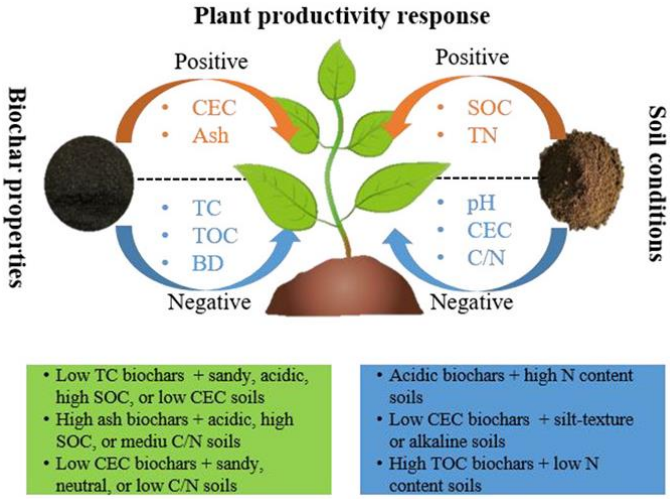

Figure 2.9. The combined effect of biochar and soil properties (TC: total carbon content; TOC: total organic carbon content; TN: total N content;) [333].

Table 2.2. Biochar application's direct and indirect effects on long-term SOC increase agro-ecosystems and potential mechanisms [171].

Pathway	Observed effect	Potential mechanism	Reference
Direct	Increase in stabilized SOC fraction	The increased fused aromatic ring structure	[169], [170]
		Physical entrapment by metal oxides; increase in micro-aggregation and molecular-level associations	[172]
	Deepening of SOC distribution	Reduction in losses by erosion and leaching; increased translocation to subsoil layers; increased stabilization in the subsoil and more anaerobic soil layers	[154], [327]
Indirect	Higher crop yield and/or aboveground productivity	Increased water holding capacity	[82], [27], [155], [159]
		Increased aggregation; increased soil alkalinity (liming effect)	[164]
		Increased soil P and K concentrations; increased tissue K concentration	[161]
		Increased CEC	
	Higher total and belowground productivity of annual plant species	Reduced sensitivity to toxic biochar compounds	[164]

2.3.4. Biochar as carbon sequestering material

Biochar has excellent potential to reduce CO_2 emissions. For example, 1 ton of dry feedstock is equivalent to about 870 kg of CO_2, of which carbon capture and storage capacity account for about 62~66% [173]. Biochar's climate mitigation potential stems primarily from its highly tolerant nature [174], [175]. Reducing atmospheric carbon requires moving carbon into a stable or stagnant passive carbon pool. (Table 2.3) Therefore, moving even the tiny amount of carbon circulating between the atmosphere and plants into the slower biochar cycle would help reduce atmospheric CO_2 concentrations. It will reduce GHGs in the atmosphere as it is more than eight times more effective than plants artificially removing CO_2 [176]. Biochar exists in a chemically stable molecular structure than the carbon structure of biologically existing biomass. It is challenging to emit even with CO_2, so it has high potential as a material for carbon sequestration (Fig 2.10) [177]. Converting even 1% of a plant's annual net carbon uptake to biochar could mitigate nearly 10% of current anthropogenic carbon emissions [18]. Biochar acts as a carbon sink in the soil for an extended period. It has high resistance to chemical and biological degradation, increasing terrestrial carbon stocks over a long period. Although soils generally contain more than 80% of organic carbon stocks [178], soils are less likely to accumulate carbon with forest growth [18]. Therefore, biomass conversion to biochar through pyrolysis and biochar application in soil should be approached as a long-term way to reduce carbon in terrestrial ecosystems.

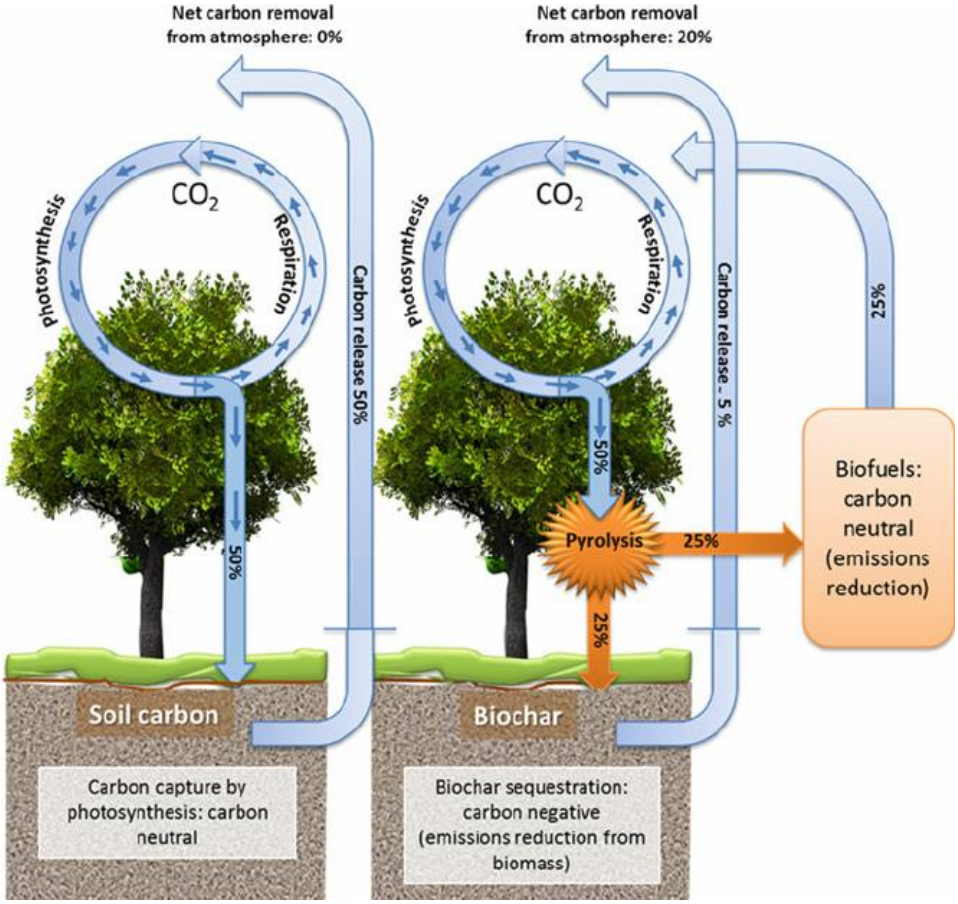

Figure 2.10. Comparison of carbon-negative biochar sequestration to carbon-neutral photosynthesis [7]

Table 2.3. Application of several types of biochar for soil improvement, carbon sequestration, and GHG reduction [176].

Biochars	Soil	Experiment type	Biochar application Rate (t/ha)	N fertilization (kg/ha)	Time (day)	Soil carbon	CO_2 emission	CH_4 emission	N_2O emission	References
Bamboo	Paddy soil	Bottle (anaerobic)	2.50%	-	49	-	No difference	51. 1% decreased	-	[179]
Cornstalk	Paddy inceptisol	Pot	24	250	116	Soil DOC increased	-	63% decreased	-	[180]
Cornstalk	Paddy inceptisol	Pot	24	250	116	Soil DOC increased	-	61% decreased	-	
Maize straw	Vegetable field	Pot	20	400	67	-	-	No difference	77% decreased	[92]
Maize straw	Vegetable field	Pot	40	400	67	-	-	No difference	82% decreased	
Mixed sawdust	Cornfield	Serum vial	20~60%	-	100	-	Decreased	Decreased when biochar ≥ 20%	57~74% decreased	[181]
Municipal biowaste char	Grassland soil	Petri dish	10%	-	3	-	-	-	89% decreased	[182]
Pinus radiata D	Dairy farm soil	Soil core	20	760	55	No Difference initially and then increased	-	-	No difference	[70]
Pinus radiata	Pasture soil	Headspace chamber bases	30	133	70	-	-	-	70% decreased	[183]
Pourltry Manure & Wood	Alfisol	Column	10	45	183	-	Fluctuated	-	14~73% decreased	[184]
Pourltry Manure & Wood	Vertisol	Column	10	45	183	-	Fluctuated	-	23~52% decreased	
Straw	Paddy soil	Bottle (anaerobic)	2.50%	-	49	-	No difference	91. 2% decreased	-	[179]
Wheat straw	Agricultural soil	Pot (40% moisture)	1%	150	55	Soil DOC decreased	Increased	-	Decreased	[185]
Wheat straw	Agricultural soil	Pot (40% moisture)	3%	150	55	Soil DOC increased	3.3. times increased than 1%	-	Decreased	
Wheat straw	Rice paddy	Field	40	300	150	-	-	34% increased	40~51% decreased	[186]
Wheat straw	Rice paddy	Field	40	0	150	-	-	41% increased	21~28% decreased	
Wood	Wheat soil	Field	30	222	420	-	No difference	No difference	25~76% decreased	[187]
Wood	Wheat soil	Field	60	222	420	-	No difference	No difference	59~88% decreased	

2.3.5. Biochar as energy

Power generation that causes environmental pollution, such as thermal power generation, is becoming a global problem. Thus, switching to alternative energy sources that do not increase environmental pollution is essential in sustainable social and economic development. Therefore, a clean energy utilization plan that can reduce the consumption of fossil fuels is needed to meet current energy demands [188], [189].

Generally, the materials used to develop energy storage devices are not renewable because inorganic materials containing graphite and rare metals are used as core elements. However, biochar may be used instead of graphite. Biomass-based materials are environmentally friendly, are naturally abundant, and have various structures so that they can be used together with other materials because of their inherent mechanical strength and flexibility. Therefore, biochar is being studied to develop storage devices (lithium-ion batteries, fuel cells, and supercapacitors) that use waste rather than char as fuel as an alternative to simple fossil fuel [190].

Chapter 3. Sorptive removal of nitro explosives and metals using biochar

3.1. Introduction

Biochar provides an environmental benefit as a sorbent in natural environments. Biochar has been increasingly investigated as a sorbent in soils and sediments because of its high surface area and strong sorption affinity for aromatic organic compounds [191], [192]. Yang and Sheng (2003) showed that black carbon (BC) formed from the burning of crop residue is primarily responsible for the sorption of aromatic pesticides in soils [193]. The existence of ashes, including BC, may determine their environmental fate in soils. They showed that surface functional groups also significantly reduce the sorption capacity of wheat-derived BC for pesticides compared with activated carbon [194]. Changes in pH also affect the sorptive capacity of wheat char according to the surface charge of the char and protonation of pesticides [194], [195]. Chun et al. (2004) [191] showed that sorptive properties of crop residue–derived chars are strongly related to the surface area, surface functional groups, organic matter contents, and oxygen contents according to a pyrolysis temperature. They suggested that the relatively high affinity of biochar for polar aromatic compounds (e.g., nitrobenzene) could attribute to the functional groups (acidity or basicity) on the biochar surface. Zhu and Pignatello (2005) [127] proposed that π–π electron donor-acceptor (EDA) interactions between organic sorbates and BC best explain the sorption behavior. Namely, electron-rich, and poor regions of graphene moieties in BC could explain the sorption of π-acceptors (e.g., nitrobenzene, 2,4-dinitrotoluene [DNT], and 2,4,6-trinitrotoluene [TNT]) and π-donors (e.g., naphthalene and phenanthrene), respectively [127], [196]. They reported that dyes and phenol atrazine could be removed from soil and water when various biochars were used. [197]-[199]. It has also been shown that nonpolar and polar aromatic compounds could be sorbed to the surface of pine needle biochar through partition or adsorption depending on the properties of the biochar, including

carbonizing and the organic matter contents according to pyrolysis temperatures [192], [200]. Ambrosia trifida–derived biochar was evaluated as a sorbent for TNT and hexahydro-1,3,5-trinitro-1,3,5-triazine (RDX) [201]. They showed that the maximum sorption capacity onto biochar synthesized at 700 ℃ was 76.9 and 55.6 mg/g, respectively.

Biochar has also been examined to remove toxic metals and anions in soils and water. Seredych and Badosz (2006) [202] showed that copper (Cu) sorption to sludge-derived char is comparable to activated carbon. They attributed the sorption of Cu onto char to cation exchanges on the surface of char, surface complexation, and surface precipitation. Machida et al. (2006) [203] showed that lead (Pb) is sorbing to an oxygen-free BC surface due to localized electrons in the graphene layer (aka C_π electrons). However, when oxygen-containing functional groups existed on the surface of BC, Pb sorption to the BC surface switched from the graphene layer to carboxyl/lactonic functional groups. Mohan et al. (2007) [204] showed that considering the sorbed amount of Pb and cadmium (Cd) to activated carbon per unit surface area, bark-derived char's sorptive capability for Pb and Cd is far superior. Lima et al. (2009) [205] showed that broiler manure char could remove more Cu and Zn (58 and 63 mg/g, respectively) than other chars synthesized from coal, wood, or coconut. Cao et al. (2009) [118] reported that Pb is sorbing to dairy manure–derived biochar via surface precipitation (84~87%) and surface sorption (13~16%). The surface sorption was attributed to C_π–cation interactions and H^+~Pb^{2+} exchanges in the surface functional groups. Uchimiya et al. (2010) [206] showed that the addition of broiler litter–derived biochar immobilizes Cd, Cu, Ni, and Pb by increasing pH and ion exchanges in surface functional groups. When the metals were sorbed to biochar synthesized at high temperatures, the importance of cation exchanges decreased as C_π–cation interactions and surface precipitation increased. They explained the sorption of Cu to biochar by several mechanisms (e.g., electrostatic interactions, ash components sorption surface, functional groups complexation, π electron-cation interaction, and surface precipitation). They

concluded that biochar's immobilization ability for cationic metals correlates with the amount of oxygen functional groups representing the O:C molar ratio, PZC, and total acidity [207], [208]. Recently, Lu et al. (2012) [209] summarized Pb adsorption mechanisms to sludge-derived biochar, including cation exchange, complexation with surface functional groups (carboxyl or hydroxyl), surface precipitation, and electrostatic sorption. Attempts to apply biochar for phosphate and sulfate removal in water have also been recently made [210], [211].

In the present study, we evaluated biochars, which were pyrolysis from various biomasses, for treating nitro explosives and toxic metals in water. We determined the physical and chemical properties of biochars synthesized using various agricultural wastes and biomasses, including fallen leaves (Oak trees), rice straws, corn stalks, used coffee grounds, biosolids from wastewater treatment facilities, and poultry litter. Granular activated carbon (GAC) and graphite were also characterized as reference materials. We hypothesized that biochar might be an alternative sorbent for nitro explosives and metals in contaminated water. We examined the feasibility of using biochar as a sorbent through batch sorption experiments. We obtained the maximum sorption capacity for nitro explosives, including DNT, TNT, RDX, and toxic metals, including As, Cd, Cu, Pb, and Zn. We determined the factors affecting the sorption of nitro explosives and metals to biochar and investigated possible mechanisms responsible for the sorption of nitro explosives and metals to biochar.

3.2. Materials and methods

3.2.1. Chemicals

2,4-Dinitrotoluene (DNT) (97%), a nitroaromatic compound, was purchased from Aldrich. Hanwha Corp provided TNT and RDX. Cadmium chloride (98%), $CuCl_2$ (97%), $PbCl_2$ (98%), $ZnCl_2$ (97%), and $Na_2HAsO_4 \cdot 7H_2O$ (98%) were purchased from Aldrich. Methanol (HPLC grade) was purchased from SK Chemicals and used as received without further purification. For reference, BC material, high purity graphite powder (<20 mm, 99.9%), and charcoal-based GAC were purchased through Aldrich and DC Chemical. The GAC contained C (79.8%), H (0.56%), O (2.81%), and N (0.59%). The graphite and GAC surface areas were 13.6 and 738.8 m^2/g, respectively, as determined by the Brunauer-Emmett-Teller (BET) method with N_2.

3.2.2. Synthesis and characterization of biochars

Poultry litter (PL) and biosolid (BS) biochars were prepared via pyrolysis from dried pellets of PL and wastewater biosolids. The PL pellets (<6 mm in diameter) were obtained from Perdue Agri Recycle, Inc., and the BS was collected from a municipal wastewater treatment facility in Ulsan, South Korea. Poultry litter biochar was prepared through slow pyrolysis of dried PL pellets at 400°C for 8 h at a Delaware State University facility. A detailed description of the PL biochar has been published elsewhere [212]. The sampled biosolids were dried and pyrolyzed at a pilot-scale plant located at a company in Ulsan for 4 h at 400 ℃. In addition, four other types of biochar were synthesized from fallen leaves (oak tree) (FL), used coffee grounds (CF), rice straws (RS), and corn stalks (CS), which were generated in the city of Ulsan. The biochars were pyrolysis using a laboratory-scale, gas flow–controlled, tube-type furnace at 550 ℃ for 4 h under N_2 at 1000 mL/min flow rate. The synthesized biochars use without further treatment. Therefore, particle size analysis was not performed. However, analysis observed the diameter of the biochar particles to be <4.75 mm. Properties of the reference BC

materials and synthesized biochars, pH, BET surface area, CEC, PZC, and elemental contents are summarized in Table 3.1. A Nicole 380 spectrometer (Thermo Scientific) and K-Alpha system (Thermo Scientific) were used to determine the surface functional groups of the reference BC material and biochar. As a result, Fourier transforms infrared spectroscopy (FT-IR) spectra and X-ray photoelectron spectroscopy (XPS) were obtained. In addition, SEM images of BC materials and biochars were obtained using a JSM 600F (JEOL).

Table 3.1. Properties of the black carbon and biochars used in the present study.

Types of black carbon [1)]	pH[2)]	BET surface area[3)] (m^2/g)	CEC[4)] ($cmol_c/kg$)	PZC[5)]	Elemental contents[6)] (%)			
					C	H	O	N
Graphite	3.73	13.6	5.40	4.94	97.5	0.06	<0.01	<0.01
GAC	6.42	739	11.6	6.89	79.8	0.56	2.81	0.59
PL biochar	9.81	11.0	72.5	8.26	37.1	2.30	13.9	5.20
BS biochar	8.31	123	8.61	7.12	31.8	3.40	19.4	4.41
FL biochar	9.52	12.9	7.03	8.33	56.5	2.43	13.6	1.99
CF biochar	9.81	18.7	5.32	8.13	77.4	3.12	10.7	4.22
RS biochar	9.10	16.7	3.11	8.22	56.1	2.77	12.7	1.92
CS biochar	11.7	16.8	11.9	8.24	56.4	2.13	13.4	2.29

[1)] BS: biosolids; CF: coffee grounds; CS: corn stalks; GAC: granular activated carbon; PL: poultry litter; FL: fallen leaves; RS:
rice straw.
[2)] Determined by the method of Rump and Krist (1988) using deionized water [213].
[3)] Brunauer, Emmett, and Teller surface area analyzed by nano POROSITY-XQ (Mirae Scientific Instrument) using N_2.
[4)] Cation exchange capacity, determined by the method of Hesse (1971) [214].
[5)] Point of zero charge, determined by the method of Faria et al. (2004) [215].
[6)] Analyzed by Vario EL Elemental Analyzer (Elementar, GmbH, Germany)

3.2.3. Batch sorption experiments

Batch sorption experiments were performed using a 40 mL amber vial containing 20 mL of solution and reference BC or biochar (0.05~5 g) at 25 ± 2 ℃. After sealing with screw caps with PTFE-silicon septa, vials were shaken by an orbital shaker at 180 rpm throughout the experiment except during sampling. Duplicate vials were prepared for each batch to ensure reproducibility and to estimate experimental errors. Preliminary experiments indicated that the sorption of explosives and metals to biochar reached equilibrium after 24 h. Initial concentrations of explosives and metals were 40 to 50 mg/L and 100 to 180 mg/L, respectively. We obtained equilibrium concentration (Ce), sorbed concentration (q), and equilibrium pH by changing the number of sorbents. In addition, the sorption isotherm data are obtained by changing the metals' concentrations to determine the effect of different equilibrium pH by changing the number of sorbents. We added no salts to provide ionic strength in solutions.

Furthermore, maintained pH at 4, 7, and 10 using acetate, N-[2-hydroxyethyl] piperazine-N-[2-ethanesulfonic acid], and 3-[cyclohexylamino]-2-hydroxy-1-propane sulfonic acid buffers. The reason was to check the effect of pH on the adsorption of explosives. For the metal sorption experiments, the initial pH was adjusted to 5 to 5.5 to prevent possible precipitation and maintain the initial concentration. After we reached equilibrium, aliquots were withdrawn using glass syringes and immediately passed through a 0.025 mm cellulose membrane filter (Millipore) to analyze explosives and metals. Furthermore, set up a set of control vials under identical conditions without biochar to consider possible sorption to the inside surface of the vial. Gardea-Torresdey et al. (1990) [216] and Chen and Yang (2006) [217] blocked the carboxyl and hydroxyl functional groups through the method proposed.

Afterward, we investigated the effect of carboxyl and hydroxyl functional groups on the adsorption of explosives and metals on BC materials and biochar. For the blocking of carboxyl functional groups, a 1000 mL flask containing 9 g of FL or RS biochar, 633 mL of methanol,

and 5.4 mL of 0.1 mol/L HCl was shaken at 100 rpm for 6 h at 25 ℃. After centrifugation at 4000 rpm for 10 min in a centrifuge, we removed the solution, and the biochar was washed with deionized water for at least 2 min using a Vortex shaker. After washing with deionized water at least three times, the biochar was dried in a dry oven at 40 ℃ for 12 h. For blocking hydroxyl functional groups, a 250 mL flask containing 5 g of the biochar and 100 mL of 1%, HCHO solution was shaken at 100 rpm for 24 h at 25 ℃. After the HCHO solution removing by filtration with a 0.025 mm cellulose membrane filter, the biochar was washed with deionized water at least three times and dried at 40 ℃ for 12 h. Using carboxyl/hydroxyl-blocked biochars. Sorption experiments were performed under identical conditions.

3.2.4. Chemical analysis

2,4-Dinitrotoluene, TNT, and RDX were analyzed using a Dionex Ultimate-3000 high-performance liquid chromatograph equipped with a Dionex Acclaim 120 guard column (4.3 × 10 mm) and an Acclaim 120 C-18 column (4.6 × 250 mm, 5 mm). The analytical methods and conditions for quantifying DNT, TNT, and RDX are described elsewhere [218], [328]. The concentrations of As, Cd, Cu, Pb, and Zn are determined by an atomic absorption spectrophotometer (5100 ZL, PerkinElmer) equipped with a graphite furnace. We used analytical duplicates, standards, and blank samples for quality control of the data we obtained.

3.3. Results and discussion

3.3.1. Characteristics of the biochars

The physical and chemical properties of the reference BC materials and biochars are summarized in Table 3.1. Graphite and GAC showed acidic pH (3.73 and 6.42, respectively), but biomass-derived biochars were alkaline (8.31 ~ 11.7). As previously reported, the possible existence of carbonate materials (e.g., $CaCO_3$ and $MgCO_3$) may account for the alkaline pH of biomass-derived biochars [219]. The deprotonated surface functional groups of biochar (e.g., COO- or O-) can also affect the alkalinity of biochar [54]. Brunauer–Emmett–Teller (BET) surface areas of biochar showed various ranges. Compared with GAC (738.8 m^2/g), most of the biochars surface areas were one order of magnitude smaller (11.0~18.7 m^2/g), except for BS biochar (123 m^2/g). Due to being synthesized at 400 or 550 ℃, the six biochars may have included organic impurities (residues), accounting for biochar's relatively low surface area. According to a previous report [107], further elevated temperatures (700–900 ℃) can result in the increased surface area through removal of organic residues and formation of aromaticity (graphene layer). The CEC of the biochars was not significantly different from those for graphite and GAC, except for PL biochar (72.5 $cmol_c/kg$). Compared with the CEC of minerals in soil (2~15 $cmol_c/kg$ for kaolinite, 10~40 $cmol_c/kg$ for biotite and muscovite, and 80~150 $cmol_c/kg$ for montmorillonite) [220], the CEC of biochar was in the lower range of minerals in the soil. PL biochar may likely sorb toxic cations (discussed below). The biochars' PZC ranged from 7.12 to 8.33. Elemental analysis indicated that their compositions of C, H, O, and N differed depending on the biomass types. The diverse ranges in properties of biochar may result in different sorptive capacities for nitro explosives and metals.

XPS and FT-IR analyzes were performed to confirm the presence of surface functional groups. Compared with pure graphite, the intensity spectra (C1s) of the six biochars of XPS were significantly higher in C-O (286.5 eV), C=O (287.5 eV), and COO (289.1 eV) (Fig. 3.1),

and this result indicates that oxygen This is because functional groups including. On the other hand, the spectrum of GAC was much close to that of graphite, indicating that oxygen-containing surface functional groups were not dominant on the GAC surface. The FT-IR analysis confirmed the development of C-H bonds (at 2750~2950 cm^{-1}), carboxylic bonds (COOH) (at 1700 cm^{-1}), and aromatic bonds (C=C) (at 1600 cm^{-1}) at the surface of the biochar (Figure. 3.2). Compared with the six biochars, the FT-IR spectra of GAC and graphite show that the oxygen-containing function is not developing. SEM images showed that biomass-derived biochars have various shapes in their surface morphology and porous structures and that some biochars may include impurities on their surface (Figure. 3.3).

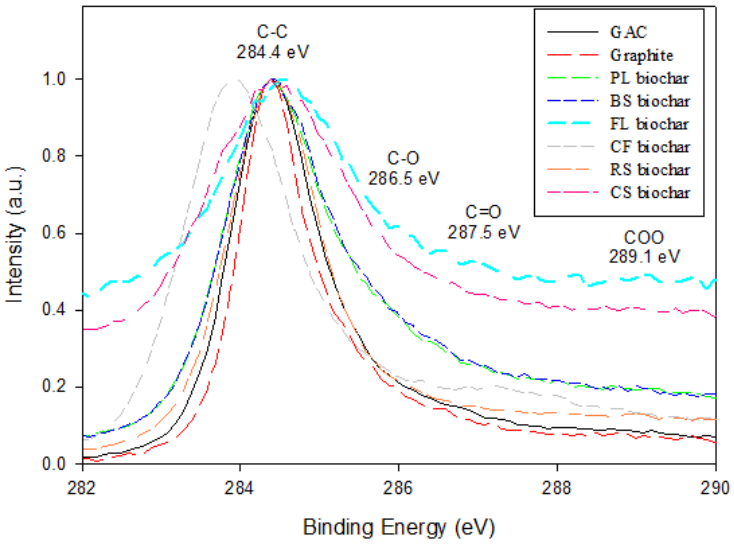

Figure 3.1. XPS spectra (C1s) of the black carbon and biochars used in the present study (X-ray source: monochromatic Al Ka; spot size: 400 mm, Ar ion gun 1 keV).

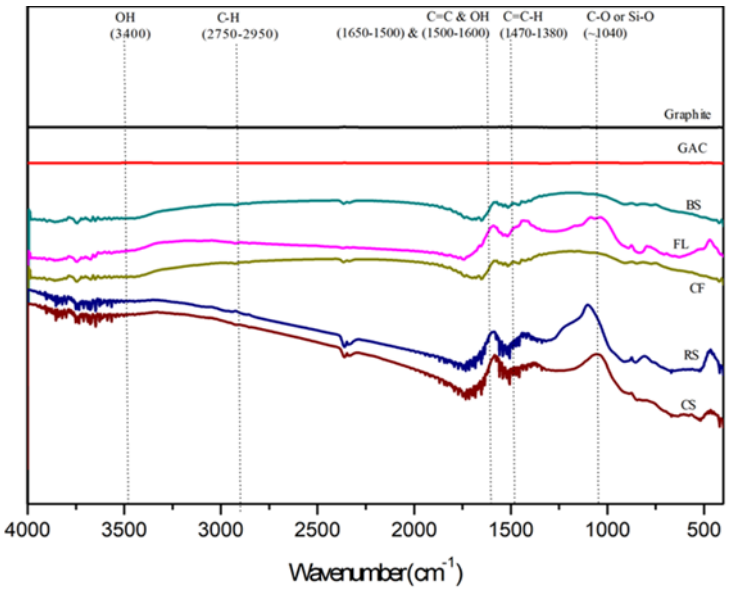

Figure 3.2. FT-IR spectra of the black carbon and biochars used in the present study. (BS: BS biochar; CF: CF biochar; CS: CS biochar; GAC; PL: PL biochar; FL: FL biochar; RS: RS biochar).

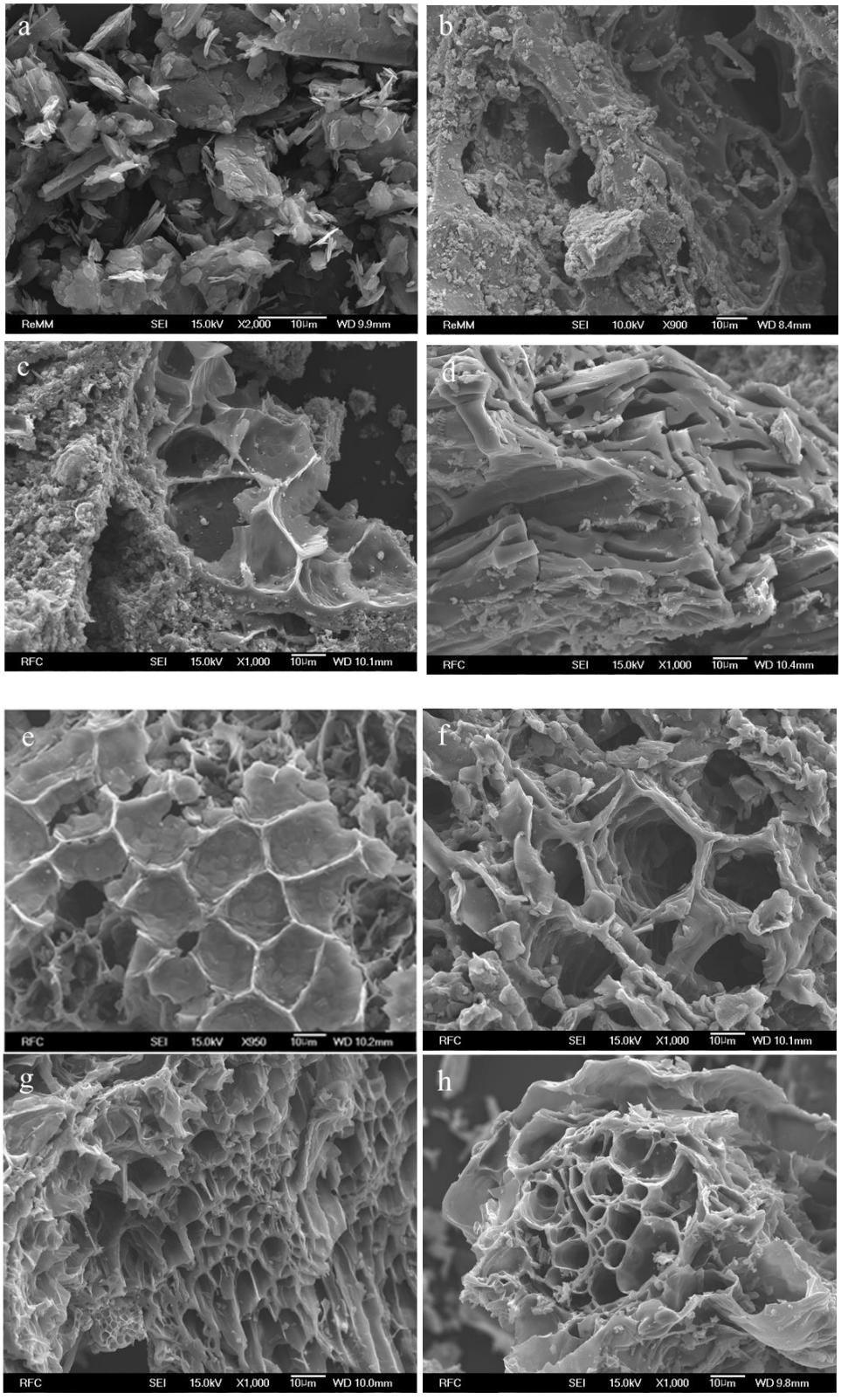

Figure 3.3. SEM images of the black carbon and biochars used in the present study (a: graphite, b: GAC, c: PL biochar, d: BS biochar, e: FL biochar, f: CF biochar, g: RS biochar, h: CS biochar).

3.3.2. Sorption of explosives to biochars

By changing the number of sorbents and the concentrations of explosives in the solution, the Langmuir sorption isotherm was established (R^2= 0.87 ~ 0.98), and maximum sorption capacities for DNT and TNT and the RDX of graphite, GAC, and the six biochars were determined (Figure. 3.4). Granular activated carbon showed the highest sorption capacity for DNT, TNT, and RDX (15.48, 10.17, and 10.67 mg/g, respectively), probably due to its high surface area (738.8 m^2/g) and high carbon content (79.8%). Graphite also showed a relatively high sorption capacity (10.11, 7.07, and 7.68 mg/g, respectively). Previously, π–π EDA interactions have been reported to account for the sorption of nitroaromatics to BC [196], [127]. DNT, TNT, and RDX (K_{ow} = 2.00, 2.05, 0.87) and the low surface area of graphite (13.6 m^2/g) explain the adsorption mechanism of nitro explosives on graphite. This result is mainly attributed to the π–π EDA interaction between the electron-withdrawing nitro functional group and the electron-rich moiety in graphite [221]. However, we cannot exclude the possibility of hydrophobic sorption to graphite and GAC.

Maximum sorption capacities of the six biochars for DNT, TNT, and RDX were lower than those of GAC and graphite. The development of surface functional groups, explained by the low carbon and high oxygen contents (Table 3.1), may reduce the sorption capacity of the biochars for explosives. Sorption capacities of the PL and CS biochars for DNT were as good as graphite. Excepting these cases, other biochars showed about 35 to 70% sorption capacities of graphite. These results imply that the mechanisms of explosive sorption to BC and biochar may not be related to properties affecting pHs, such as surface charge and surface functional groups. Our results suggest that some selected biochars (i.e., PL and CS biochars) may have competitive sorption capacities compared with GAC and graphite.

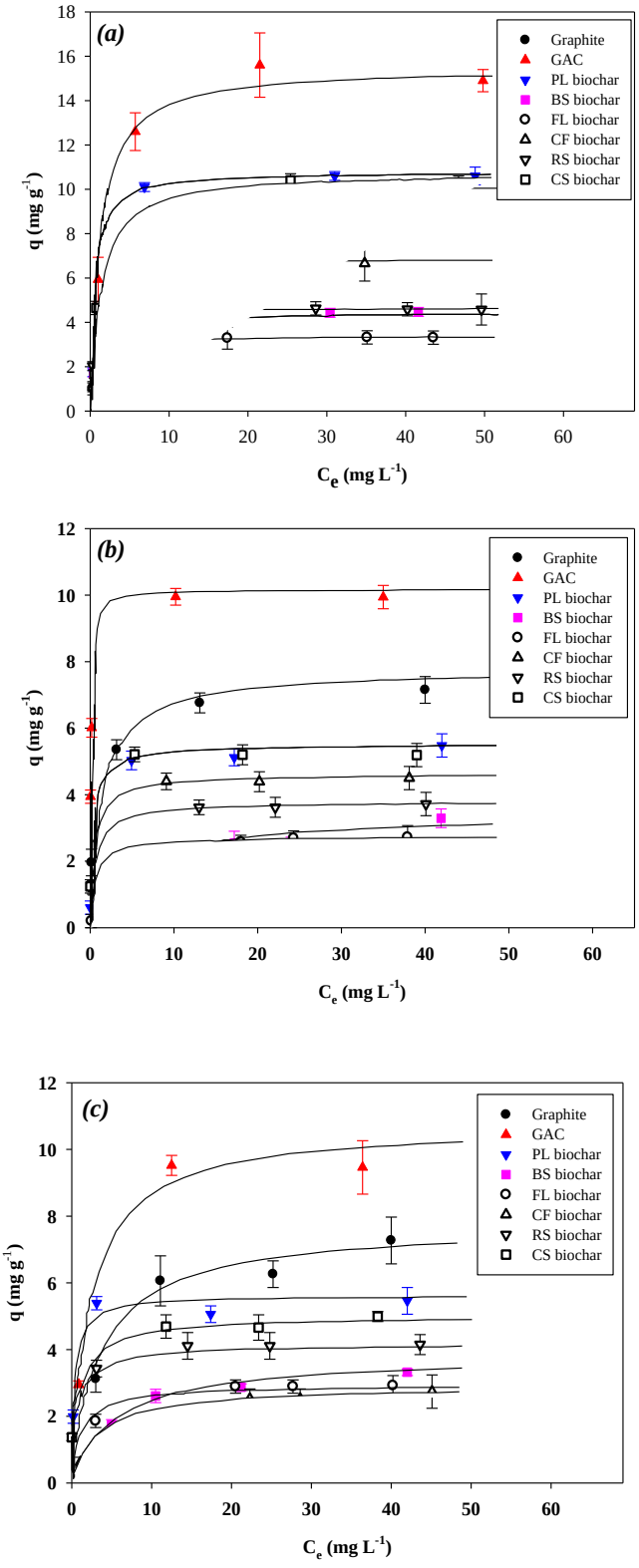

Figure 3.4. Langmuir sorption isotherm of black carbon and biochars for (a) DNT, (b) TNT, and (c) RDX. Data points are the average of duplicate samples, and error bars represent 1 SD.

3.3.3. Sorption of metals to biochars

The maximum sorption capacity of As and cationic metals are summarized in Figure. 3.5 by fitting the data obtained with the Langmuir sorption isotherm model. In the case of As, the sorbed amounts of As to GAC, graphite, and other biochars were negligible or minimal (0 mg/g for graphite, FL, CF, RS, and CD biochars; 0.11 mg/g for PL biochar; 0.56 mg/g for GAC; and 0.91 mg/g for BS biochar). Due to its existence as an anion in solution, the sorption of As (as a form of arsenate [$HAsO_4^{2-}$ or AsO_4^{3-}]) to BC and biochar could be different from those of cationic metals. Although As a result adjusted the initial pH to 5 to 5.5, the presence of carbonate minerals in GAC and biochars (except graphite) increased the pH to 11 as the dosage of BC materials increased. Considering their PZCs (Table 3.1), the net surface charges of GAC and biochars were negative. Therefore, the repulsive force arising from anions and an opposing surface may hinder the sorption of As. Because the presence of graphite decreased the solution pH to 4 and the PZC of graphite is 4.9, it may be favorable for arsenate to be sorbed onto the surface of graphite. However, the sorbed amount of As onto graphite was negligible. This result suggests that the electrostatic sorption of arsenate to the graphite surface having a net positive charge may not be essential. These results suggest that other factors such as surface complexation or ion exchange may be responsible for arsenate sorption.

In cationic metals, the sorptive capacity of graphite was not significant compared with GAC and other biochars (Figure 3.5). This result may be related to the positive surface charge due to the PZC of graphite (4.9) and its low pH in the solution (Figure 3.6). The adsorption number of cationic metals for GAC and 6 biochars was significantly higher. Especially for PL biochar, maximum sorption capacities for Cd, Cu, Pb, and Zn were 18.0, 18.8, 37.7, and 8.05, respectively, by far more extensive than the other biochars and GAC (Figure 3.5). It appears that the high CEC (72.5 $cmol_c/kg$) is responsible for the significant number of cationic metals sorbed onto PL biochar. It was considering the low carbon and high oxygen and nitrogen

contents (Table 3.1) and the spectra of XPS and FT-IR (Figure. 3.2 and 3.3), surface functional groups would be well developed on the surface of PL biochar accounting for the high CEC. For the other biochars, maximum sorption capacities for most cationic metals were comparable to GAC's (Figure. 3.5). Only CF, RS, and CS biochars had lower sorption capacities for Pb compared with GAC. Like PL biochar, other biochars have surface functional groups according to elemental and spectroscopic analyses (Table 3.1; Figure 3.2 and 3.3). The removal of cationic metals to biochar could also be related to the increased pH in biochar–water systems. For all six biochars, the pH increased by increasing the amount of biochar (Figure 3.6). CS biochar, adding a small amount of biochar resulted in steep increasing pH up to 11. Therefore, electrostatic sorption of cationic metals to a negatively charged surface and the possibility of surface precipitation as metal-hydroxides may be more critical at an elevated pH. Different equilibrium pH by different amounts of biochar (Figure 3.6) may affect maximum sorption capacity. However, the sorption isotherm data obtained by changing the concentrations of metals at constant equilibrium pH confirmed that different pH showed similar maximum sorption capacity. It appears that pH difference may not significantly change the sorption isotherm data.

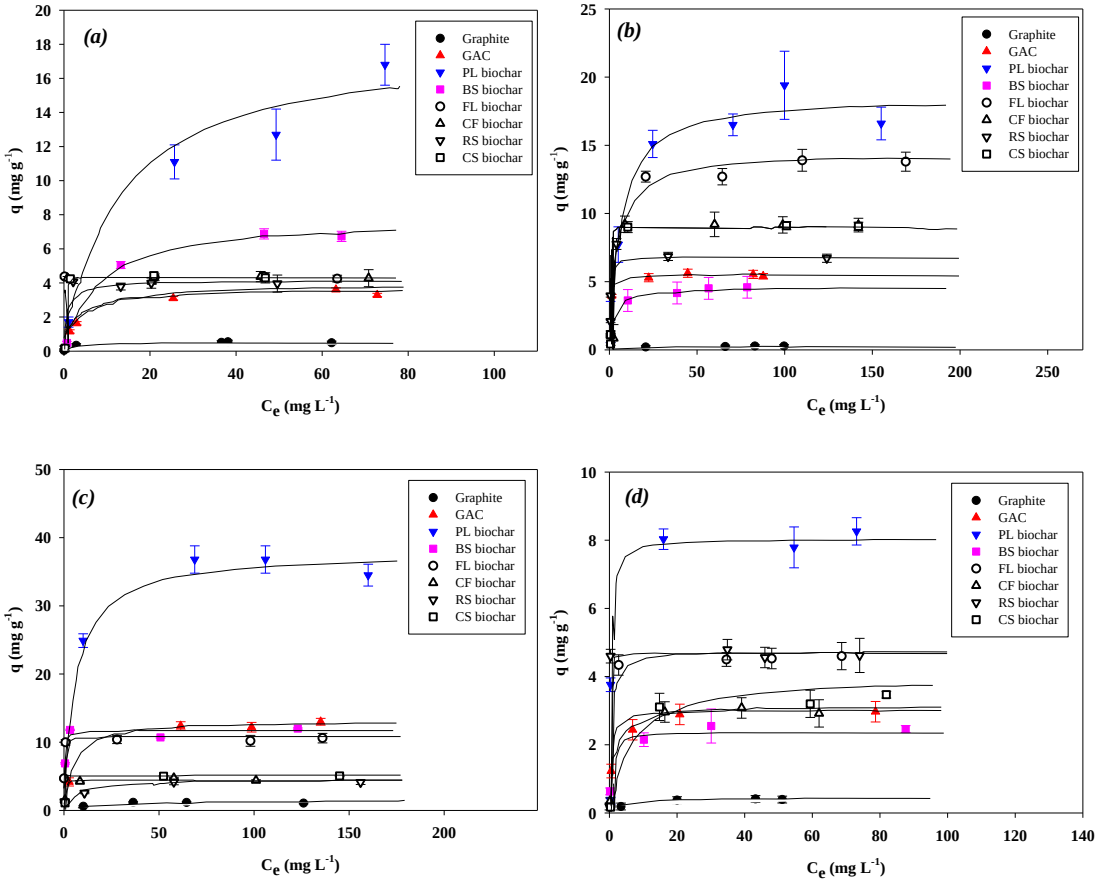

Figure 3.5. Langmuir sorption isotherm of black carbon and biochars for (a) Cd, (b) Cu, (c) Pb, and (d) Zn. Data points are the average of duplicate samples, and error bars represent 1 SD.

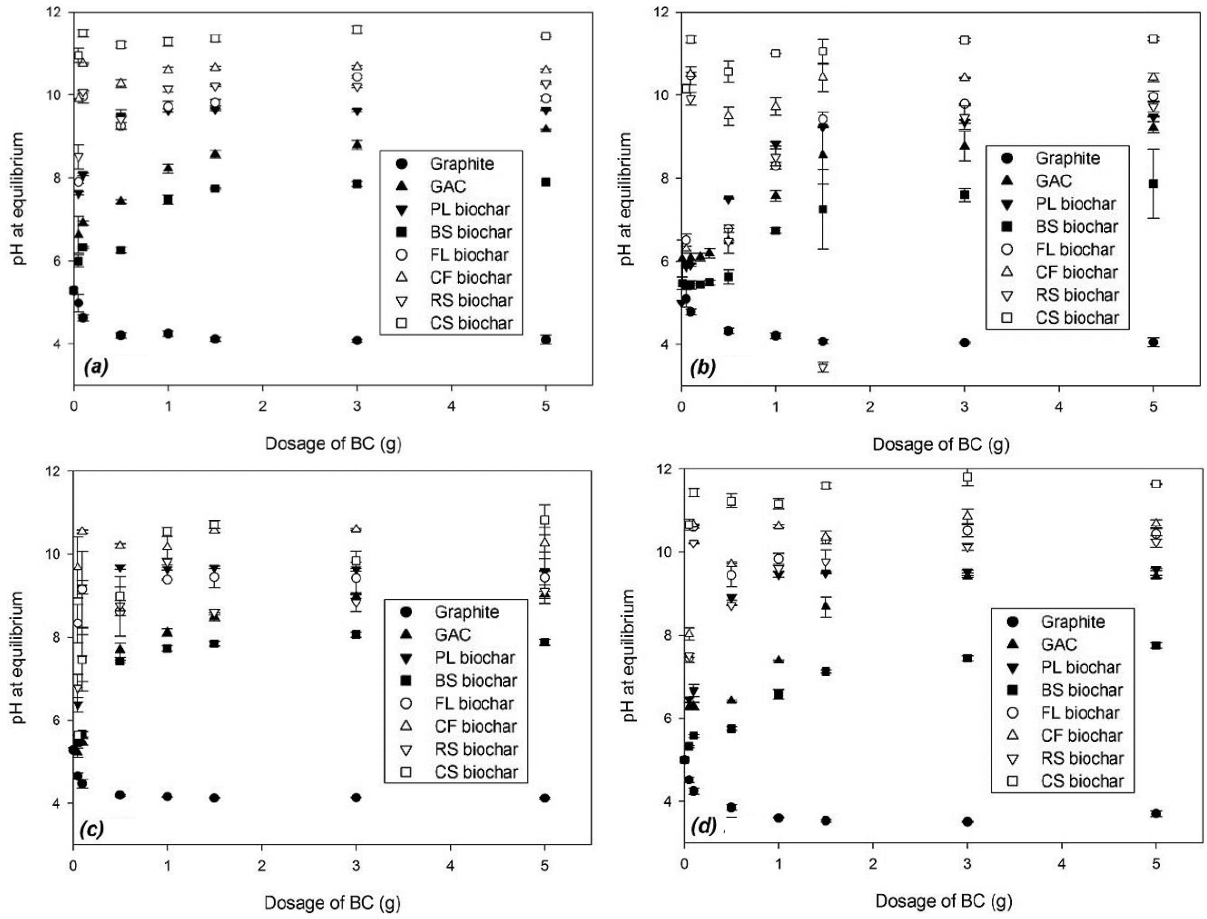

Figure 3.6. Change in pH over dosage of biochars during sorption experiments for (a) Cd, (b) Cu, (c) Pb, and (d) Zn. Data points are the average of duplicate samples, and error bars represent 1 SD.

3.3.4. Factors affecting the sorption of explosives and metals to biochars

According to the analysis of sorption data, possible sorption mechanisms in the sorption of nitro explosives to biochar could be attributing to π–π EDA interactions and hydrophobic sorption. In cationic metal sorption, possible sorption mechanisms could be explained by surface functional groups (represented by CEC) via cation exchanges and surface complexation, surface precipitation due to increases in pH, and electrostatic sorption. Regarding the factors affecting the adsorption of nitro explosives and metals on biochar, we analyzed the correlation between biochar characteristics and the maximum adsorption capacity of nitro explosives and cationic metals. Sorptive capacities of nitro explosives had positive correlations with surface area and carbon contents and negative correlations with hydrogen, nitrogen, and oxygen contents and O:C and H:C ratios (Table 3.2). These results strongly support that nitro explosives' sorption was not related to surface functional groups and that π–π EDA interactions and possible hydrophobic sorption could account for the sorption of explosives [127]. The adsorption capacity of cationic metals was positively correlated with pH, CEC, PZC, oxygen, and nitrogen content and negatively correlated with carbon content (Table 3.2). The results indicate that the sorption of cationic metals is related to net surface charge and surface functional groups and that surface complexation, ion exchange, electrostatic sorption, and surface precipitation can be possible sorption mechanisms [207], [209]. The correlation between maximum sorption capacity and XPS spectrum ratio [(C-O + C=O + COO):(C-C)] also showed that the sorption of cationic metals is related to surface functional groups in biochar (Table 3.3).

To obtain evidence supporting the adsorption mechanism of nitro explosives and cationic metals, we used FL and RS biochars with surface functional groups removed to adsorb nitro explosives and metal ions. For nitro explosives, regardless of carboxyl or hydroxyl functional group blockage, the maximum sorption capacity did not show any significant difference (Table

3.4). However, blockage of a carboxyl or hydroxyl functional group for cationic metals resulted in a marked reduction of sorption capacity (Table 3.4).

Table 3.2. The correlation coefficient between maximum sorption capacities and properties of black carbon and biochars.

Contaminant	pH	BET S.A.	CEC	PZC	C	H	O	N	O:C	H:C
DNT	-0.29	0.65#	0.32	-0.34	0.40	-0.71#	-0.63#	-0.32	-0.49*	-0.59*
TNT	-0.55*	0.78#	0.09	-0.52*	0.58*	-0.81#	-0.79#	-0.51*	-0.62*	-0.68#
RDX	-0.62*	0.78#	0.10	-0.59	0.49*	-0.86#	-0.76#	-0.59	-0.53*	-0.63#
Cd	0.40	-0.15	0.93#	0.42	-0.72#	0.36	0.50*	0.78#	0.59*	0.54
Cu	0.69#	-0.26	0.75#	0.75#	-0.56*	0.42	0.49	0.64#	0.33	0.30
Pb	0.43	0.07	0.95#	0.50	-0.56*	0.32	0.49	0.78	0.46	0.33
Zn	0.62*	-0.19	0.76#	0.74#	-0.63#	0.40	0.48	0.56*	0.35	0.33
As	-0.21	0.55	-0.05	-0.21	-0.36	0.12	0.24	0.18	0.53	0.49

# $p<0.1$
* $p<0.2$

Table 3.3. The correlation coefficient between maximum sorption capacities and XPS spectrum ratios of black carbon and biochars.

Log (contaminant)	Log [(C-O + C=O + COO):(C-C)]
Log (DNT)	-0.491*
Log (TNT)	-0.702#
Log (RDX)	-0.666#
Log (Cd)	0.481
Log (Cu)	0.643#
Log (Pb)	0.415
Log (Zn)	0.549*
Log (As)	N/A

* $p < 0.2$
# $p < 0.1$
N/A: Not available

Table 3.4. The maximum sorption capacities of FL and RS biochars using the Langmuir sorption isotherm when blocked by hydroxyl or carboxyl functional groups.

Contaminant	FL biochar			RS biochar		
	No blocking	Carboxyl blocked	Hydroxyl blocked	No blocking	Carboxyl blocked	Hydroxyl blocked
	-mg/g-					
DNT	3.36	3.35	3.78	4.63	4.73	3.88
TNT	2.73	2.43	2.86	3.77	3.99	3.98
RDX	2.90	2.79	2.59	4.13	3.58	3.66
Cd	4.27	3.88	3.81	4.08	3.17	1.22
Cu	12.8	3.64	3.07	6.85	4.19	1.75
Pb	10.9	5.73	5.83	4.59	3.88	2.49
Zn	4.74	4.17	2.63	4.98	4.57	1.44

3.4. Conclusions

In the present study, our results showed that biochar has a porous structure and a high surface area, which is favorable for the sorptive removal of nitro explosives and toxic cationic metals. Compared with GAC, biochar is an effective sorbent for removing Cd, Cu, Pb, and Zn from contaminated water. Compared with graphite and GAC, some biochars can also effectively sorb nitro explosives. Correlation analysis showed that the sorption capacity of nitro explosives is related with BET surface area and carbon content. It also shows that the sorption capacity of biochar for cationic toxic metals is related to pH, CEC, O:C, and H:C. X-ray photoelectron spectroscopy and blocking experiments showed that surface functional groups are responsible for the sorption of cationic metals to biochar. In contrast, carbon contents account for the sorption of nitro explosives possibly through π– π EDA interaction and hydrophobic sorption. Our results suggest that the application of biochar may be an attractive and alternative option in environmental remediation for nitro explosives and cationic metals in water through sorption and immobilization. The synthesis of biochar via pyrolysis adds extra cost. In South Korea, after ocean dumping of biosolids was banned in 2012, about 900 ton/d of biosolids are being treated via pyrolysis.

Therefore, biosolids-derived biochar could be easily provided free of charge. To use biochar derived from other biomasses, a cost-effective pyrolysis process should be developed, and additional cost analysis needs to be conducted. Disposal of metal/explosive-laden spent biochar remains to be examined.

Chapter 4. Sorption of halogenated phenols and pharmaceuticals to biochar: affecting factors and mechanisms

4.1. Introduction

Thermal decomposition is an effective and standard option to treat combustible organic waste in South Korea, with limited landfill sites. Among thermal decomposition processes, pyrolysis has drawn substantial attention due to the production of energy (bio-oil and biogas) and solid biochar, a product used for waste treatment. As a form of char, such can store carbon in biomass without further oxidation to carbon dioxide. Because it is relatively stable and resistant to biodegradation in soil and sediment, biochar has been studied as a carbon sequestration method to mitigate the release of CO_2 to the atmosphere [18], [222]. Amendment of soil with biochar provides additional benefits such as enhancing soil fertility and productivity, providing, storing nutrients, and creating habitat for microorganisms. Biochar also conveys environmental benefits as a sorbent to control the fate and transport of contaminants in natural environments [223], [125].

In the last decade, numerous studies have investigated the extent and mechanisms of contaminant sorption to biochar. Due to the large surface area and well-developed functional groups on the surface of biochar, immobilization with biochar suggested removing toxic metals in natural water and soil. Biochars synthesized from various biomasses, such as coal, wood, bark, biosolid (sludge), manure, and broil litter, were evaluated as sorbents to remove cationic metals and toxic anions [118], [202]-[206], [209]-[211], [224], [225]. The extent of metal sorption to biochar was strongly affected by the properties of the biochar, including pH, surface area, PZC, surface functional groups, oxygen and hydrogen contents, and aromaticity. Some biochars can even sorb toxic metals as effectively as activated carbon. The mechanisms involved in the sorption of metals to biochar were attributing to cation exchange between toxic

cations and H^+ in surface functional groups, surface complexation, π electrons cation interaction, electrostatic sorption according to surface charge, and surface precipitation [118], [202], [209], [226].

Due to their porous structure and strong affinity for aromatic organic compounds [191], [192], biochars have also been intensively studied for their sorption of organic contaminants. We investigated the adsorption mechanisms of pesticides, polycyclic aromatic hydrocarbons (PAHs), phenols, nitro-aromatics, and dyes utilizing different types of biochar [192], [193], [197]-[200], [227]. Depending on the types of organic compounds and the properties of the biochar, the sorption of organic compounds to biochar has been controlled by several factors, including pH, surface functional groups, organic matter residuals, surface area, degree of carbonization, and development of nanopores [191], [194], [228], [229]. The sorption of organic compounds to biochar was explained using several possible mechanisms, such as hydrophobic sorption, hydrogen bonding, pore-filling, and electrostatic interactions. For some polar aromatic compounds, which include electron-withdrawing functional groups (e.g., $-NO_2$), π-π EDA interaction between organic sorbates and biochar is suggested to explain the sorption behavior [127], [196]. In the current study, we investigated the sorption of nitro explosives to biochars synthesized from poultry litter, biosolids, fallen leaves, rice straw, corn stalk, and ground coffee waste [230]. The sorption capacity of explosives was proportional to the carbon content of the biochar. Statistical and experimental results showed that the sorption of nitro explosives was primarily due to π-π EDA interactions. The sorption of halogenated aromatic compounds to other types of carbonaceous materials was also studied. It has previously been shown that chlorophenols' sorption to activated carbon fibers is due to π-π EDA interactions, solvent effect, hydrophobicity, molecular dimensions, and electrostatic interaction [231], [232]. Wang et al. (2007) [231] showed that lower pH values are favorable for the sorption of 2,4-dichlorophenol (DCP) to activated carbon fibers. Hamdaoui and

Naffrechoux (2007) [233] showed that the sorption of chlorophenols to granular activated carbon was proportional to molecular weight, hydrophobicity, and degree of chlorination. Yang et al. (2008) [234] suggested that the sorption of chlorophenols to carbon nanotubes may be attributed to hydrogen bonding interactions between H-donor (solute) and H-acceptor (carbon nanotube), π-electron polarizability, and van der Waals forces.

To date, numerous studies have been conducted on the sorption of nonionic organic compounds to control and determine their fate in natural water and soil. Recently, some efforts were made to study the sorption of ionizable organic contaminants to biochar. Ni et al. (2011) [235] showed that de-protonated aromatic carboxylate ions were sorbed to biochar via proton exchange with water. Li et al. (2013) [236] proposed that ionizable compounds could be sorbed to carbon nanotubes via forming a negative charge-assisted H-bond between a carboxyl group of the solute and carboxylate or phenolate functional groups on the surface. However, limited research has been performed on this subject, and the extent and mechanisms of various types of ionizable organic compounds remain to be determined.

This study investigated the adsorption of halogenated phenols, triclosan, ibuprofen, and organic compound ions to biochar. We hypothesized that biochar could be used as an adsorbent to remove halogenated phenols and pharmaceuticals from contaminated water. According to the properties of biochars and compounds, the sorption of halogenated phenols and pharmaceuticals to biochar may be material-dependent and predictable. We investigated the degree of adsorption of halogenated phenols and pharmaceuticals on different biochars through batch experiments and determined the adsorption capacity of each biochar using the Langmuir adsorption isotherm model. Furthermore, among the characteristics of biochar and compounds, we investigated factors affecting the adsorption of biochar through a statistical approach. Possible sorption mechanisms were discussed. The effects of pyrolysis temperature, ionic strength of the solution, and humic acid were also determined.

4.2. Materials and methods

4.2.1. Chemicals

Nine halogenated phenols were selected and purchased from Aldrich (Milwaukee, WI, USA): 2,4-Dichlorophenol (99%, DCP), 2-Chlorophenol (99%, 2CP), 4-Chlorophenol (99%, 4CP), 2,4-Dibromophenol (95%, DBP), 2-Bromophenol (98%, 2BP), 4-Bromophenol (99%, 4BP), 2,4-Difluorophenol (99%, DFP), 2-Fluorophenol (98%, 2FP), and 4-Fluorophenol (99%, 4FP). Phenol (99%) was purchased from Daejung Chemical (>99%, Kyunggi, South Korea). Triclosan (97%), ibuprofen (98%), and N-[2-hydroxyethyl] piperazine-N′-[ethanesulfonic acid] (HEPES) were obtained from Sigma (St. Louis, MO, USA). Humic acid and NaCl (> 98%) were purchased from Aldrich. All chemicals were used as received without further purification. The black carbon (BC) material, high purity graphite powder (<20 μm, 99.9%), and charcoal-based GAC used in the experiments were purchased from Aldrich and DC Chemical (Seoul, Korea), respectively. The GAC contained C (79.8%), H (0.56%), O (2.81%), and N (0.59%). The graphite and GAC surface areas were 13.6 and 738.8 m^2/g, respectively, as determined by the Brunauer-Emmett-Teller (BET) method with N_2. Table 4.1 summarizes the properties of halogenated phenols, triclosan, and ibuprofen.

Table 4.1. Properties of phenols and pharmaceuticals used in this study [237]-[242].

	Chemical formula	Molecular weight	Log K_{ow}	pK_a	Water solubility (mg/L)
2.4-Difluorophenol (DFP)	$C_6H_4F_2O$	130.09	1.91	8.72	8,109
2-Fluorophenol (2FP)	C_6H_5FO	112.1	1.71	8.70	14,100
4-Fluorophenol (4FP))	C_6H_5FO	112.1	1.77	9.91	12,500
2,4-Dichlorophenol (DCP)	$C_6H_4Cl_2O$	163.0	3.20	7.90	4500
2-Chlorophenol (2CP)	C_6H_5ClO	128.56	2.15	8.48	28,500
4-Chlorophenol (4CP)	C_6H_5ClO	128.56	2.39	9.41	24,000
2,4-Dibromophenol (DBP)	$C_6H_4Br_2O$	251.9	3.22	7.79	1,900
2-Bromophenol (2BP)	C_6H_5BrO	173.01	2.35	8.45	2,227
4-Bromophenol (4BP)	C_6H_5BrO	173.01	2.59	9.17	14,000
Phenol (P)	C_6H_6O	94.11	1.46	9.95	82,800
Triclosan	$C_{12}H_7Cl_3O_2$	289.54	4.76	8.14	10
Ibuprofen	$C_{13}H_{18}O^2$	206.28	3.97	4.91	21

4.2.2. Synthesis of biochar

BS biochar was prepared via pyrolysis from wastewater biosolids collected from a municipal wastewater treatment facility in Ulsan, South Korea. The sampled biosolids were dried and pyrolyzed for 4 h at 400 ℃ at a pilot-scale plant owned by a company in Ulsan. In addition, four other types of biochar were synthesized from fallen leaves (oak tree) (FL), used coffee grounds (CF), rice straws (RS), and corn stalks (CS), all of which were generated in the Ulsan. The biochars pyrolysis using a laboratory-scale gas flow-controlled tube-type furnace at 550 ℃ for 4 h under N_2 at 1000 cc/min flow rate. To determine the effect of pyrolysis temperature RS biochars, pyrolyzed at 250, 400, 550, 700, and 900 ℃ under identical conditions. The synthesized biochars use without further treatment. Although we did not perform particle size analysis, the diameter of the biochar particles was less than 4.75 mm. Properties of the reference BC materials and the synthesized biochars, pH, BET surface area, CEC, PZC, and elemental contents are summarized in Tables 3.1 and 4.2. To determine the reference BC materials surface functional groups, biochar spectra from FT-IR and XPS were

obtained using a Nicolet 380 spectrometer (Thermo Scientific, Pittsburgh, USA) and a K-alpha system (Thermo Scientific), respectively.

Table 4.2. Properties of RS biochars by temperature.

Types of black carbon	Pyrolysis temperature (°C)	pH	BET surface area (m^2/g)	CEC (cmol/kg)	PZC	Elemental contents (%)			
						C	H	O	N
RS biochar	550	9.10	16.7	3.11	8.22	56.1	2.77	12.7	1.92
RS biochar	250	6.85	7.96	24.9	6.9	40.8	5.73	39.8	0.03
RS biochar	400	7.19	10.7	21.7	8.9	53.1	3.84	17.8	1.52
RS biochar	700	8.99	38.4	15.2	11.3	59.4	1.64	6.58	1.47
RS biochar	900	11.7	116	34.2	11.3	62.5	0.97	5.20	1.83

4.2.3. Batch sorption experiments

Batch sorption experiments were performed using a 40-mL amber vial containing 20 mL of solution and biochar (0.05-5 g) at 25 ± 2 °C. After sealing with screw caps with PTFE silicone septa, duplicate vials were shaken on an orbital shaker at 180 rpm throughout the experiment, except during sampling. Preliminary experiments indicated that the sorption of halogenated phenols and the pharmaceuticals to biochar reached equilibrium after 24 h. Initial concentrations of halogenated phenols, triclosan, and ibuprofen were 50-500 mg/L. Using HEPES buffer (20 mM), we evaluated the effect of pH on the sorption of DCP and triclosan to biochar by maintaining solution pH at 7.0. To determine the effects of ionic strength and dissolved humic acid on the sorption of those compounds, predetermined ionic strength (0.01 or 0.1 M) and humic acid (20 and 100 mg/L in TOC analysis) were dissolving in DCP and triclosan solutions. Humic acid was initially dissolving in a solution of pH 11. Then, the pH was adjusted to 7 using 0.1 N HCl. The humic acid solution was filtered for use in batch experiments. After that reached equilibrium, aliquots were withdrawn using glass syringes and immediately passed through a 0.025-μm cellulose membrane filter (Millipore, MA, USA) to

determine halogenated-phenols and pharmaceuticals analytically. A set of control vials was set up under identical conditions without biochar to determine possible loss of the contaminants due to sorption to the inner surface of the vial or volatilization at elevated equilibrium pH (4.1-11.0). A set of control vials was set up under identical conditions without biochar to determine possible loss of the contaminants due to sorption to the inner surface of the vial or volatilization at elevated equilibrium pH (4.1-11.0). The adsorption amount of pollutants is calculated by taking into account the pollutant losses through batch experiments. To determine the effect of pre-hydration on biochar [243], we also performed batch experiments with 7-day hydrated biochar (RS) for the sorption of DCP by spiking concentrated DCP to solution following the procedure suggested by Pignatello et al. (2006) [243]. However, we did not see a significant difference, indicating that the pre-hydration effect on the sorption may be negligible.

4.2.4. Chemical analysis

Phenol and 9 halogenated phenols were analyzed using an Ultimate™ 3000 HPLC system (Dionex, Sunnyvale, CA, USA) equipped with an Acclaim® 120 guard column (4.3×10 mm, Dionex, Sunnyvale, CA, USA) and an Acclaim® 120 C18 column (4.6×250 mm, 5 μm, Dionex, Sunnyvale, CA). A methanol-water mixture (70:30 or 75:25, v/v) was used as the mobile phase at a flow rate of 1.0 mL/min, and the sample injection volume was 100 μL. The mobile phase used for elution to measure triclosan was a mixture of deionized water (30%) and acetonitrile (70%) passed through the column at 1 mL/min. A Discovery® RP-Amide C-16 column (4.6x150 mm, 5 μm) (Supelco, Bellefonte, PA, USA) was installed in the HPLC system to analyze the ibuprofen concentration. The mobile phase used for elution was 25 mM KH_2PO_4 at pH 3.0 (40 %) and acetonitrile (60 %), delivered at 1 mL min−1 through the column. We used a sample injection volume of 100 μL, and the wavelength of the UV detector was 230 nm. and performed a calibration plot for quantification purposes within the range of experimental

concentrations used (coefficient of determination (R^2) greater than 0.99).

4.3. Results and discussion

4.3.1. Sorption of halogenated phenols, triclosan, and ibuprofen to biochar

Deprotonation of chloro-phenols and the net surface charge of sorbents can determine according to the compound's pKa, PZC of the sorbent, and solution pH. Therefore, solution pH is a critical factor in determining the sorption of ionizable compounds. In the presence of graphite, GAC, BS, FL, RS, CS, or CF biochars, solution pH at equilibrium after 24 h of shaking was 4.1, 8.9, 7.9, 10.5, 10.1, 11.0, and 10.9, respectively. The possible existence of carbonate materials (e.g., $CaCO_3$ and $MgCO_3$) or deprotonated surface functional groups (e.g., COO− or O−) of biochar may account for the alkaline pH of biomass-derived biochars [54], [219]. The abrupt increase in pH mainly occurred within 1 h, after which the pH slowly increased. Except for the graphite sample, the pH increased, and the final pH value was higher than the PZC (Table 4.2). Therefore, the net surface charge of GAC and the six biochars was dominantly negative. The degree of deprotonation may differ according to the pK_a of the compound. For example, DCP and 2CP are more deprotonated than 4CP and phenol, possibly due to the relatively lower pK_a values at alkaline pH.

Sorption of DCP, 2CP, 4CP, and phenol to reference BC materials and biochars is summarized in Figure 4.1. Comparing data sets between aqueous and sorbed concentrations at equilibrium determined maximum sorption capacity via a Langmuir sorption isotherm model. Compared to the sorption capacities of other biochars (less than 6 mg/g), BS biochar showed a higher sorption capacity for 2CP (24.6 mg/g) (Figure. 4.1a). This difference may attribute to slight differences between the final pH and PZC of biochars. In the case of the other biochars (except BS biochar), sorption to the biochar surface may be difficult due to repulsive forces between deprotonated anionic 2CP (pH: 10.1-10.9) and the negatively charged biochar surface (PZC: 8.13-8.33). However, unlike other biochars, the solution pH was only increased to 7.9

in the presence of BS biochar (PZC = 7.1 in Table 3.1), resulting in a less negatively charged surface. In addition, different from other biochars, the final pH for BS biochar (7.9) was lower than the pK_a of 2CP (8.48). Therefore, deprotonation of 2CP did not occur in the presence of BS biochar. For these reasons, the sorption of 2CP to BS biochar was higher than for other biochars. The sorption capacity of graphite (8.35 mg/g) was also higher than that of other biochars (except BS). The lack of deprotonation and a slightly positive net charge (PZC= 4.9 and pH= 4.1) may be responsible for this result. A higher surface area of BS biochar (123 m^2/g) (Table 4.2) may explain the higher sorption capacity. As a result, it cannot completely rule out possible roles of surface functional groups or impurities in BS biochar.

Similar to 2CP sorption to biochar, the sorption of 4CP to BS biochar was much higher than that of other biochars (Figure. 4.1b). The sorption capacity of BS biochar for 4CP was higher than that for 2CP (47.7 mg/g), probably due to the higher pK_a of 4CP (9.41), though higher log K_{ow} (2.39 for 4CP vs. 2.15 for 2CP) may also be responsible. Steric effects or electron density differences between 4CP and 2CP might also account for this difference [233]. DCP and phenol adsorption tendencies (pK_a = 7.90 and 9.95, respectively) were like those of 2CP and 4CP, respectively (Figure. 4.1c, d). It appears that, due to the higher hydrophobicity of DCP (log K_{ow} = 3.20), the maximum sorption capacity of BS biochar for DCP (34.4 mg/g) was higher than that for 2CP (24.6 mg/g). Similarly, the lower hydrophobicity of phenol (log K_{ow}=1.46) might result in decreased sorption to BS biochar (23.7 mg/g). Sorption to GAC showed similar behavior (Figure 4.1e). Due to the high surface area of GAC (739 m^2/g), the sorption capacity was much higher. The sorption capacity for 2CP (60.9 mg/g) was the smallest, probably deprotonated, and less hydrophobic than DCP and 4CP (Table 4.1). Interestingly, DCP showed the highest sorption capacity even though it was deprotonated (259 mg/g). Likely, both the hydrophobicity of compounds and the effect of pH (deprotonation and surface charge) affected the sorption to GAC. The sorption capacities of reference BC materials and biochar

for bromophenols (DBP, 2BP, and 4BP) and fluorophenols (DFP, 2FP, and 4FP) were obtained similarly (Figure 4.2 and 4.3). The estimated sorption capacities are summarized in Table 4.3.

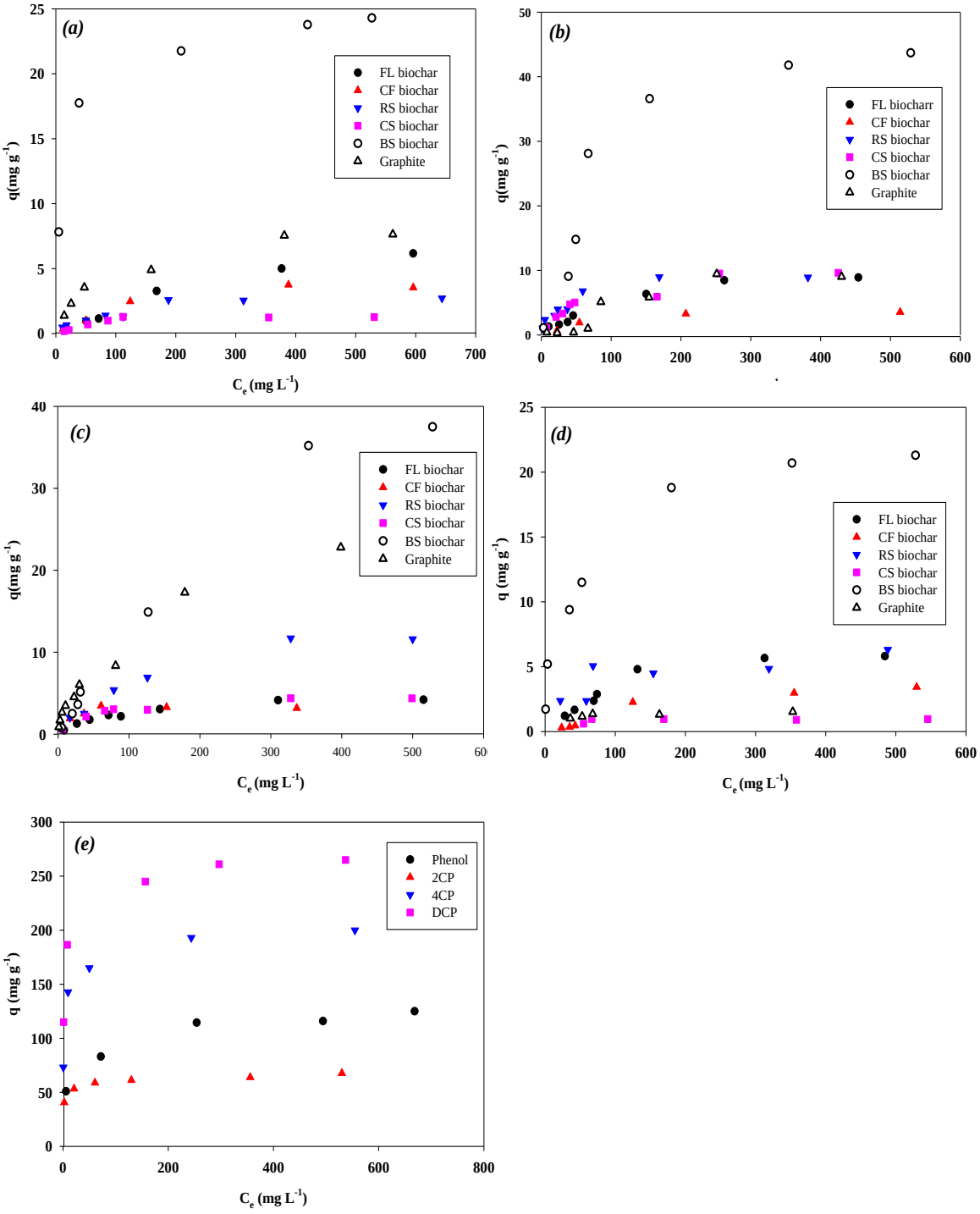

Figure 4.1. Sorption of chlorophenols and phenol to black carbon and biochar ((a):2CP; (b): 4CP; (c): DCP; (d): Phenol; (e): GAC).

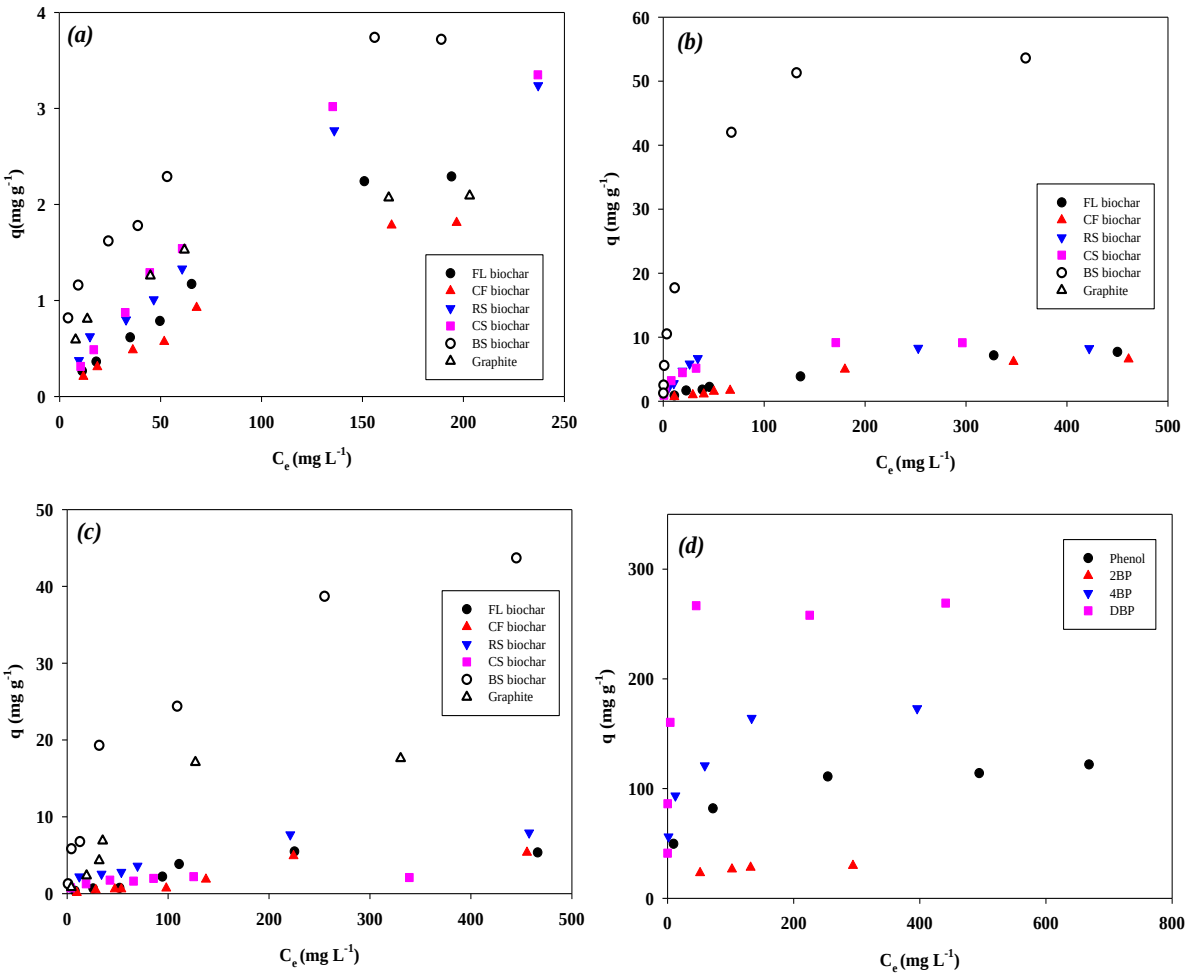

Figure 4.2. Sorption of bromophenols to black carbon and biochar ((a):2BP; (b): 4BP; (c): DBP; (d): GAC).

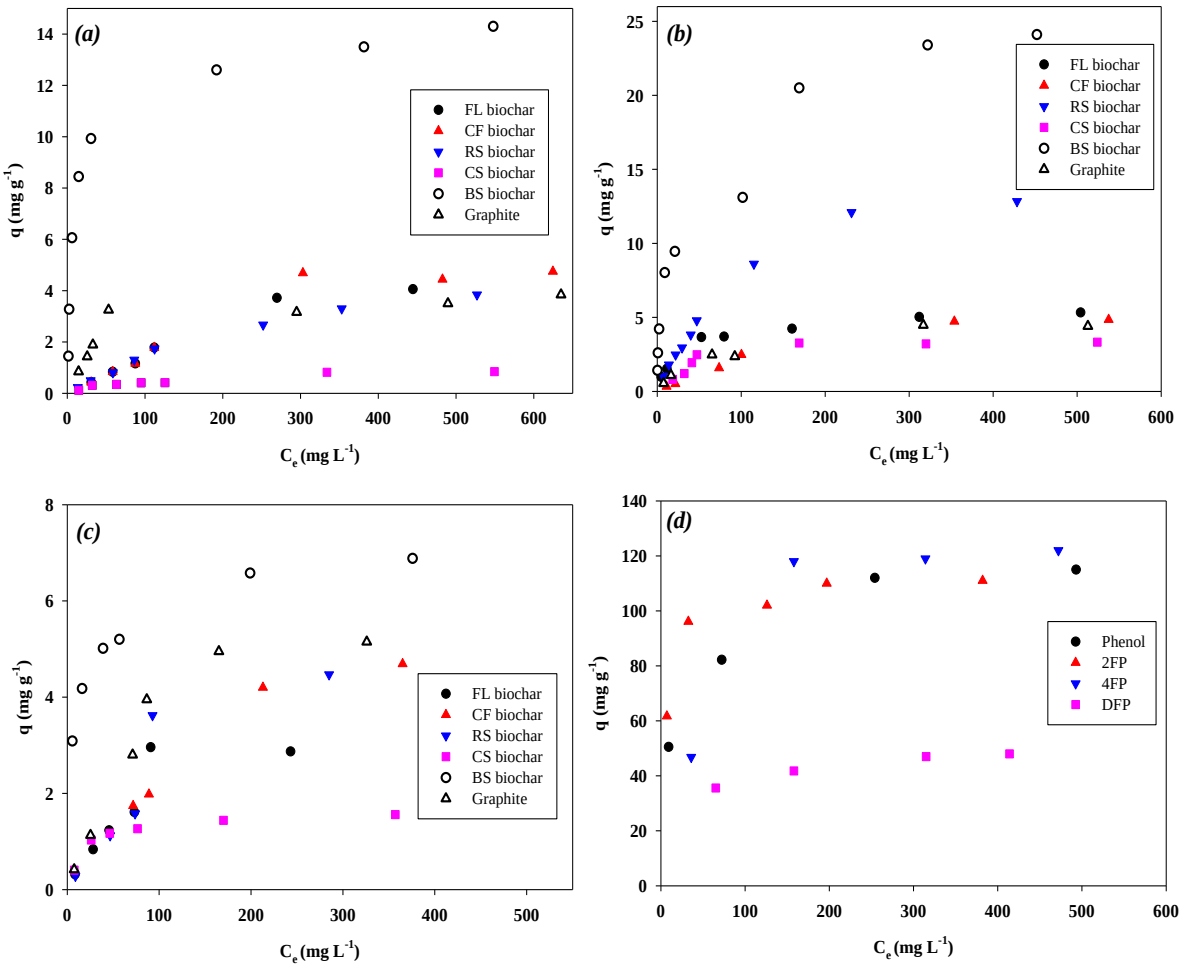

Figure 4.3. Sorption fluorophenols to black carbon and biochar ((a):2FP; (b): 4FP; (c): DFP; (d): GAC).

Table 4.3. Maximum sorption capacities (mg/g) of black carbon and biochars using the Langmuir sorption isotherm for halogenated-phenols and pharmaceuticals.

	Graphite	GAC	BS biochar	FL biochar	CF biochar	RS biochar	CS biochar
2FP	3.88	110	13.2	4.65	4.66	4.93	1.14
4FP	4.52	127	24.3	4.94	4.96	13.2	3.67
DFP	5.40	51.2	6.63	2.80	4.56	5.11	1.55
2CP	8.35	60.9	24.6	5.48	4.31	2.53	1.64
4CP	8.66	203	47.7	8.13	4.13	10.7	10.4
DCP	22.4	259	34.4	4.81	3.35	10.9	4.81
2BP	2.08	33.5	3.32	2.48	2.44	2.94	3.24
4BP	7.20	171	47.2	7.57	5.97	8.80	8.98
DBP	16.9	253	43.5	5.63	5.43	8.33	2.10
Phenol	1.49	107	23.7	6.28	12.3	5.33	1.05
Triclosan	97.8	277	209	3.03	3.73	4.20	2.58
Ibuprofen	97.8	109	10.7	0.45	0.30	0.43	0.85

Sorption of triclosan (pK_a = 8.14) showed a similar trend, controlled by the effect of pH and hydrophobicity (Figure 4.4). Due to being fully deprotonated in the presence of FL, CF, RS, or CS biochars at elevated pH (10.1–10.9), the sorption capacity for triclosan was less than 4 mg/g. on the other hand, the presence of graphite, GAC, or BS biochar (pH=4.1, 8.9, and 7.9, respectively) resulted in less deprotonation of triclosan. Furthermore, GAC and BS biochar have high surface areas. Therefore, combined with high hydrophobicity (log K_{ow}=4.76), the sorption capacity was much higher (Figure 4.4). The sorption capacity for ibuprofen (pK_a=4.91, log K_{ow}=3.97) also showed a similar trend, as shown in Figure 4.5. The estimated maximum sorption capacities are summarized in Table 4.3.

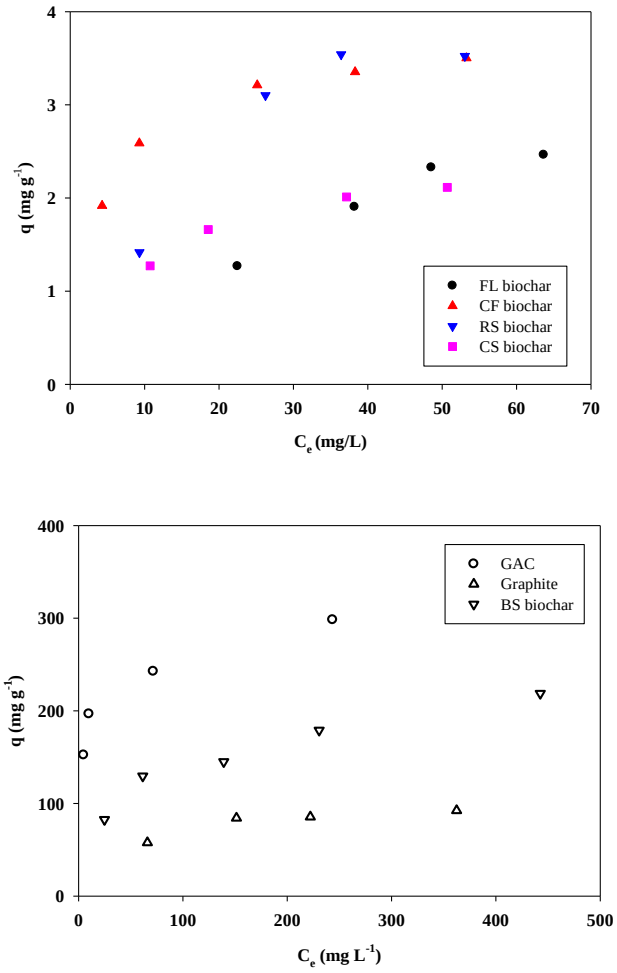

Figure 4.4. Sorption triclosan to black carbon and biochar.

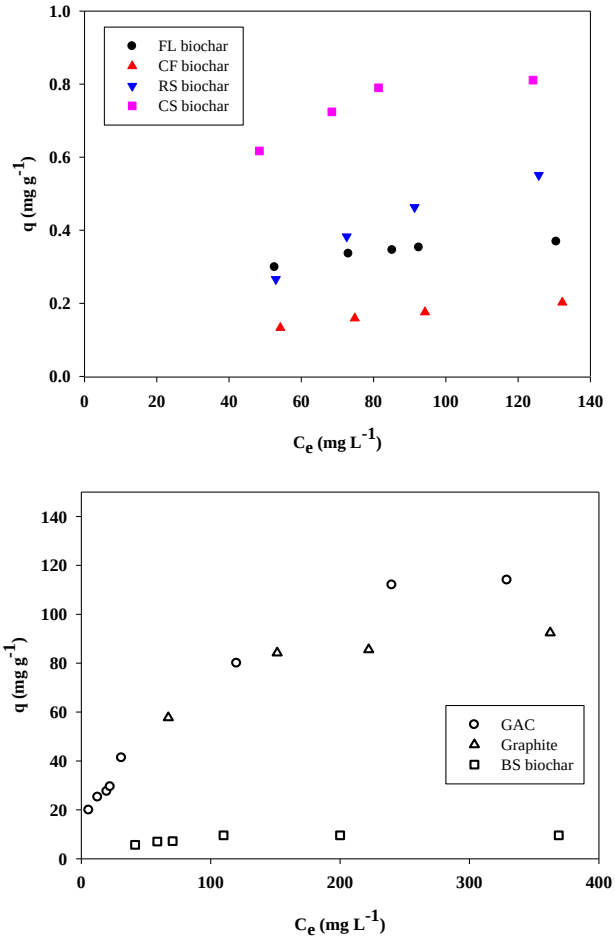

Figure 4.5. Sorption ibuprofen to black carbon and biochar.

4.3.2. Effect of pyrolysis temperature on the sorption capacity of biochar

Several studies distinguished the properties of biochar according to the pyrolysis temperature. In general, biochars synthesized at high temperatures have a higher surface area, lower hydrogen and oxygen contents, and greater aromaticity [107], [191]. Pyrolysis temperature strongly affects the sorption of metals and organic compounds to biochar [192], [226]. Ahmad et al. (2013) [244] showed that the sorption of trichloroethylene to pine needle biochar was proportional to pyrolysis temperature (300-700 ℃) due to the large surface area and low polar increased aromaticity. On the other hand, Lattao et al. (2014) [245] showed that sorption of benzene, naphthalene, and 1,4-dinitrobenzene was maximizing at 500 ℃ (among 300-700 ℃) and that it did not show any typical trends with surface area, micropore, and mesopore volumes, or H/C and O/C ratios. To investigate the effect of pyrolysis temperature on the sorption of ionizable compounds on biochar, we investigated the sorption of DCP and triclosan using RS biochar synthesized at 250-900 ℃. The properties of those biochars are summarized in Table 4.2. As shown in Figure. 4.6., the extent of sorption to biochar at lower pyrolysis temperatures (250 and 400 ℃) was much more significant than those seen with biochars produced at 550, 700, 900 °C. Likely, part of the biomass is not entirely pyrolysis, and therefore, a range of sorption domains may exist. It appears that, at lower pyrolysis temperatures (250 and 400 ℃), other factors/mechanisms may be involved. Partitioning to organic residuals remaining on biochar due to low pyrolysis temperatures could be dominant [192]. At the elevated temperatures (550-900 ℃), sorption capacity linearly increased with pyrolysis temperature, suggesting that increasing surface area and aromaticity and decreasing polarity may account for the sorption of DCP and triclosan.

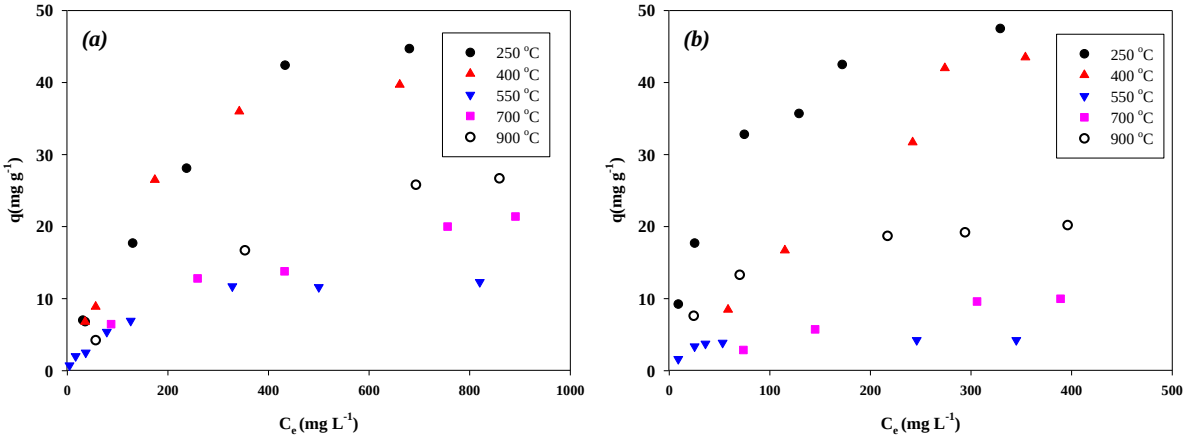

Figure 4.6. Sorption of (a) DCP and (b) triclosan to RS biochars pyrolyzed at different temperatures.

4.3.3. Effect of biochar properties on the sorption capacity biochar

To investigate the factors affecting the adsorption of ionizable compounds on biochar, we performed a correlation analysis between the properties of biochar and the maximum adsorption capacity of ionizable compounds. As shown in Table 4.4, the sorption capacities of the halogenated-phenols and pharmaceuticals had positive correlations with surface area, CEC, and carbon content and negative correlations with pH, PZC, and hydrogen, oxygen, and nitrogen contents. These results strongly support the theory that sorption of the ionizable compounds was not related to the surface functional groups. Hydrophobic sorption could account for the sorption of ionizable compounds. The negative correlations with pH indicate that the lack of deprotonation at lower pH may be favorable for the sorption of the ionizable compounds. The correlations with CEC and PZC suggest that the negative charge of the biochar surface may be favorable for the sorption of the ionizable compounds.

This finding is not consistent with the presence of a repulsive force between protonated compounds and the negatively charged surface in electrostatic sorption. It appears that the negatively charged surface may be related to electron-rich portions of the biochar. Due to the electron-withdrawing nature of halogenated functional groups, biochar may involve π-π EDA

interactions in the overall sorption of the compounds [231], [232]. Further studies are needed to clarify the involvement of π-π EDA interactions.

Table 4.4. Correlation coefficients between maximum sorption capacity and properties of black carbon and biochars.

	pH	BET S.A.	CEC	PZC	C	H	O	N
2CP	-0.41	0.97[a]	0.55	-0.29	0.12	-0.41	-0.34	-0.26
4CP	-0.34	1.00[b]	0.58	-0.20	0.16	-0.44	-0.38	-0.33
DCP	-0.39	0.99[b]	0.53	-0.24	0.30	-0.54	-0.51	-0.44
2BP	-0.33	0.99[b]	0.54	-0.18	0.28	-0.50	-0.48	-0.40
4BP	-.033	1.00[b]	0.58	-0.20	0.13	-0.41	-0.35	-0.30
DBP	-0.38	1.00[b]	0.53	-0.23	0.28	-0.52	-0.49	-0.41
2FP	-0.34	1.00[b]	0.53	-0.18	0.25	-0.47	-0.45	-0.37
4FP	-.034	1.00[b]	0.53	-0.18	0.18	-0.44	-0.40	-0.35
DFP	-0.35	1.00[b]	0.54	-0.19	0.26	-0.49	-0.46	-0.39
Phenol	-0.31	1.00[b]	0.53	-0.15	0.18	-0.39-	-0.37	-0.27
Triclosan	-0.55	0.82[b]	0.48	-0.50	0.02	-0.37	-0.26	-0.17
Ibuprofen	-0.86	0.67[b]	0.25	-0.81	0.69	-0.91	-0.87	-0.75

[a] $p < 0.1$; [b] $p < 0.05$

4.3.4. Effect of compound properties on the sorption capacity of biochar

Table 4.5 summarizes the correlation between the properties of compounds and the adsorption capacity to confirm the effect of hydrophobicity and deprotonation of chemicals. It appears that reference black carbon materials and biochars can classify into two groups. In graphite, GAC, and BS biochar (group 1), the sorption capacity was positively correlated with formula weight and log K_{ow} (negative correlation with water solubility), indicating that hydrophobic sorption is dominant. In the other biochars (group 2), pK_a showed a positive correlation with sorption capacities, indicating that the sorption is mainly driven by decreased deprotonation of compounds at elevated pH.

Table 4.5. Correlation coefficients between maximum sorption capacity and properties of halogenated phenols and pharmaceuticals.

	Formula weight	Log K_{ow}	pK_a	Solubility
Graphite	0.72[a]	0.89[c]	-0.73	-0.38
GAC	0.60[c]	0.63[a]	-0.07	-0.24
BS biochar	0.64[a]	0.66[b]	0.02	-0.16
FL biochar	-0.37	-0.43[b]	0.66[b]	0.45
CF biochar	-0.35	-0.47[c]	0.57[c]	0.80[a]
RS biochar	-0.17	-0.16	0.50[a]	0.03
CS biochar	-0.07	0.01	0.34	-0.05

[a] $p < 0.05$; [b] $p < 0.1$; [c] $p < 0.2$

4.3.5. Effects of pH, ionic strength, and humic acid on the sorption capacity of biochar

To determine the effects of pH, ionic strength, and humic acid, GAC, and RS biochar were selected to evaluate the sorption of DCP and triclosan. When pH was controlled at 7.0 using HEPES buffer (Figure 4.7), the sorption was markedly enhanced, indicating that the increase of pH was not favorable for ionizable compounds. When pH was controlled at 7.0 using HEPES buffer (Figure 4.7), the sorption was markedly enhanced, indicating that the increase of pH was not favorable for ionizable compounds. For both GAC and RS biochar, the sorption of DCP and triclosan was not significantly affected by increasing the ionic strength to 0.1 M (Figure. 4.8). Theoretically, increasing ionic strength could shrink the diffuse double layer, which can adsorb counter-charged dissolved solutes [220]. As a result, the sorption is reduced. A lack of effect by altering ionic strength indicates that the attractive interaction between the charged surface and counter-charged solute is not dominant. On the other hand, the increase of humic acid concentration to 100 mg/L resulted in decreased sorption capacity (Figure. 4.9). Pore blockage with humic acid or complexation with humic acid may hinder the sorption of DCP and triclosan to GAC and biochar [243], [329].

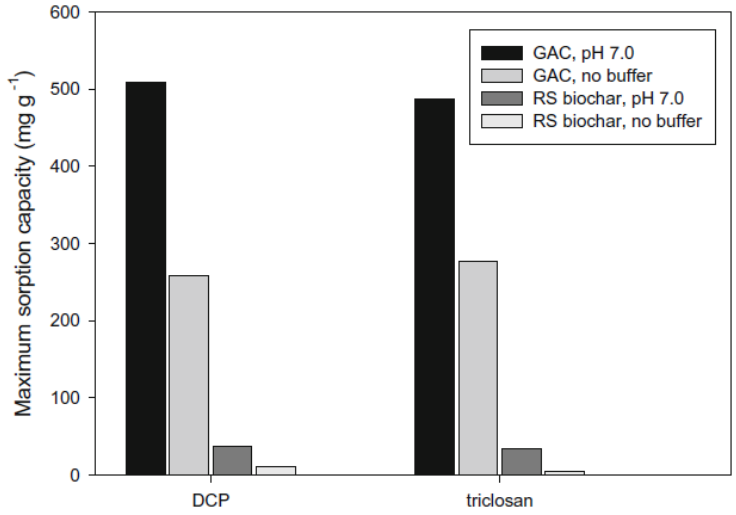

Figure 4.7. Effect of pH on the maximum sorption capacity of GAC and biochar for DCP and triclosan.

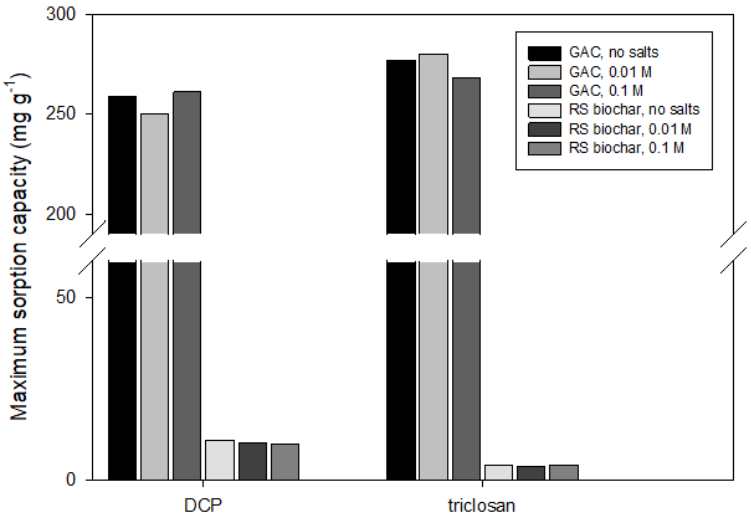

Figure 4.8. Effect of ionic strength on the maximum sorption capacity of GAC and biochar for DCP and triclosan.

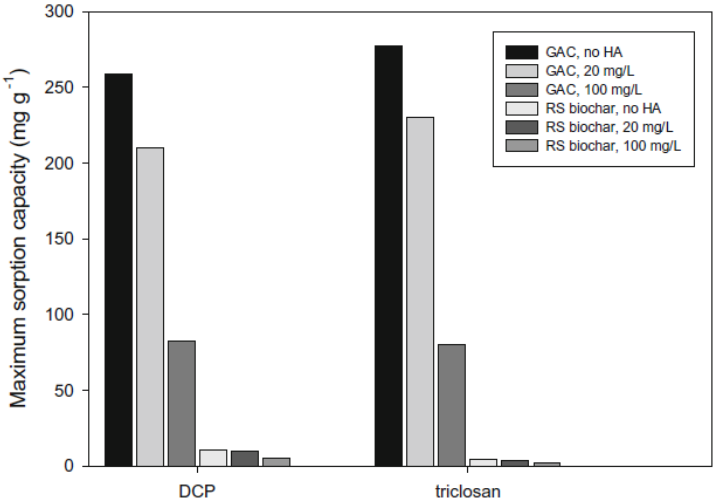

Figure 4.9. Effect of humic acid on the maximum sorption capacity of GAC and biochar for DCP and triclosan.

4.4. Conclusions

In this study, our results showed that, compared to other biochars, BS biochar can effectively remove halogenated phenols, triclosan, and ibuprofen from solution due to its high surface area. The sorption of these compounds to biochar is dependent on the hydrophobicity of the compound, the surface area of biochar, and solution pH. Electrostatic interactions (mostly repulsion) and hydrophobic sorption are the main mechanisms to explain the sorption of the compounds to biochar. The sorption was not affected by ionic strength but was influenced by dissolved humic acid. These results suggest that specific conditions may be required to remove ionizable organic compounds from water and soil using biochar. Involvement of other possible mechanisms, such as π-π EDA interactions and hydrogen bonding, remain to be determined.

Finally, it should be noted that BS biochar may have a potential to include other contaminants (e.g., toxic metals), which can be released when the biochar is applied as a sorbent. Therefore, cautious application should be needed to avoid possible contamination of water and soil.

Chapter 5. Redox and catalytic properties of biochar-coated zero-valent iron for the removal of nitro explosives and halogenated-phenols

5.1. Introduction

Pyrolysis is a thermochemical decomposition of organic materials at elevated temperatures in the absence of oxygen. Biochar, a carbon by-product derived from biomass pyrolysis, has been intensively investigated for carbon sequestration due to its immediate impact on reducing CO_2 released into the atmospheric environment [18]. In addition to the disposal of biomass wastes and increasing crop productivity, biochar has also been investigated as a sorbent and an electron transfer mediator for environmental applications, such as water treatment, soil remediation, stormwater management, mine reclamation [123], [219], [246]-[248]. The properties of biochar, which are affected by the type of biomass and the pyrolysis conditions, significantly changed the effectiveness and performance of biochar in various applications. Therefore, improvement and consistent maintenance of biochar quality were critical for its efficient usage in the environmental engineering field.

For redox-sensitive contaminants, in situ or ex situ chemical reduction is one of the best treatment options in natural environments [249]. As a result, biological or abiotic degradability is generally improving, and the toxicity of pollutants is reducing through reductive transformation. Among the various reducing agents, zero-valent iron [Fe(0)] and iron oxide (combined with ferrous iron) have been extensively investigated for contaminant treatment due to their strong redox potential and catalytic effect [250], [251].

Several attempts have been made to develop upgraded biochar materials in combination with iron-bearing materials, such as biochar-nano Fe(0) composites and biochar–iron oxide composites [252]-[260]. Combined with Fe(0), biochar can provide additional benefits, such as simultaneous or stepwise sorption, reducing redox-sensitive contaminants, and preventing

the coagulation of nanoparticles. However, the synthesis of iron–biochar composites can be costly due to the different chemical reactions (e.g., reduction with $NaBH_4$ or thermochemical reduction) after pyrolysis of biochar [255], [257], [258], [260]. In addition, biochar was primarily used as an embedded matrix to hold well-spread nano-Fe(0) to maximize the reaction rate [252]-[254], [257].

Our research group also examined the improvement of biochar quality via simple and cost-effective co-pyrolysis of biomass and zero-valent iron [Fe(0)]. By changing the amount of rice straw and Fe(0), Fe(0)-biochar was synthesized via co-pyrolysis [261]. We characterized the synthesized Fe(0)-biochar (hereafter referred to as Fe(0)–biochar) and determined the optimal Fe(0)-to-biochar ratio to maximize the removal of DNT and DCP, both of which are priority pollutants according to the U.S. EPA. The synthesized Fe(0)-biochar rapidly removed DNT and DCP from the solution. Molecules adsorbed on the surface of Fe(O)-coated biochar were further reduced to reduction products. Biochar significantly enhanced reduction due to the catalytic role of Fe(0) in Fe(0)-biochar supported by the distribution and yield of reducing intermediates. Until now, limited studies on synthesized Fe(0)-biochar have been conducted to examine its application for treating other contaminants. It is necessary to examine how effectively we can remove other contaminants with Fe(0)-biochar. The mechanism of biochar catalytic role in Fe(0)-biochar is still under investigation. In the present study, different nitro explosives and halogenated-phenols were selected as redox-sensitive compounds, and their transformation with Fe(0)–biochar was investigated.

Fe(0)-biochar can effectively treat nitro explosives and halogenated phenols, and Fe(0) in Fe(0)-biochar and biochar act as reducing agents and adsorbents/catalysts, enabling reductive transformation. Batch experiments conducting to determine the extent of enhancement in reducing the nitro explosives and halogenated phenols in the presence of Fe(0)-biochar. TNT, RDX, DBP, and DFP were chosen as nitro explosives and halogenated-phenols due to their

toxicity, detrimental effects on human and living creatures, and similarity to previously studied compounds (DNT and DCP). We conducted cyclic voltammetry (CV), XPS, and X-ray absorption near edge structure (XANES) analyses to characterize the redox properties of Fe(0)–biochar. Possible mechanisms for the biochar-mediated reduction in the Fe(0)-biochar system were examined via surface blocking experiments.

5.2. Materials and methods

5.2.1. Chemicals

TNT and RDX obtain from Hanwha Corp. (Seoul, South Korea). 2,4-Dibromophenol (95%, DBP), 2-Bromophenol (98%, 2BP), 4-Bromophenol (99%, 4BP), 2,4-Difluorophenol (99%, DFP), 2-Fluorophenol (98%, 2FP), 4-Fluorophenol (99%, 4FP), and Phenol (98%) were purchased from Aldrich (Milwaukee, WI, USA). Formaldehyde (HCHO, >99.8%) and HEPES (N-[2-hydroxyethyl] piperazine-N0-[ethanesulfonic acid]) were obtained from Sigma (St. Louis, MO, USA). Acetonitrile and methanol (each HPLC grade) purchasing from SK Chemicals (Ulsan, South Korea). All the solutions prepared with deionized water—all the chemicals used as received without further treatment. Zero-valent iron [Fe(0)] (<212 mm, Fe 99%) obtained from Acros Organics (Geel, Belgium). BET surface area measured by N_2 adsorption and carbon content of the Fe(0)-biochar was 13.1 m^2/g and 0.24%, respectively.

Fe(0)-biochar was synthesized via co-pyrolysis of rice straw and Fe(0) (95: 5 v/v) at 550 ℃ for four h using a tube-type electrical furnace under N_2. Fe(0)–biochars catalytic properties were well developing at 550 ℃, and further increase of the pyrolysis temperature did not show a significant difference. Scanning electron microscopy (SEM) observations confirmed that Fe(0) particles were entirely covered with biochar, which was pyrolysis from an excessive amount of rice straw. The particle size of the synthesized Fe(0)-biochar ranged from 100~200 mm. The synthesized Fe(0)-biochar was stored in a sealed glass bottle before batch experiments.

The pH, BET surface area, measured by N_2 adsorption, CEC, PZC, and carbon content of Fe(0)-biochar was 10.8, 12.9 m^2/g, 51.7 meq/100 g, 10.0, and 15.6%, respectively.

5.2.2. Spectroscopic analysis

CV, XPS, and XANES analyses were conducted to determine the redox properties of Fe(0)–biochar. XPS analysis was conducted using a K-alpha system (Thermo Scientific, Pittsburgh, USA). The obtained spectra for Fe2p, C1s, and O1s were compared with standard spectra provided by the manufacturer and previously reported spectra (http://xpssimplified.com), and the existence of each elemental form was predicted. The atomic ratio of Fe^{2+}-to-Fe^{3+} was determined via curve fittings with standard Fe2p spectra [262]. X-ray absorption spectra for XANES analysis were determined at the Fe K-edge in transmission mode using a Si (1 1 1) double-crystal monochromator at the beamline 10C at the Pohang Accelerator Laboratory, South Korea. The pure Fe_2O_3, Fe_3O_4, and FeO spectra were used as the reference spectra for Fe^{3+}, $Fe^{2.65+}$, and Fe^{2+}. Pure Fe foil was used as a reference for Fe(0).

5.2.3. Batch experiments

The procedure for the batch experiments has been described in detail elsewhere [261]. In brief, 40 mL amber vials filled with 4 g of the Fe(0)-biochar and 20 mL of deoxygenated solution were shaken sideways at 180 rpm using a rotating shaker. An excessive Fe(0)-biochar was added to the batch system to determine the pseudo-first-order rates. Because the reduction of organic contaminants with Fe(0) was affected by pH [263], the solution pH was maintained at 7.4 with 0.1 M HEPES buffer to minimize the effect of pH at relatively neutral pH. The initial concentration of nitro explosives and halogenated phenols was between 40.4 and 52.4 mg/L. Triplicate vials were sacrificed at each sampling time and filtered through a 0.22 mm cellulose membrane filter (Millipore, MA, USA) for chemical analysis. Reduction control

experiments were also conducted with only Fe(0) under identical conditions. We conducted control sorption experiments; adsorption fractions for nitro explosives and halogenated phenols were 40-55%. Chemical control experiments without Fe(0)-biochar showed that the chemical loss during sampling and analysis was less than 5% of the initial concentration. To determine the effects of surface functional groups as electron transfer mediators to enhance the electron transfer from iron corrosion to sorbed molecules, we blocked the surface functional groups following the modified methods suggested by Gardea-Torresdey et al. (1990) [216]. Chen and Yang (2006) [217] Procedures for blocking the surface functional groups have been described elsewhere [230]. Fe(0) surface functional groups–biochar pyrolyzed at 250 ℃ were sequentially blocked with methanol and formaldehyde. The surface functional group-blocked Fe(0)-biochar was used for DBP sorption under identical conditions.

In order to determine the possible role of surface functional groups in biochar, the reduction of DNT and DBP with pre-reduced biochar was investigated. RS-derived biochar (2 g) pyrolyzed at 550 ℃ in a 50 mL deoxygenated solution was pre-reduced to Fe(0) (5 g) at pH 7.4 (0.1M HEPES) in an anaerobic glove box (Jisico, Seoul, South Korea). The mixture of biochar and Fe(0) in HEPS solution was mixed sideways at 180 rpm for 1 h. After Fe(0) was completely removed using a magnetic retriever more than 5 times, 50 mL of deoxygenated DNT/DBP solution was added. At pre-determined sampling times, 1 mL of aliquot was collected, filtered, and analyzed for DNT/DBP and their reduction products using HPLC.

5.2.4. Chemical's analysis

The concentrations of TNT, RDX, DBP, and DFP, and their reduction products were determined using a Dionex Ultimate®-3000 high-performance liquid chromatography system (HPLC, Sunnyvale, CA, USA) equipped with a Dionex Acclaim® 120 guard column (4.3×10 mm) and an Acclaim® 120 C-18 column (4.6×250 mm, 5 mm). The analytical methods and

conditions for quantifying TNT, RDX, and halogenated phenols have been described elsewhere [219], [263]. Formaldehyde was determined using the Dionex HPLC system through derivatization with Nash's reagent (0.02 M of 2,4-pentanedione and 2 M of ammonium acetate, pH 6) [264]. 2,4,6-Triaminotoluene (TAT) was analyzed using a Dionex HPLC with an Alltima C18 column (250 x 4.6 mm, 5 mm, Grace, Columbia, MD, USA) and an Alltima guard column (7.5 x 4.6 mm, Grace). The analytical methods and conditions for TAT and formaldehyde have been described elsewhere [251], [265]. 2,4,6-Triaminotoluene (TAT) was analyzed using a Dionex HPLC with an Alltima C18 column (250×4.6 mm, 5 mm, Grace, Columbia, MD, USA) and an Alltima guard column (7.5×4.6 mm, Grace). The analytical methods and conditions for TAT and formaldehyde have been described elsewhere [251], [265]. Bromide (Br^{-1}) and fluoride (F^{-1}) were analyzed using Dionex ICS-100 ion chromatography. A mixture of Na_2CO_3 (4.8 mM) and $NaHCO_3$ (1.0 mM) was used as the eluent. The injection volume and flow rates were 10 mL and 1.5 mL/min, respectively. The suppressor current was set to 40 mA. Analytical duplicates, standards, and blank samples were used for quality control of the obtained data to guarantee precision and accuracy.

5.3. Results and discussion

5.3.1. Degradation of nitro explosives and halogenated-phenols with Fe(0)-biochar

The removal of TNT and RDX with Fe(0)-biochar is summarized in Figure 5.1. Direct reduction of TNT with Fe(0) showed only 34% of removal after 12 h. The removal of TNT with Fe(0) was somewhat slower than that with other types of Fe(0) detailed in a previous report [265], indicating that different types of Fe(0) could significantly affect removal kinetics. Due to the slow removal rate, the concentration of TAT, which was a final reduction product, was less than 1% of the initial molar concentration of TNT. In the presence of Fe(0)–biochar, the removal of TNT was markedly improved. More than 90% of TNT was removed in 5 h.

Compared to direct reduction with Fe(0) (0.044 ± 0.009 h^{-1}, $R^2 = 0.905$), the removal rate with Fe(0)-biochar was approximately 40 times faster (1.607 ± 0.292 h^{-1}, $R^2 = 0.985$). The coated biochar played the role of a sorbent to remove TNT rapidly. On the other hand, to direct reduction control with Fe(0), the TAT was gradually formed, and 18% of the initial TNT was transformed into TAT in 12 h (Figure 5.1a). Like TNT, RDX removal was also enhanced in the presence of Fe(0)-biochar (Figure. 5.1b). Fe(0)-biochar also rapidly removed RDX in solution, with 69% removal of the initial RDX in 12 h. Formaldehyde, one of the reduction products [265], was steadily produced, and the mass recovery for formaldehyde in 12 h was 19% (Figure. 5.1b). Under identical conditions, Fe(0) only showed 31% removal in 12 h. These results indicated that the removal of TNT and RDX with Fe(0)-biochar was enhanced due to the coated biochar. The sorbed molecules on the outside of the biochar were further transformed into reduction products. The mechanisms for electron transfer between the sorbed molecules and Fe(0) in the Fe(0)-biochar will be discussed later.

The removal of DBP and DFP with Fe(0)-biochar was also enhanced. Direct reduction with Fe(0) was slow, and only 36% and 38% of the initial DBP and DFP were removed in 24 h. Reduction products were not produced within 24 h (Figure 5.2). Previous studies [266]-[269] suggest dehalogenation of brominated compounds and halogenated phenols with microscale Fe(0) was extremely slow. Thus, it appears that the removal of DBP and DFP may be primarily due to sorption to the iron surface. Compared to direct reduction with Fe(0), the removal of DBP and DFP was significantly enhanced, showing 68% and 72% removal in 24 h, respectively. On the other hand, to the reduction control with Fe(0), phenol, a final reduction product, was produced for DBP and DFP systems. In 24 h, phenol was responsible for 29% and 4.1% of the initial DBP and DFP molar concentrations, respectively. These results strongly supported the indication that the presence of biochar in the Fe(0)-biochar could also markedly enhance the reductive transformation of DBP and DFP. It is likely that the dehalogenation of DBP with

Fe(0)-biochar was more favorable than that of DFP. As reduction intermediates, small amounts of 2BP and 2FP were identified, indicating that dehalogenation by electrons in a para position was predominant. The preference of electron transfer in the para position was probably due to the steric effect from the electron density in a phenol structure [261], consistent with results in a previous study [270]. As dehalogenation proceeded, bromide (Br^{-1}) and fluoride (F^{-1}) were formed as products in the DBP and DFP systems. Considering the amount of Br^{-1} and F^{-1} released from biochar under identical conditions (3.36 and 6.33 mg/L, respectively, from 0.624 g of biochar based on 15.6 C% in Fe(0)–biochar), the formation of Br^{-1} and F^{-1} was determined. As shown in Figure 5.2, compared to the initial Br and F concentrations in DBP and DFP (0.211 and 0.408 mM, respectively), 28.4% of Br and 37.6% of F were recovered as the released anions. The difference between removing and forming products in DBP and DFP systems may be due to the possible retention (physical or chemical sorption) of the anions on Fe(0)–biochar. Further studies may be needed to establish mass balance in the Fe(0)-biochar system. Like nitro explosives (Figure 5.1), after some hours, the removal of halogenated phenols was slow (Figure 5.2). It appears that the removal of contaminants with Fe(0)-biochar has two stages, rapid sorption to outside biochar and relatively slow reductive transformation of sorbed molecules to daughter products. In summary, our results showed that Fe(0)-biochar could effectively remove nitro explosives and halogenated-phenols and further transform them into reduction daughter products, which may have less toxicity and better degradability in subsequent biotic and abiotic transformations.

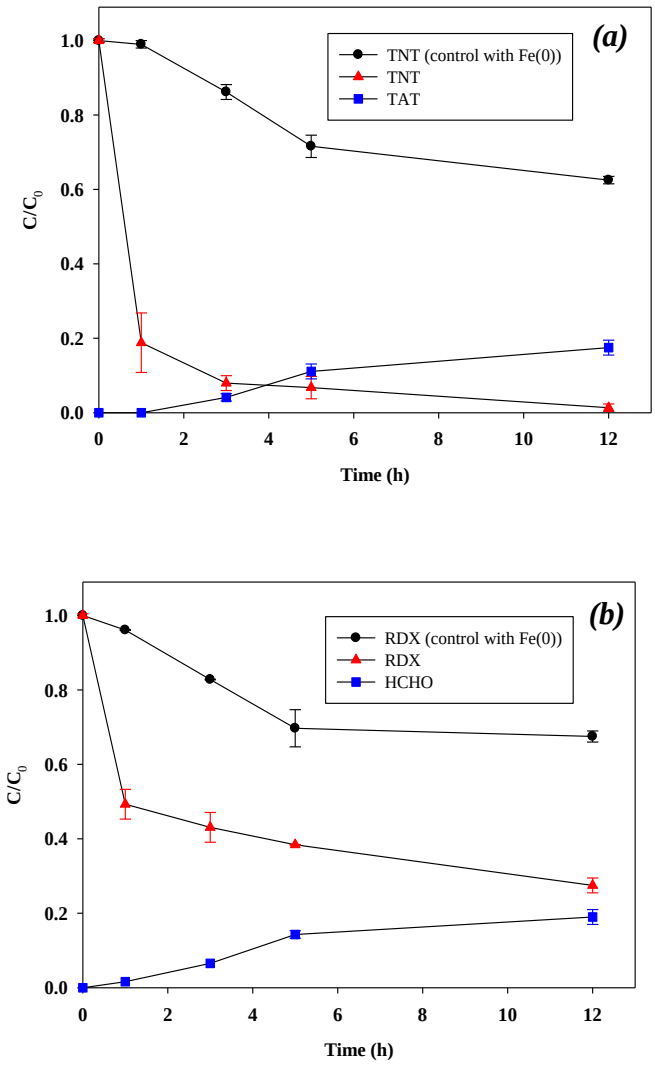

Figure 5.1. Removal of (a) TNT and (b) RDX with Fe(0)-biochar pyrolyzed at 550 °C (unit: relative C concentration). Data points are average values, and the error bars represent one standard deviation.

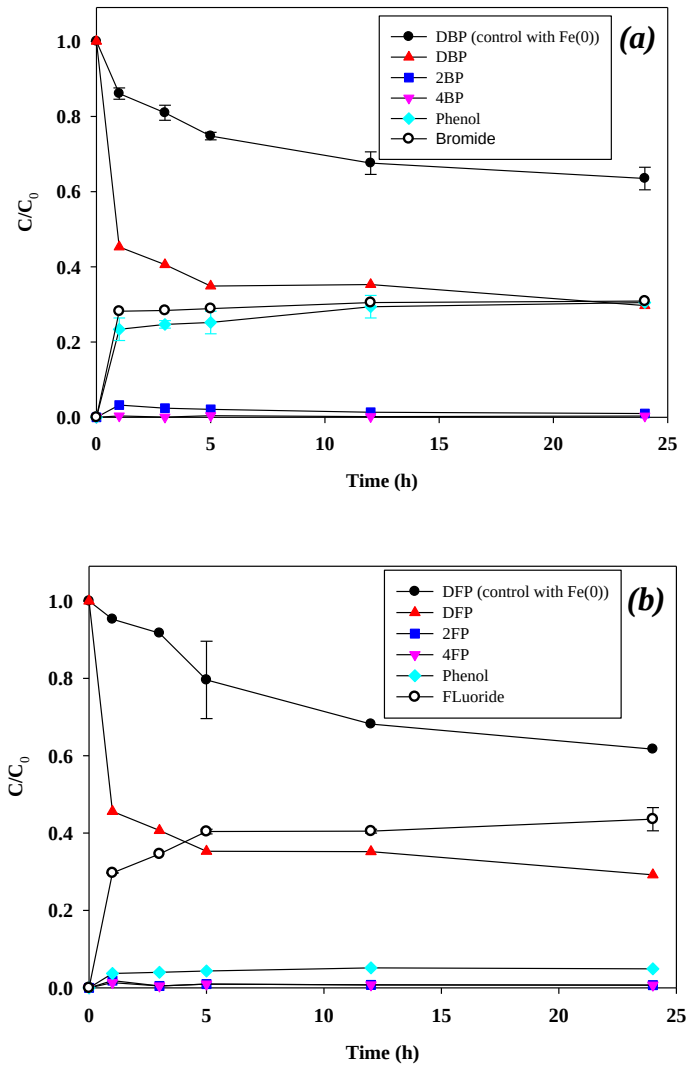

Figure 5.2. Removal of (a) DBP and (b) DFP with Fe(0)-biochar pyrolyzed at 550 °C (unit: relative C concentration). Data points are average values, and the error bars represent one standard deviation.

5.3.2. Redox properties of Fe(0)-biochar

After co-pyrolysis with an excessive amount of rice straw and Fe(0), we obtained Fe(0)-biochar, which could be used as a sorbent and reductant. Even though we showed nitro explosive and halogenated phenol removal promotion (Figure. 5.1 and 5.2), electron transfer mechanisms from iron corrosion to sorbed molecules were not examined in detail. The electron-donating properties of Fe(0)-biochar were investigated through cyclic voltammetry (CV) analysis. In our previous report [261], cyclic voltammograms of Fe(0) and Fe(0)-biochar were similar, which strongly suggested that the remaining redox potential originated from the Fe(0) in the Fe(0)-biochar. As we changed the scan rate from 10 mV/s to 1 mV/s, the Fe oxidation peaks and reduction peaks at ~ -0.83 V (Fe/Fe^{2+}), ~ -0.62 V (Fe^{2+} / Fe^{3+}), and ~ -0.98 V (Fe^{3+} / Fe^{2+}), respectively, were more clearly observed (Figure. 5.3). In batch experiments, the solution pH slightly increased even when the pH was controlled at 7.4 with 0.1 M HEPES, indicating that Fe(0) corrosion occurred although the outside of the Fe(0) was fully covered with biochar. It appears that wetting and saturation of the coated biochar with water molecules was followed by Fe(0) corrosion in the Fe(0)–biochar. In batch experiments, the solution pH slightly increased even when the pH was controlled at 7.4 with 0.1 M HEPES, indicating that Fe(0) corrosion occurred although the outside of the Fe(0) was entirely covered with biochar. It appears that wetting and saturation of the coated biochar with water molecules was followed by Fe(0) corrosion in the Fe(0)-biochar.

XANES analysis was conducted to determine the state of iron in Fe(0)-biochar. As shown in Figure 5.4., regardless of the dosage of Fe(0) and rice straw, the spectra of Fe(0)-biochar did not vary significantly, and they were similar to those of Fe(0). This similarity indicated that thermochemical reactions during pyrolysis under N_2 did not change the state of iron. Compared to the spectra of pure Fe foil, the spectra of Fe(0) and Fe(0)-biochar showed a similar pattern but somewhat higher absorbance at the pre-edge part (7110~7120 eV). This difference was

probably due to changes in the ligand at the Fe(0) surface or the coordination number of Fe(0) [271]. Compared to the spectra of reference FeO (Fe^{2+}), Fe_2O_3 (Fe^{3+}), and Fe_3O_4 ($Fe^{2.65+}$), the 8 spectra of Fe(0) and Fe(0)-biochar were different, suggesting that the number of valence electrons in Fe seemed to be mixed and affected by other factors. Overall, the spectra of Fe(0) and Fe(0)-biochar showed a similar pattern to those of pure Fe, and the little bit of drift from pure Fe was due to exposure to different outside conditions.

XPS analysis was also conducted to examine the oxidation state of C and Fe in Fe(0)-biochar (Figure 5.5). As the dosage of rice straw was increased, C–C (284.4 eV), C–O (286.5 eV), C=O (289.5 eV), and COO (289.1 eV) peaks in the C1s spectra increased. As the carbon amount was increased to between 292 and 294 eV, higher binding energy was observed, indicating that a π–π satellite structure was developed due to delocalized electrons (e.g., aromatic rings) (Figure. 5.5a). Similarly, as the Fe(0) dosage was increased, the Fe_2O_3 (710.8 eV $Fe2p_{3/2}$, and ~724 eV $Fe2p_{1/2}$) and FeO (709.6 eV Fe $2p_{3/2}$) peaks in the Fe 2p spectra increased (Figure. 5.5b). To clarify the state of Fe, the spectra of Fe(0) and Fe(0)-biochar was fitted following the method suggested by Yamashita and Hayes (2008) [262] (Figure 5.6). Compared the $Fe2p_{1/2}$ and $Fe2p_{3/2}$ peak positions of reference Fe^{2+} from Fe_2SiO_4, and Fe^{3+} from Fe_2O_3 and Fe_3O_4, the peak positions of Fe(0) and Fe(0)-biochar were the closest to that of Fe_3O_4 (Table 5.1), indicating that the outside of Fe(0) in Fe(0)-biochar was Fe_3O_4, which is known for its electron-conducting capability [272]. Thus, electrons produced from iron corrosion could be transported to the outside through coated Fe_3O_4. The spectra of O1s showed that metal oxides (e.g., Fe-oxides, 529–530 eV) existed in Fe(0). As the carbon content was increased in Fe(0)-biochar, the peak was shifted to organic C–O and C=O (531.5 ~ 532 eV, 533 eV) (Figure. 5.5c), consistent with C1s and Fe2p spectra. In summary, XANES and XPS analyses showed that Fe(0) in the Fe(0)-biochar was intact and had a similar redox potential after pyrolysis and that the outside of Fe(0) beneath biochar was mostly coated with Fe_3O_4. According to the

elemental contents in the synthesized biochar, the oxidation state of carbon (Co_x) was also calculated using the following equation [273]: $Co_x = (2[O] - [H] + 3[N])/[C]$, where [ ] is the molar concentration of each element. The Cox of the rice straw (-0.1135) further decreased to -0.1649 and -0.2815 for biochar and Fe(0)–biochar, respectively, suggesting that carbon existed in a more reduced state after pyrolysis.

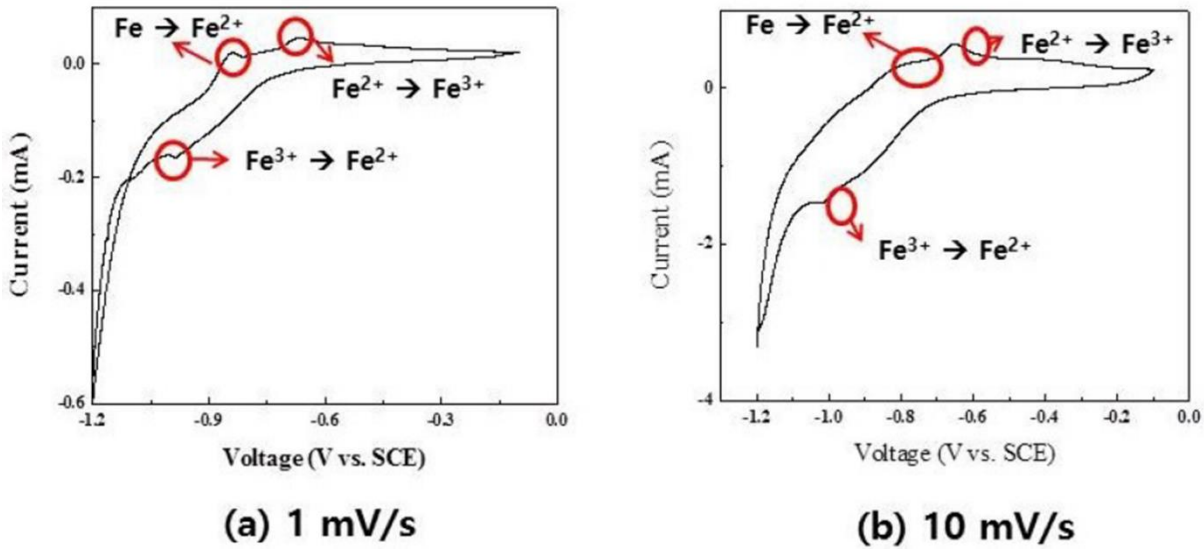

Figure 5.3. Cyclic voltammograms of Fe(0)-included biochar at different scan rates ((a) 1 mV/s and (b) 10 mV/s). Electrochemical measurements were carried out using an IVAMSTAT instrument with a three-electrode configuration. The working electrodes were prepared using 7:3 of active material and polytetrafluoroethylene (PTFE). The electrodes were formed and attached to a nickel mesh. In the three-electrode configuration, Fe(0)-included biochar (5 v% Fe) was used as the working electrode, saturated calomel electrode (SCE) was used as the reference electrode, and platinum wire was employed as the counter electrode. 6.0 M KOH served as the electrolyte. The electrodes were determined at a potential range of -1.2 to -0.1 V.

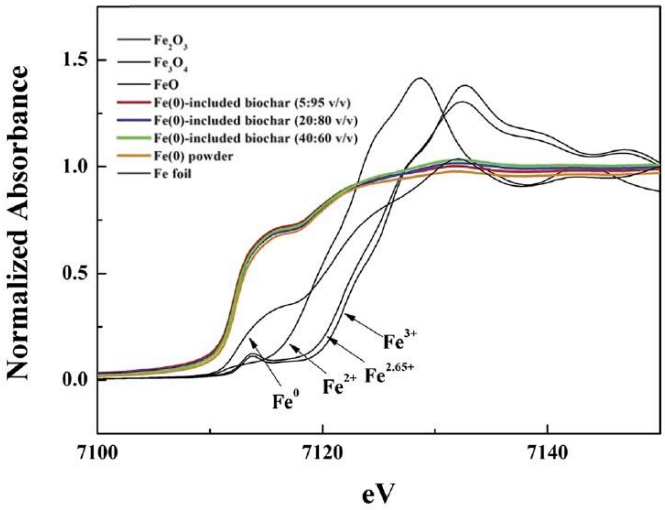

Figure 5.4. XANES spectra of Fe(0), Fe(0)–biochar, and Fe-bearing reference materials.

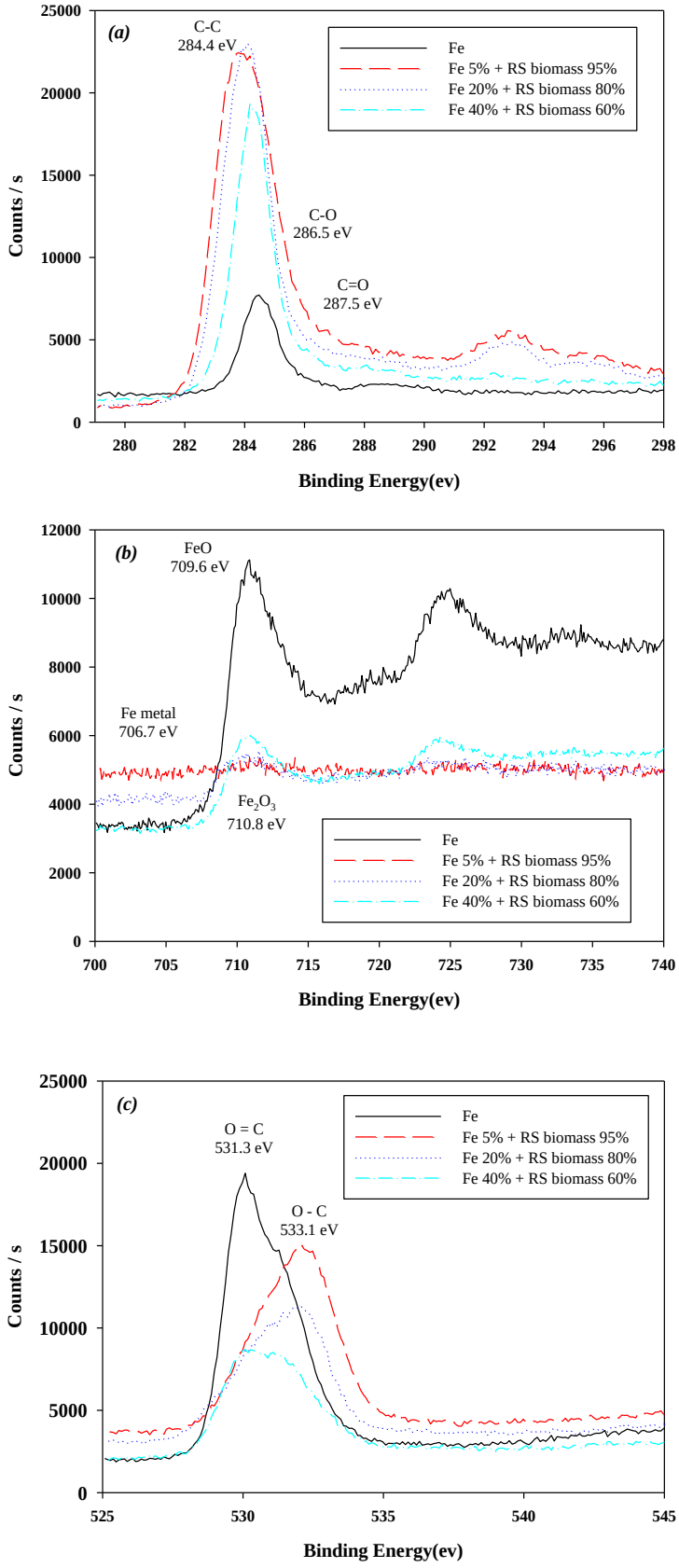

Figure 5.5. XPS spectra [(a) C1s, (b) Fe2p, and (c) O1s] of Fe(0) and Fe(0)–biochar pyrolyzed at 550 °C.

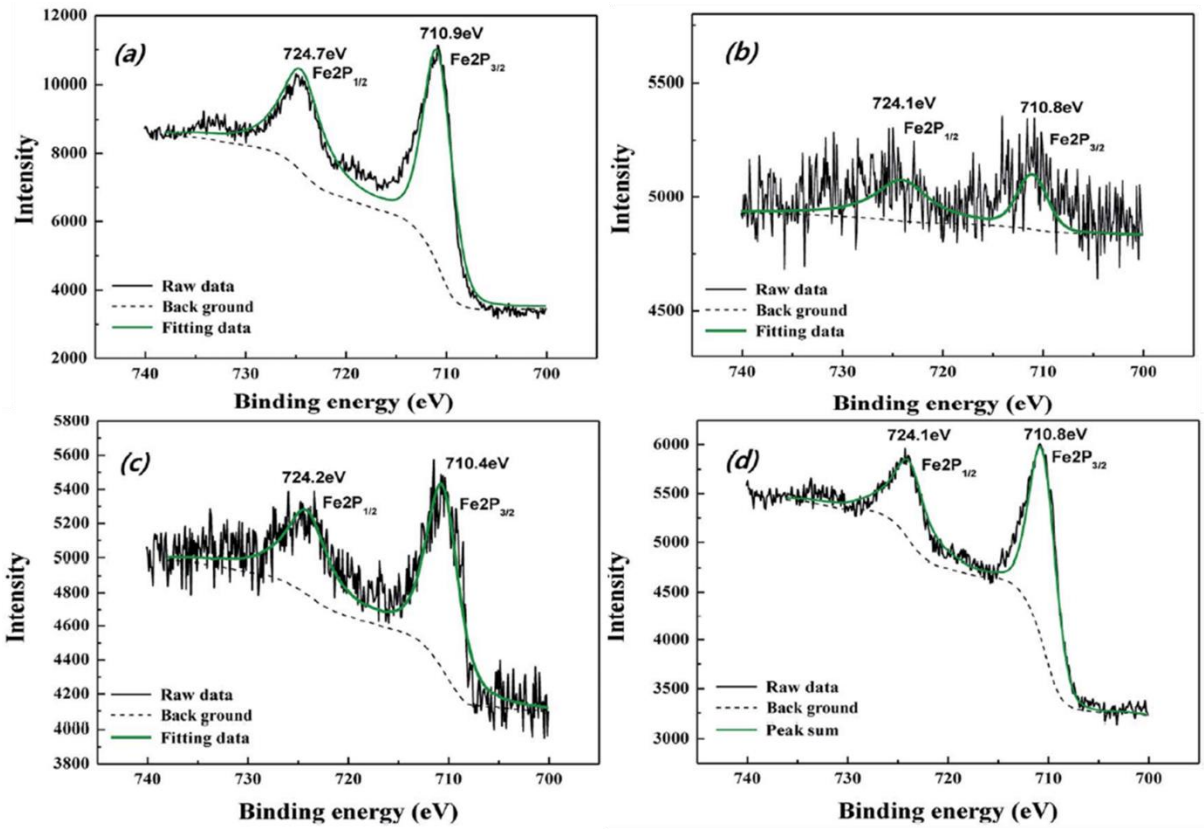

Figure 5.6. Results of curve fitting for the Fe2p XPS spectra of Fe(0) and Fe(0)–biochar to analyze Fe^{2+} and Fe^{3+}. [(a) Fe(0), (b) Fe(0)–biochar (Fe(0) 5 v%), (c) Fe(0)–biochar (Fe(0) 20 v%), and Fe(0)–biochar (Fe(0) 40 v%)].

Table 5.1. Peak positions and FWHM of the XPS Fe2p peak for Fe(0) and Fe(0)–biochar.

	$Fe2p_{1/2}$		$Fe2p_{3/2}$		x^2
	Peak position	FWHM[a]	Peak position	FWHM	
Fe(0)	724.2 eV	5.00	710.9 eV	3.40	7.32
Fe(0)-biochar (Fe(0) 5 v%)	724.1 eV	6.60	710.8 eV	3.50	2.75
Fe(0)-biochar (Fe(0) 20 v%)	724.2 eV	5.01	710.4 eV	.3.87	2.88
Fe(0)-biochar (Fe(0) 40 v%)	724.1 eV	3.87	710.8 eV	3.10	1.71
Fe^{3+} obtained from Fe_2O_3[b]	724.6 eV	-	711.0 eV	-	-
Fe^{2+} obtained from Fe_2SiO_4[b]	722.6 eV	-	709.0 eV	-	-
Fe_3O_4[b, c]	724.07 eV	-	710.6 eV	-	-

[a.] Full width at half maximum for the specific peaks.
[b.] [262]
[c.] Atomic ratio of Fe^{2+}-to-Fe^{3+} = 0.35 : 0.65.

5.3.3. Catalytic properties of Fe(0)-biochar

Based on the redox properties of Fe(0)–biochar, the reductive transformation of sorbed molecules can be explained by stepwise electron transfer from iron corrosion via Fe_3O_4 and biochar. Electron transfer through biochar has been interpreted as either electron conductivity or surface functional groups (e.g., quinone) [219], [274]-[276]. The linear correlation between the electrical conductivity of biochar and the pseudo-first-order rate of contaminant degradation with biochar strongly supported the catalytic role of biochar in electron transfer [219], [276]. It has been previously reported that Fe(0)–biochar pyrolyzed at 900 ℃could reduce sorbed molecules onto the outside biochar surface [261]. This result indicated that electron conductance through biochar was due to the primarily graphitic structure because no surface functional groups were observed on the surface of the outside biochar. However, the possibility of surface functional groups in biochar could not be completely ruled out because both the electrical conductivity from the graphene region and the surface functional groups co-existed in biochar pyrolyzed at 550 ℃. Fe(0)–biochar was pyrolyzed at 250 ℃ to determine the role of the surface functional groups of biochar, where surface functional groups were dominant and graphitic regions were not significantly developed, and the removal of DNT and DBP was examined.

The effect of the surface functional group on electron transport was confirmed by blocking the surface functional group under the same conditions. As shown in Figure. 5.7, Fe(0)–biochar pyrolyzed at 250 ℃ could remove DNT and DBP and reduce them further into the reduction products, DAT and phenol, respectively. On the other hand, the reductive transformation of DNT and DBP was inhibited after blocking (Figure. 5.7b and d). Only a tiny formation of DAT and 2BP was observed. Unlike DNT, DBP was further sorbed to the blocked surface. These results suggested that the surface functional groups of biochar may also facilitate electron transfer in Fe(0)–biochar. It should be noted that the possibility that contaminants in the water

permeated into the outside biochar and were directly reduced by electrons from the corrosion of inside iron cannot be completely ruled out.

Goeringer et al. (2001) [277] suggested that oxygen-containing surface 9 functional groups can be changed to oxidized or reduced forms with oxidants or reductants to function as catalysts for redox reactions. Since various types of oxygen-containing surfaces, functional groups can be developed on biochar surfaces [175], [278], [279]. Electrons generated from the corrosion of inside Fe(0) can transform oxygen-containing surface functional groups on the outside biochar into reduced forms, which may be responsible for reducing sorbed nitro explosives and halogenated-phenols. The reduction of DNT and DBP with pre-reduced biochar was examined through batch experiments to determine the role of surface functional groups in Fe(0)–biochar. As DNT and DBP were removed with biochar, 2A4NT and 2BP formed, although their concentrations were somewhat low [Figure 5.7]. The yields of 2A4NT and 2BP as reduction intermediates were consistent with those in the Fe(0)–biochar system. These results suggested that Fe(0) corrosion could give surface functional groups on the biochar surface the reducing capability to transform sorbed nitro explosives and halogenated-phenols in the Fe(0)–biochar system. Considering the redox and catalytic properties of Fe(0)–biochar, the reductive removal of contaminants with Fe(0)–biochar can be summarized by the following five steps: (1) sorption of contaminants to the outside biochar surface; (2) corrosion by permeated water molecules; (3) electron transfer from iron to biochar through Fe_3O_4; (4) electron transfer through biochar to sorbed molecules via the graphene regions or surface functional groups; (5) re-partitioning of reduction products between the sorbed and aqueous phases.

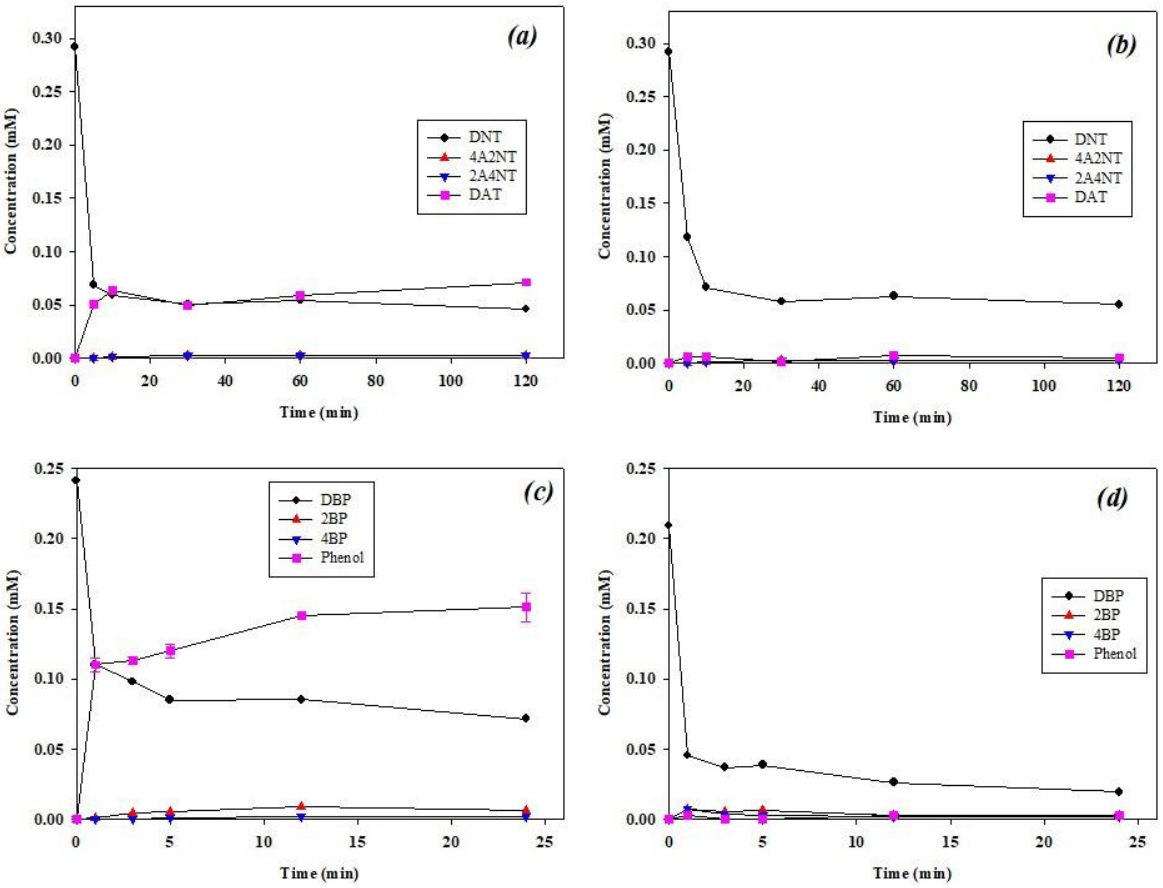

Figure 5.7.The effects of the surface blockage of functional groups (hydroxyl and carboxyl) on the reductive removal of DNT and DBP with Fe(0)–biochar pyrolyzed at 250 °C. Data points are average values, and the error bars represent one standard deviation. [(a) DNT without blocking, (b) DNT after blocking, (c) DBP without blocking, and (d) DBP after blocking].

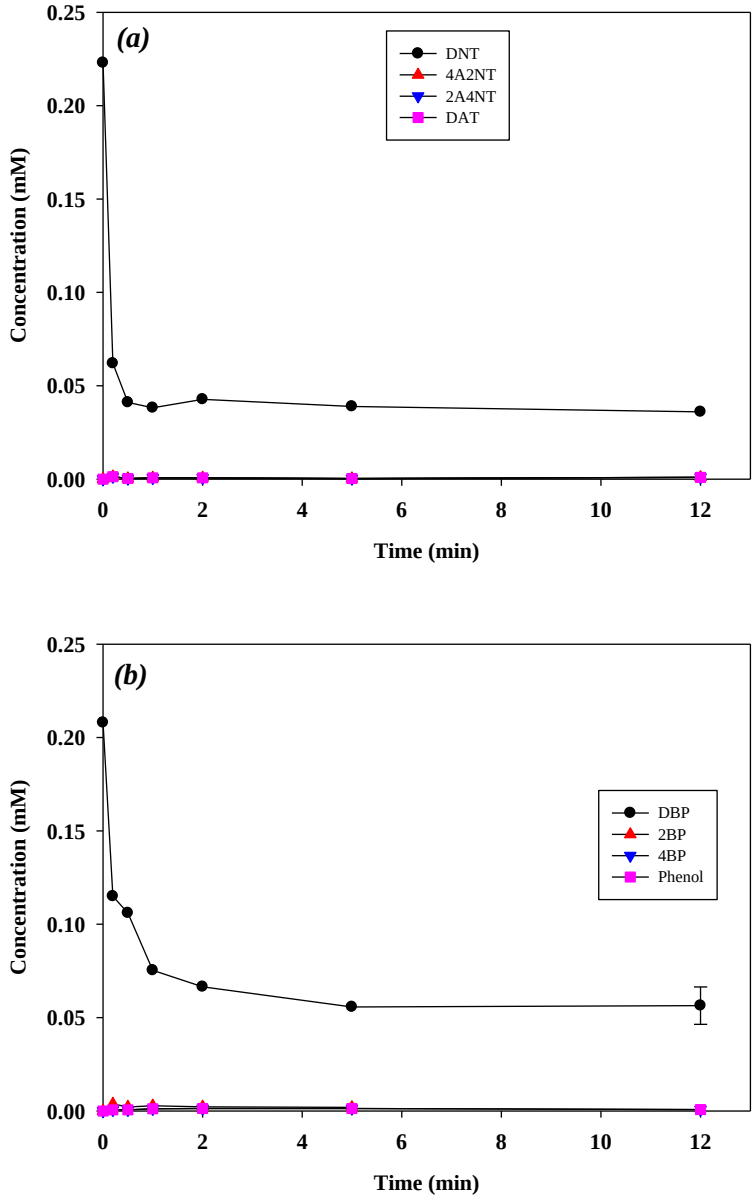

Figure 5.8. Reduction of (a) DNT and (b) DBP by pre-reduced biochar by Fe(0). Data points are average values, and the error bars represent one standard deviation. The biochar was pyrolyzed at 550 °C and pre-reduced by Fe(0) at a pH of 7.4 for 1 h.

5.4. Conclusions

Our results showed that TNT, RDX, DBP, and DFP were rapidly removed, and further transformed into reduction products in the presence of Fe(0)–biochar. XANES and XPS analyses showed that the redox properties of Fe(0) were not changed after co-pyrolysis with rice straw. Surface blocking experiments showed that surface functional groups may also be involved as an electron transfer mediator in the reduction of sorbed molecules with Fe(0)–biochar. The novel Fe(0)–biochar may be a promising active strategic material to sorb and transform redox-sensitive contaminants for long-term remediation actions for contaminated soils and sediments.

Chapter 6. Polymer/biomass-derived biochar for use as a sorbent and electron transfer mediator in environmental applications

6.1. Introduction

Since plastics (mainly composed of synthetic organic polymers) were introduced in the early 1930s, plastic materials have become integral to human life, and many polymers are used in everyday life. The global plastic production in 2010 was 264 million tons [280]. According to the Korean Ministry of Environment, approximately 6000 tons/day of plastic/polymer wastes were generated in South Korea in 2014. Currently, about 60% of plastic wastes are recycled via physical and chemical processes in South Korea. Plastics have a high resistance to biodegradation, limiting plastic waste's final disposal to incineration and landfilling. Because polymers have high carbon and hydrogen content, much research in the last few decades has focused on recovering valuable energy from thermal decomposition processes, such as pyrolysis [281], [282]. Pyrolysis of plastic wastes produces pyrolysis oil and gas, which can be further treated to produce a product that can be used for practical purposes [283], [284].

Disposal and treatment of agricultural and biomass wastes have also been intensively examined. Unlike plastic wastes, biological treatment (e.g., composting) is a primary option because most biomass wastes are readily biodegradable [285]. Recently, pyrolysis of biomass wastes was proposed as an alternative process for developing alternative energy in response to climate change [7]. The pyrolysis of biomass wastes has also been shown to reduce the release of carbon dioxide by converting the biomass to biochar, a relatively stable form that is resistant to degradation; this is a type of carbon sequestration [7], [132]. Pyrolysis is not only used to treat biomass waste, but it can also be used to produce reusable energy such as heat, bio-oil, and syn-gas [7], [286]. On the other hand, to pyrolysis oil produced from plastic/polymer wastes, the crude bio-oil produced from biomass is not satisfactory for use in fuels [100]. Bio-

oil is acidic and contains high water and oxygen content [42]. Furthermore, the properties of the produced bio-oil varied depending on the composition of the biomass wastes (e.g., lignin, cellulose, hemicellulose, and other compositions) [100], [42]. The quality of bio-oil could be enhanced using several treatment processes (e.g., catalytic hydroprocessing) to produce transportation or engine fuels [287], [288]. For the practical use of bio-oil, the required upgrading treatment processes are costly. Attempts have also been made to improve the quality of crude bio-oil, including fast catalytic pyrolysis [289], [290]. However, the improvement in the quality of the crude bio-oil was limited.

One way to improve bio-oil quality is to use plastics/polymer wastes and biomass together in pyrolysis. Co-pyrolysis of polymer and biomass has significantly improved bio-oil quality due to the synergistic effect of the high carbon and hydrogen content in the polymers. The addition of polymers to biomass pyrolysis has resulted in increased bio-oil yield and higher heating values [291]-[293]. Co-pyrolysis of polymers with biomass resulted in upgraded bio-oil by reducing the acidity, density, and oxygen content [291], [294]. Catalytic co-pyrolysis of polymers with biomass also significantly improved the quality of bio-oils [295]. Studies on char produced from co-pyrolysis of biomass and polymers were also conducted. Compared to biochar, the yield of char was reduced, and the calorific values were improved [296]-[298]. The co-pyrolysis also resulted in aromaticity via the growth of polycyclic aromatic hydrocarbons (PAHs) [299], [300]. Bernardo et al. (2012) [301] suggested that the upgraded biochar made from the co-pyrolysis of biomass and polymers can be used as an adsorbent.

Many studies have been conducted on using biochar as an alternative sorbent to immobilize toxic metals and organic compounds in environmental applications [248]. Various types of biochar have been synthesized based on the pyrolysis conditions, and their sorption characteristics were different. In general, the sorption of contaminants to biochar was less than the sorption on activated carbon. The sorption of contaminants to biochar was enhanced

through surface activation with acids and oxidants. However, the sorption capacity was still less than activated carbon due to the low carbon content and small surface area. To overcome this limitation, we propose a co-pyrolysis of biomass and polymer to upgrade the properties of biochar. Though bio-oil from the co-pyrolysis of polymer and biomass has been well characterized, limited attempts have been made to study biochar produced from co-pyrolysis of polymers and biomass for environmental applications. We hypothesized that polymer/biomass-derived biochar might improve the properties of biochar for sorbents and catalysts due to residues from the polymers. The objectives of this study were to characterize biochar that was co-pyrolyzed with polymer and biomass and evaluate the polymer/biomass-derived biochar as a sorbent and an electron transfer mediator. DNT and Pb were selected as model contaminants because their sorption to biochar was previously investigated in detail [230]. By pyrolysis of rice straw and high molecular compounds (polypropylene, polyethylene, and polystyrene) together, polymer/biomass-derived biochar was synthesized and characterized. The sorption of DNT and Pb were determined in batch experiments. The role of the electron transfer mediator was examined during the reductive transformation of DNT using a model reductant, dithiothreitol (DTT) (Eh^0 = -0.33 V at pH 7).

6.2. Materials and methods

6.2.1. Chemicals

Polypropylene (PP, amorphous, average molecular weight ~ 14,000), polyethylene (PE, low density, melt index 25 g/10 min), polystyrene (PS, average molecular weight ~ 19,200), 2,4-Dinitrotoluene (DNT, 97%), 2-Amino-4-Nitrotoluene (2A4NT, 99%), 4-Amino-2-Nitrotoluene (4A2NT, 97%), 2,4-Diaminotoluene (DAT, 98%), and $PbCl_2$ (98%) purchasing from Aldrich (Milwaukee, WI, USA). HEPES (N-[2-hydroxyethyl] piperazine-N'-[ethanesulfonic acid]) was obtained from Sigma (St. Louis, MO, USA). All chemicals were

used as received without further purification.

6.2.2. Synthesis of polymer/rice straw-derived biochar

Rice straw (RS) collected from rice farms in Ulsan, Korea, was used as biomass to synthesize polymer/biomass-derived biochar. The sampled RS was dried in an oven at 105 ± 5 ℃ for at least 2 h. After storing in a desiccator overnight, the dried RS was pulverized to smaller sizes (less than 5 mm) using an electric mixer. Then, one of the purchased polymers was mixed with the RS at volumetric ratios of 40:60, 20:80, and 5:95. The wholly mixed polymer/RS mixtures were co-pyrolyzed at 550 ℃ for 4 h using a tube-type electrical furnace under N_2 at 1000 cc/min. A relatively high nitrogen flow rate was maintained to prevent ash formation from biomass during the pyrolysis process. After cooling down to room temperature, the co-pyrolyzed polymer/RS-derived biochar was put in a desiccator for additional drying. To determine the effect of pyrolysis temperature, we changed the temperature to 700 and 900 ℃. The synthesized polymer/RS-derived biochar properties were characterized, including pH, BET surface area, CEC, pH at PZC, and elemental compositions (Table 6.1). FT-IR (Nicolet iS5 ThermoFisher Sci., Waltham, MA, USA) spectra and SEM (JSM 600F, JEOL, Japan) images were also obtained to identify the surface functional groups and investigate the surface morphology. Thermogravimetric analysis (TGA) was conducted to determine the mass change as a function of the pyrolysis temperature under anaerobic conditions using a TGA system (STA409C/3/F, Netzsch, Germany).

Table 6.1. Properties of the polymer/rice straw-derived biochars.

Polymer type	Polymer contents before pyrolysis (v%)	Pyrolysis temp. (°C)	pH	BET S.A. (m^2/g)	CEC (meq/100 g)	PZC	Elemental contents (%)			
							C	H	O	N
-	0	550	9.12	16.4	77.5	8.4	55.8	2.88	13.1	2.02
PP	5	550	11.0	18.7	224	9.8	57.1	2.13	8.83	0.75
	20	550	10.6	21.9	258	9.6	57.2	2.10	8.69	0.64
	40	550	11.1	27.5	321	9.7	57.9	2.10	7.43	0.54
	40	700	11.1	33.6	99.9	9.8	56.8	1.55	6.46	0.40
	40	900	11.4	34.8	98.9	10.0	56.6	0.75	5.14	0.37
PE	5	550	10.5	17.1	114	9.7	57.0	2.59	7.12	0.60
	20	550	10.4	23.5	186	9.8	57.5	2.30	6.76	0.56
	40	550	10.4	25.7	260	10.4	57.7	2.13	6.64	0.52
PS	5	550	10.7	16.6	97.6	9.4	57.0	1.87	5.18	1.10
	20	550	10.7	17.9	144	9.7	57.2	1.67	4.86	0.62
	40	550	10.5	20.0	191	9.8	58.1	1.56	4.71	0.54

6.2.3. Batch sorption experiments

DNT and Pb stock solutions were prepared using a magnetic stirrer and an Erlenmeyer flask (1 L) to concentrations of 200 mg/L and 1000 mg/L, respectively. A couple of drops of 1 N HCl were added to prevent precipitation of Pb in the stock solution. Batch sorption experiments were conducted using a 40-mL amber vial having 20 mL of solution and polymer/RS-derived biochar (0.05 ~ 5 g) at room temperature. The initial concentrations of the explosives and metals were 50 ~ 100 and 100 ~ 200 mg/L, respectively. Equilibrium concentrations of DNT and Pb were determined by changing the amount of biochar or the initial concentrations of the solutions. For Pb sorption experiments, the initial solution pH was adjusted to 5 ~ 5.5 to prevent possible precipitation. After sealing the vials with screw caps having PTFE-silicon septa, three vials per sample were shaken using an orbital shaker at 180 rpm throughout the experiment, except during sampling. Preliminary experiments indicated that sorption of DNT and Pb to the polymer/rice straw-derived biochar reached equilibrium after 12 h. After equilibrium was reached, aliquots were withdrawn using glass syringes. These aliquots were immediately passed through a 0.22 μm cellulose membrane filter (Millipore, MA,

USA) for the analytical determination of DNT and Pb. Control experiments were conducted under identical conditions without biochar to consider possible sorption to the inside surface of the vial. The effect of dissolved DNT (~50 mg/L) on the sorption of Pb to polymer/RS-derived biochar was also examined using PP/RS-derived biochar under identical conditions.

6.2.4. Batch reduction experiments

To determine the role of the electron transfer mediator, we investigated the reductive transformation of DNT in the presence of polymer/ RS-derived biochar by dithiothreitol (DTT) via batch experiments. The batch reduction experiments were conducted using sealed 250 mL borosilicate amber bottles in an anaerobic glove box (Jisico, Seoul, Korea) under N_2. Each bottle contained 200 mL of DNT solution and 1 g of the synthesized polymer/RS-derived biochar. The initial concentration of DNT was 0.289 mM. The DNT solution was deoxygenated by purging with N_2 for at least 30 min. The solution pH was maintained at 7.4 using a 0.1 M HEPES buffer. To each bottle, 120 mg of dithiothreitol were added as a model reductant. Each bottle was sealed with a Mininert®valve (VICI, Baton Rouge, LA, USA) and low-permeability vinyl tape (Scotch 471, 3 M, St. Paul, MN, USA). The bottles were placed horizontally in an orbital shaker at 180 rpm throughout the experiment except during sampling. A 1 mL aliquot was withdrawn at each sampling time using a glass syringe and immediately passed through a 0.22 μm cellulose membrane filter before analysis. Two experiments were conducted under identical conditions without dithiothreitol or biochar as sorption and reduction controls, respectively.

6.2.5. Chemical analysis

DNT and its reduction products were analyzed using a Dionex Ultimate®-3000 HPLC (Sunnyvale, CA, USA) equipped with a Dionex Acclaim® 120 guard column (4.3×10 mm) and

an Acclaim® 120 C-18 column (4.6×250 mm, 5 um). The analytical methods and conditions for quantifying DNT and its reduction products are described in detail elsewhere [303]. The concentrations of Pb were determined using an atomic absorption spectrophotometer (AAS, 5100 ZL, Perkin Elmer, Waltham, MA, USA). Analytical duplicate, standard, and blank samples were used for quality control of the data we obtained.

6.3. Results and discussion

6.3.1. Characteristics of polymer/RS-derived biochar

Properties of the polymer/RS-derived biochar are summarized in Table 6.1. Compared to RS-derived biochar, the addition of polymer increased the pH (from 9.12 to 10.4~11.1), the CEC (from 77.5 to 97.6~321 meq/100 g), the pH_{PZC} (from 8.4 to 9.4–10.4), and the carbon content (from 55.8 to 57.0~58.1%). The BET surface area slightly decreased from 16.4 to (16.6~27.5) m^2/g. On the other hand, significant decreases were observed in hydrogen (from 2.88 to 1.56–2.59%), oxygen (from 13.1 to 4.71~8.83%), and nitrogen (from 2.02 to 0.52~1.10%) content. However, substantial amounts of hydrogen, oxygen, and nitrogen remained on the biochar, indicating that surface functional groups remained. These results indicated that carbon-containing residuals remaining on the surface of the biochar greatly affected the properties. Regardless of polymer type, increasing the amount of polymer also slightly increased the BET surface area, CEC, and carbon content (Table 6.1). Hydrogen, oxygen, and nitrogen content also slightly decreased. As shown in the SEM images (Figure. 6.1), the addition of PP resulted in some rough impure residues on the surface of the biochar, which were not present on the RS-derived biochar. FT-IR spectra also showed information related to the functional groups on the surface of the biochar. Due to impurity and heterogeneity in biochar, peaks in the spectra were somewhat weak and broad. Carbonyl C=O (1720~1730 cm^{-1}) and phenolic C-O (1200 cm^{-1}) stretch originated from cellulose in the biomass [300], and these remained after adding polymers (Figure. 6.2). Methyl C-H (2927~2847 cm^{-1}), in-ring C-C (1600 cm^{-1}), aromatic C-H out-of-plane bending (825~880 cm^{-1}), and aromatic C-H (712 cm^{-1}) stretching polymers develop with the increasing amount or remain undamaged. These results indicate the development of condensed aromatic rings and the remaining intact polysaccharide residues [300].

To determine the effect of temperature on the formation of polymer/RS-derived biochar

in the pyrolysis process of PP and RS biomass (40 v%: 60 v%), we increased the pyrolysis temperature to 700 and 900 °C. Because polymers remained after co-pyrolysis with RS at low temperatures (250 and 400 ℃), the effect of pyrolysis temperature was only evaluated at high temperatures. Increasing the temperature did not significantly change the pH and pHPZC (Table 6.1). Similar to conventional biochar [302], increasing the temperature increased PP/RS-derived biochar (from 27.5 to 33.6 and 34.8 m^2/g). On the other hand, hydrogen, oxygen, and nitrogen contents decreased significantly (Table 6.1.). FT-IR spectra revealed that increasing pyrolysis temperature resulted in reduced surface functional groups at 700 and 900 ℃, consistent with previous results from conventional biochar synthesis at 700 and 900 ℃ [302]. In addition, CEC decreased from 321 to 99.9 and 98.9 meq/100 g for pyrolysis temperatures of 550, 700, and 900 ℃, respectively. TGA experiments were conducted to confirm the amount of remaining polymer residue. Compared with the control group using RS-derived biochar, PP/RS-derived biochar did not show a significant decrease in weight when the temperature was increased from 400 to 800 ℃ (Figure. 6.3). These results indicate that residues of the PP remain in the biochar. Regardless of PP amount (5~40 v%), the difference in weight loss was not significant as temperature increased, suggesting that the number of residues may be similar.

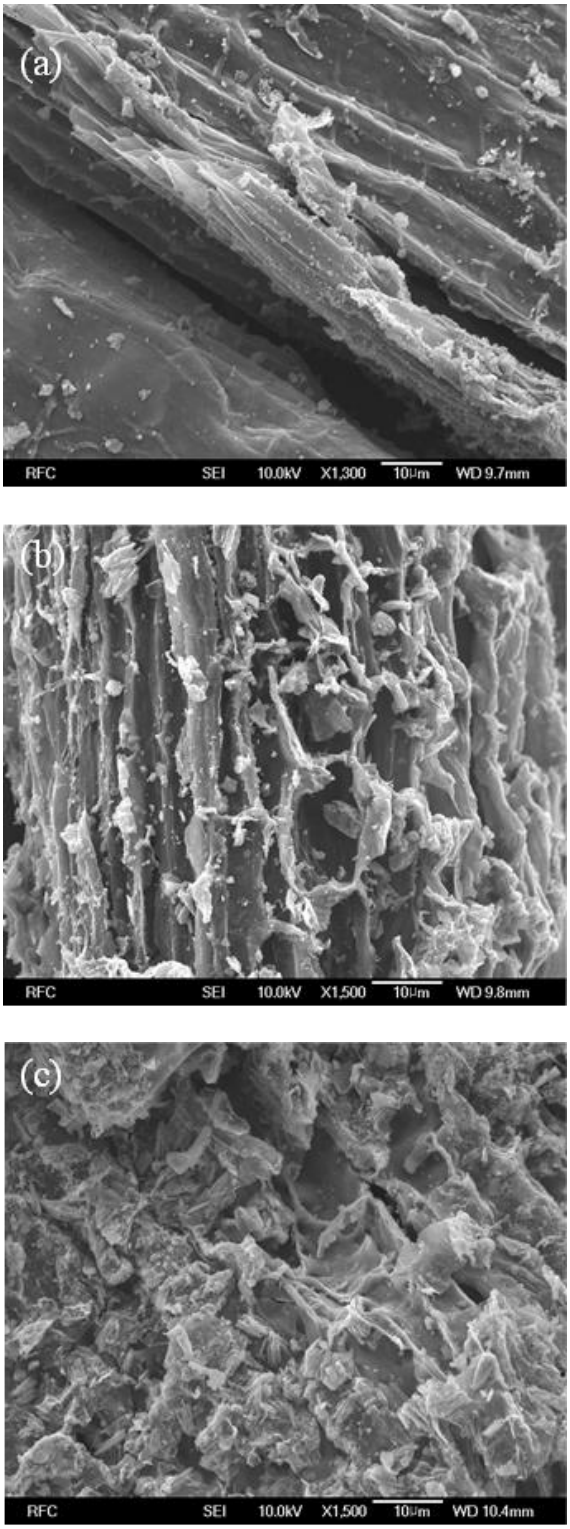

Figure 6.1. SEM images of PP/RS-derived biochar pyrolyzed at 550 ℃: (a) RS only, (b) 5 v% PP, and (c) 40 v% PP.

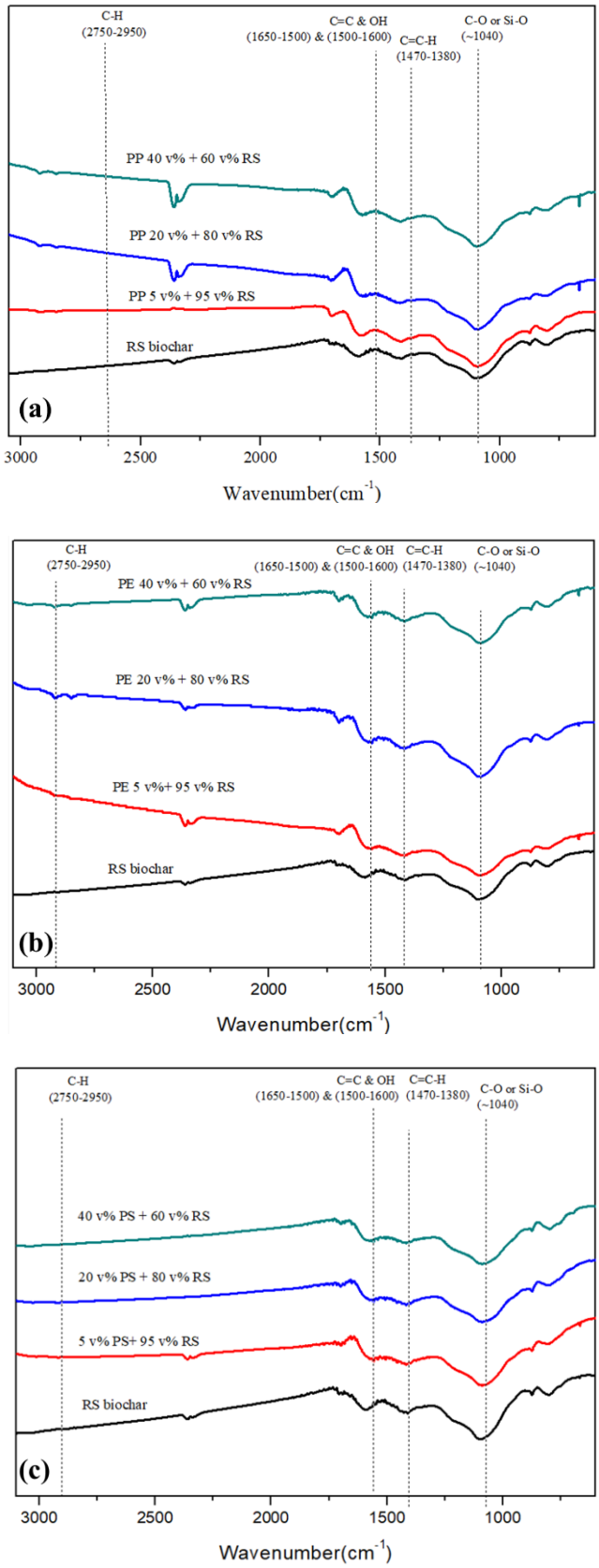

Figure 6.2. FT-IR spectra of (a) PP/RS-, (b) PE/RS-, and (c) PS/RS-derived biochars pyrolyzed at 550 °C.

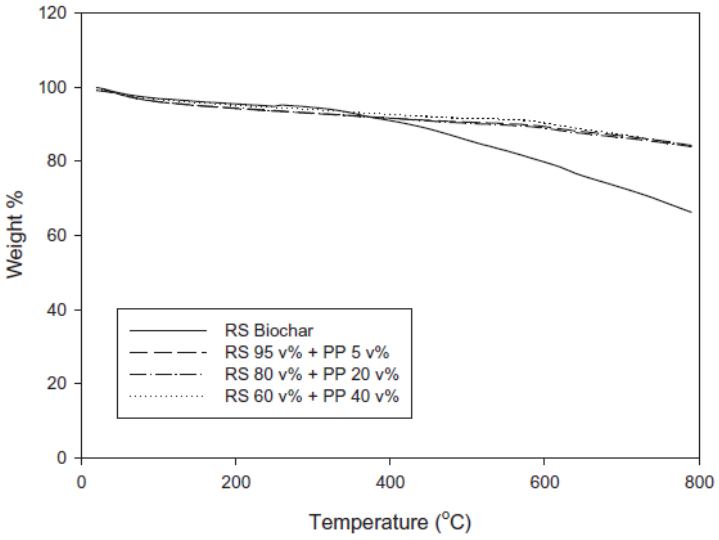

Figure 6.3. Thermogravimetric analysis (TGA) curves of PP/RS-derived biochars pyrolyzed at 550 °C.

6.3.2. Sorption of DNT and Pb to polymer/RS-derived biochar

The sorption of DNT to PP/RS-, PE/RS-, and PS/RS-derived biochar is summarized in Figure 6.4. The maximum sorption capacity in a Langmuir sorption isotherm model was estimated using the obtained data sets. In a control experiment with RS-derived biochar, the maximum sorption capacity was 4.75 mg/g, like the 4.63 mg/g obtained from our previous study [230]. Compared to RS-derived biochar, the addition of PP dramatically increased the sorption capacity. The estimated maximum sorption capacity of DNT for PP/RS (5:95 v/v)-derived biochar was 10.3 mg/g, which was about two times higher than that of RS-derived biochar (Figure 6.4a). Increases in PP did not significantly increase the sorption capacity (11.3 and 10.5 mg/g for 20:80 and 40:60 v/v, respectively). This similarity in sorption capacity may be correlated with similar weight loss values of the residues from PP in the TGA results (Figure. 6.3). The maximum sorption capacities of DNT to PE/RS- and PS/RS-derived biochar (5:95 v/v) were 15.1 and 14.2 mg/g, respectively (Figure. 6.4b and c). Increasing PE or PS did not significantly enhance the sorption capacity, consistent with the results from PP/RS-derived biochar. Among the three different types of polymers, PE is the most effective polymer for increasing the sorption of DNT. Previously, the sorption of DNT was attributed to the aromaticity arising from the graphitic structure of carbon at high pyrolysis temperatures and possible hydrophobicity from organic residues at low pyrolysis temperatures [302]. Possible sorption mechanisms were identified, including π-π EDA interactions and hydrophobic sorption [230]. Thus, the enhancement of DNT sorption to polymer/RS-derived biochar can be explained by two possible mechanisms. First, carbon residues from polymers may increase hydrophobicity. Second, the increased carbon content and aromaticity that results from pyrolysis can enhance possible π-π EDA interactions between DNT and polymer/RS-derived biochar.

The sorption of Pb to polymer/RS-derived biochar was also significantly enhanced.

However, it shows different trends than the DNT. The maximum sorption capacity of Pb to RS-derived biochar from a Langmuir sorption isotherm model was 62.1 mg/g (Figure. 6.5), which was much higher than we previously reported (4.59 mg/g) [230]. This inconsistency was probably due to the heterogeneous nature of the biochar. Though the biochar was synthesized using the same biomass under identical conditions, the properties of biochar were different from the previously reported ones [230]. Primarily, CEC markedly increased from 3.10 to 77.5 meq/100 g (Table 6.1.), and this may be responsible for increasing the sorption capacity of Pb to RS-derived biochar. The co-pyrolysis with polymer significantly enhanced the sorption of Pb to biochar. The maximum sorption capacity of Pb to PP/RS (5:95 v/v)-derived biochar was 87.4 mg/g, about 40% higher than RS-derived biochar. Increasing the amount of PP resulted in further increasing the maximum sorption capacity (109 and 122 mg/g for 20:80 and 40:60 v/v, respectively). According to previous studies [209], [230], surface complexation with functional groups, ion exchange with hydrogen in functional groups, electrostatic sorption, and surface precipitation with increasing pHs were proposed as possible sorption mechanisms of Pb to biochar. Thus, high CEC, high BET surface area, and increasing pH values may be responsible for the increased sorption capacity of Pb with increasing PP amount. Based on our results (Table 6.1), polymer and rice straw co-pyrolysis resulted in the polymer's remaining carbon residues and increased aromaticity. These property changes were favorable for the sorption of DNT (organic and polar due to nitro functional groups). At the same time, the co-pyrolysis also increased CEC, pH, and surface area, which were also favorable for the sorption of cationic metals according to factors affecting the sorption of toxic metals [230]. It appears that the co-pyrolysis of polymer and biomass produced biochar favorable for the sorption of both DNT and Pb. That different sorption mechanism was co-existed in polymer/rice straw-derived biochar.

Similar to PP/RS biochar systems, the sorption of Pb was significantly enhanced in

PE/RS-derived biochars (Figure. 6.5b). Increasing the amount of PE also enhanced the sorption capacity. The maximum sorption capacities of Pb were 91.4, 117, and 136 mg/g for 5:95, 20:80, and 40:60 v/v PE/RS-derived biochar, respectively. PS/RS-derived biochar results showed that the maximum sorption capacity significantly increased (133 mg/g for 5:95 v/v PS/RS-derived biochar). However, the sorption capacity of Pb did not increase much as the number of PS increased. FT-IR spectra showed that surface functional groups did not change much as the PS amount increased (Figure. 6.2c), indicating that changes in the PS amount had little effect. Further studies may be needed to determine the effect of the amount of PS.

The effect of pyrolysis temperature on the sorption of DNT and Pb to PP/RS (40:60 v/v)-derived biochar was investigated. The maximum sorption capacity decreased (9.34 and 8.25 mg/g) by increasing the pyrolysis temperature from 550 to 700 and 900 ℃, respectively (Figure. 6.6a). It was previously reported that increasing the BET surface area of biochar at elevated temperatures did not enhance the sorption of DNT to biochar [230]. Instead, the high carbon content at elevated temperatures made the biochar more aromatic, accounting for enhancing DNT sorption to biochar via π - π EDA interactions [302]. On the other hand, to biochar, the carbon content in PP/RS-derived biochar slightly decreased at elevated temperatures (Table 6.1), probably due to the loss of carbon residues from PP (Figure. 6.3). This removal of carbon residues may be responsible for a slight decrease in sorption capacity. The increase in pyrolysis temperature also decreased the maximum sorption capacity of Pb to PP/RS-derived biochar from 116 to 95.5 mg/g for temperatures of 700 and 900 ℃, respectively (Figure. 6.6b). The decrease in CEC, H/C, and O/C at elevated temperatures probably accounts for decreased sorption capacity (Table 6.1). For the sorption of Pb on PP/RS-derived biochar, the effect of DNT on Pb adsorption was investigated using a mixed solution of DNT and Pb. Previously, we investigated the competitive sorption between cationic metals and nitroaromatics to biochar [302]. Dissolved DNT (50 mg/L) did not significantly affect the sorption of Pb (Figure. 6.7).

This suggests that different sorption mechanisms may account for the sorption of DNT and Pb to PP/RS-derived biochar. The sorption of Pb to localized electron-rich graphene moiety may not be significant. How vital each sorption mechanism remains to be explored.

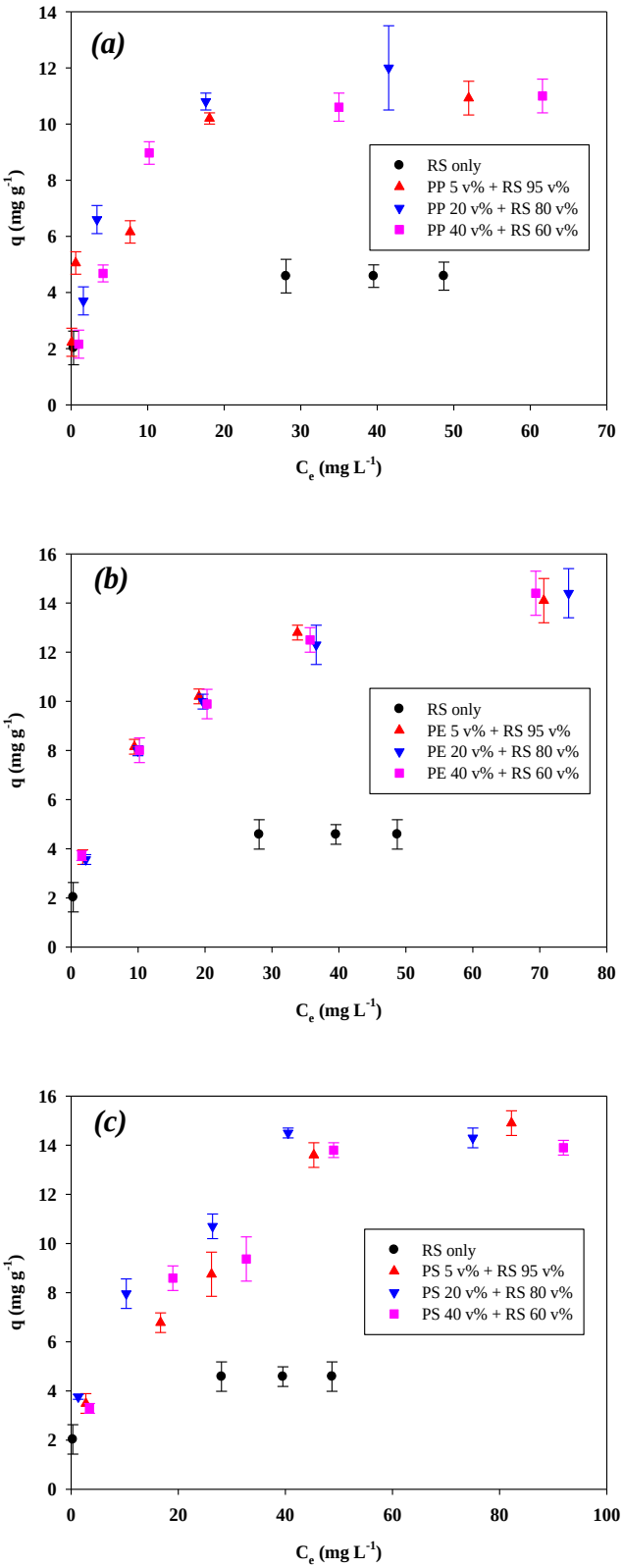

Figure 6.4. Sorption of DNT to (a) PP/RS-, (b) PE/RS-, and (c) PS/RS-derived biochars pyrolyzed at 550 °C. Data points are average values, and the error bars represent one standard deviation.

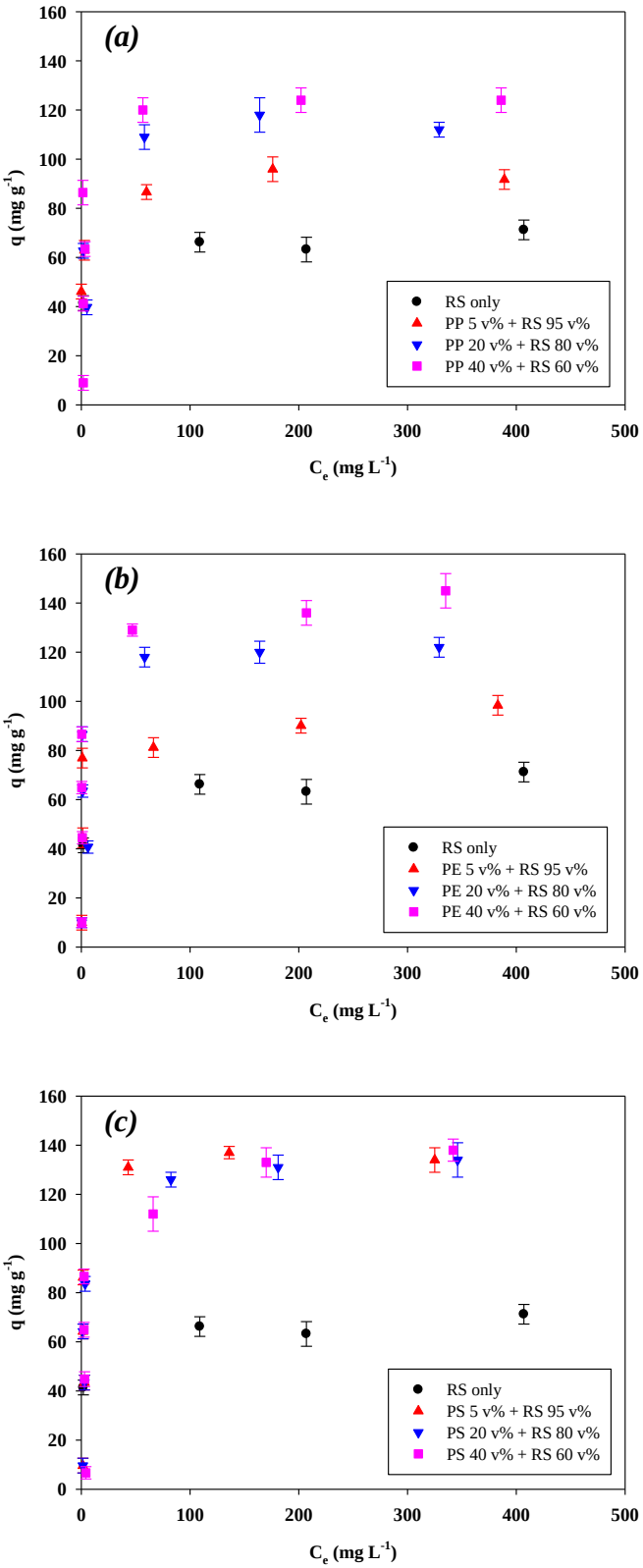

Figure 6.5. Sorption of Pb to (a) PP/RS-, (b) PE/RS-, and (c) PS/RS-derived biochars pyrolyzed at 550 °C. Data points are average values, and the error bars represent one standard deviation.

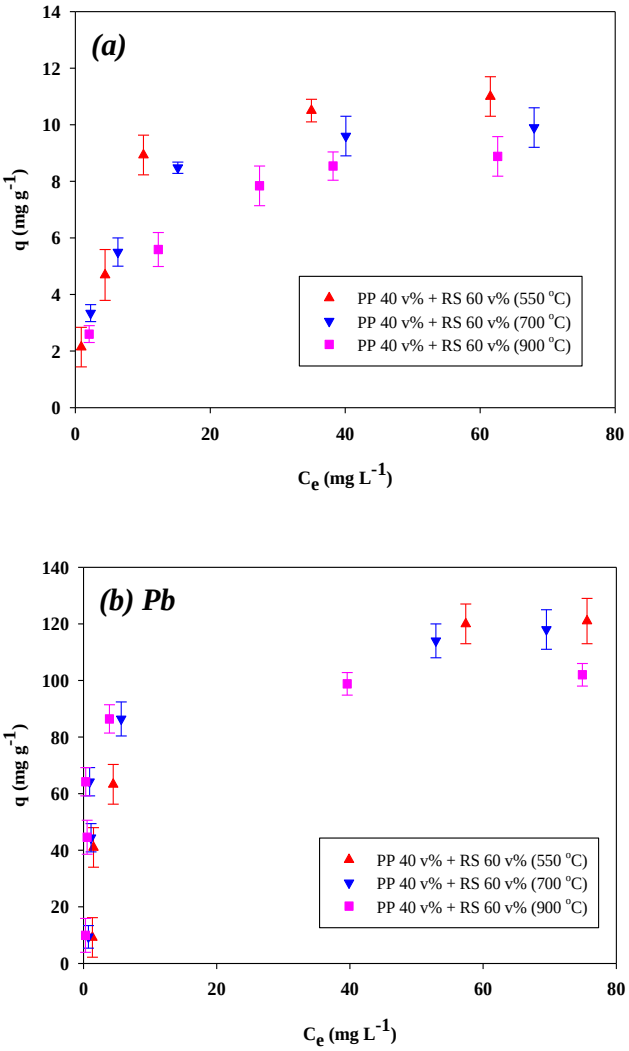

Figure 6.6. Sorption of (a) DNT and (b) Pb to PP/RS-derived biochar pyrolyzed at various temperatures. Data points are average values, and the error bars represent one standard deviation.

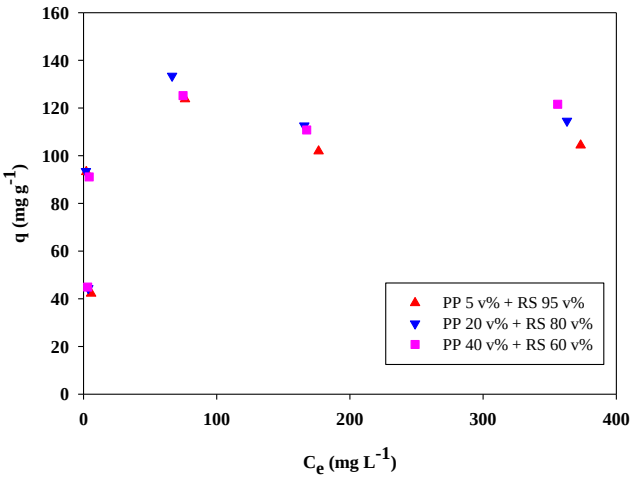

Figure 6.7. The effect of dissolved DNT (50 mg/L) on the sorption of Pb to PP/RS-derived biochar pyrolyzed at 550 °C (the concentration of DNT was 50 mg/L).

6.3.3. Reduction of DNT by dithiothreitol with polymer/RS-derived biochar

The role of polymer/RS-derived biochar as an electron transfer mediator was also investigated using dithiothreitol (DTT). Like conventional biochar [303], the existence of PP/RS-derived biochar pyrolyzed at 550 °C dramatically enhanced the reductive transformation of DNT by DTT (Figure. 6.8). Reduction with DTT only showed 10% removal in 120 h, and sorption control with PP/RS-derived biochar did not produce any reduction products of DNT. The co-existence of PP/RS-derived biochar and DTT resulted in 2A4NT and 4A2NT after 6 h (Figure 6.8). DAT was also formed as a final reduction product. After 6 h, the concentrations of 2A4NT, 4A2NT, and DAT did not significantly change. The sum of the three daughter products accounted for approximately 50% of the initial DNT concentration. The yield of two intermediates indicated that the ortho reduction pathway was dominant in the PP/RS-derived biochar-DTT-DNT system (Figure 6.8). This is consistent with the biochar-DTT-DNT system previously reported [219]. Co-pyrolyzed biochar with PS/PE and RS also showed similar results. The results suggest that polymer/RS-derived biochar may still have the catalytic ability to promote the reductive transformation of DNT in the presence of a reductant.

These results also suggest that carbon residues from the polymer may not significantly

affect the aromaticity of graphene regions in the biochar and surface functional groups. No significant difference was observed when PP/RS-derived biochars pyrolyzed at 700, and 900 ℃ were used under identical conditions (Figure. 6.9), indicating that pyrolysis at 550 ℃ is sufficient to convert the polymer/RS-derived biochar into a catalyst to promote reductive transformation.

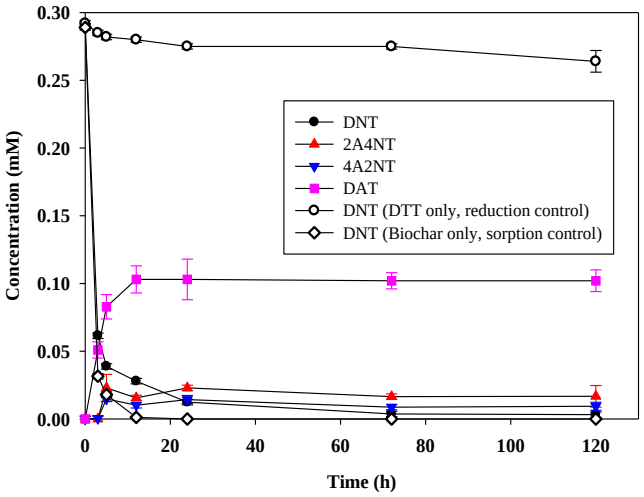

Figure 6.8. DNT reduction by DTT in the presence of PP/RS (40:60 v/v)-derived biochar pyrolyzed at 550 ℃. Data points are average values, and the error bars represent 1 SD.

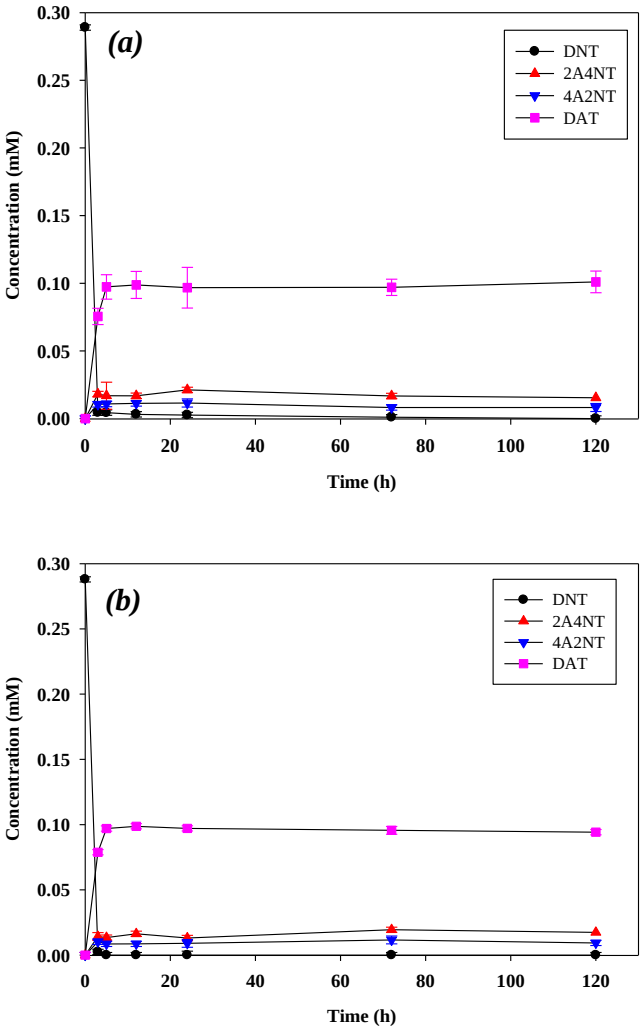

Figure 6.9. DNT reduction by dithiothreitol in the presence of PP/RS (40:60 v/v)-derived biochar pyrolyzed at (a) 700 and (b) 900 ℃.

6.4. Conclusions

Our results showed that co-pyrolysis of polymer and biomass wastes improved the properties of biochar. Increasing carbon content and the development of surface functional groups significantly enhanced the sorption capacity of DNT and Pb on polymer/RS-derived biochar. The addition of polymer did not change the catalytic role of the biochar. This suggests that the aromatic structure and surface functional groups may be responsible for the catalytic characteristics. The importance of surface functional groups and the aromaticity of polymer/RS-derived biochar as an electron transfer mediator are currently being investigated. We will report the results of this study in the near future.

Chapter 7. Evaluation of commercial biochar in South Korea for environmental application and carbon sequestration

7.1. Introduction

In the last decade, a significant amount of biochar research, a solid by-product from the pyrolysis of biomass, has been conducted due to its role in carbon sequestration, soil fertility, and amendment, and water and soil remediation [7], [36], [304]-[307]. Biochar has been used in compost, compensatory fertilizers, cosmetics, paints, filters, and medicine. It has also been used for plant protection, insulation, humidity control, and energy production [308], [309], [55]. In Korea, slashing-and-burning of fields in mountainous regions has improved soil health and crop productivity. Biochar has traditionally been synthesized from wood as a form of soot or charcoal using wood and has been used in various ways in everyday life, such as for supplementation of heating fuels, cooking, bean paste, and soy sauce production, and food storage [310]. Recently, many studies on biochar's environmental and agricultural applications have been conducted in South Korea [123], [248]. Factors affecting the sorptive removal of various contaminants have been determined, and possible removal mechanisms have been proposed [36], [307].

Many commercial biochar products can be easily purchased in large amounts from well-known online marketing sites in the U.S. Hundreds of vendors, mostly farming companies/owners, are providing various biochar products pyrolyzed from different types of agricultural wastes. On the other hand, the production of commercial biochar in South Korea is limited, and most biochar synthesis is conducted not for mass production but for the examination of biochar properties in feasibility studies. Though large bodies of research on biochar applications have been conducted in South Korea, most of the biochars used in these studies were synthesized in laboratories from various types of organic and biomass wastes.

Only two types of biochar can be obtained in bulk in South Korea. One is biochar produced via thermal carbonization of biosolid from wastewater treatment facilities (representing approximately 15% of total biosolid disposal in South Korea). Most carbonized biosolid (biochar) is being used as supplementary fuels for coal-driven power plants or municipal solid waste incinerators. The other type is commercial biochar produced in South Korea that is pyrolyzed from wood chips and used as a soil amendment on farms to increase productivity. Several attempts were made to evaluate the biosolid (BS) biochar as a catalyst and a sorbent for environmental remediation in natural environments [230], [263]. However, commercial wood chip (WC) biochar has not been evaluated for environmental processes and carbon sequestration.

In general, the construction of buildings and infrastructure using cement-based materials (e.g., concrete) generates enormous amounts of CO_2 into the atmosphere from manufacturing to the application [311], [323]. Significant efforts are needed to make the conventional construction industry more competitive in preventing climate change and the greenhouse effect. It would be desirable to adopt a mitigation process during the subsequent construction of cement-based buildings and infrastructure to compensate for CO_2 emissions [312]-[314]. Meanwhile, due to its low thermal conductivity and high-water holding capacity, biochar has been used as a plaster-mixing material to maintain a constant temperature and humidity for wine cellars in European countries [315]. Therefore, it is reasonable to consider that mixing biochar with mortar may create a carbon sink to store CO_2 in cement-based constructing materials. Additionally, some engineering properties of biochar–mortar composites may be enhanced due to the nature of biochar. Recently, adding biochar to cement mortar was made for carbon sequestration [316], [317]. By adding 2 wt% biochar to cement in mortar, the compressive strength and impermeability of the mortar were significantly improved. However, an environmental evaluation of concrete-based construction materials has not been performed.

In the present study, commercial WC biochar was examined as a sorbent for environmental applications. The competitiveness of WC biochar, in comparison with BS biochar (available in large amounts) and rice straw (RS) biochar (made from most abundant agricultural wastes in South Korea), was evaluated through batch experiments. The sorption capacities of the biochars for various types of contaminants were determined, and possible sorption mechanisms were proposed. WC biochar was also evaluated as a construction material for carbon sequestration and controlling volatile contaminants in indoor environments. It was hypothesized that the favorable properties of this biochar would make it competitive for carbon sequestration in construction materials. Mortar was chosen as a construction material, and various amounts of biochar were added for the synthesis of biochar–mortar composites. The physical and chemical properties of the biochar–mortar composites were determined, and their environmental and construction characteristics were examined, including mortar flowability, compressive strength, thermal conductivity, as well as volatile contaminant sorption capacity, and toxicity as measured by the toxicity characteristics leaching procedure (TCLP) test and Microtox® bioassay. The optimal biochar–mortar mixing ratio for construction and carbon sequestration purposes was determined.

7.2. Material and methods

7.2.1. Chemicals and biochar

DNT and DCP were purchased from Aldrich (Milwaukee, WI). TNT and RDX are provided by Hanwha Corp. (Seoul, Korea). $PbCl_2$ (98%), Na_2CrO_4, (98%), Na_2SeO_4 (> 98%), acetic acid (> 98%, ACS grade), benzene (> 99.7%), and toluene (> 99.6%) were purchased from Aldrich. Phenol (99%) was purchased from Dae-Jung Chemical (> 99%, Kyunggi, Korea). Chemicals used as received, without further treatment. We prepared all solutions with deionized water.

Three types of biochar were used for this study: WC, BS, and RS. WC biochar, which is only commercially available, was provided by a company in Yang-san, South Korea. According to the information provided by the manufacturing company, oak tree wood chips imported from South Asian countries were pyrolysis at 450 ℃ for 2 hr. In addition, biosolids were collected from a municipal wastewater treatment facility in Cheonan Gyeonggi-do, South Korea. The sampled biosolids were dried and carbonized at a pilot-scale plant located at a company in Cheonan at 400 ℃ for 2 hr. Finally, as reference biochar synthesized in the laboratory, rice straw, obtained from rice farms in Ulsan, South Korea, was pyrolyzed using a gas flow-controlled tube-type furnace at 550 ℃ for 4 hr under N_2 at a flow rate of 1,000 cc/min. The physical and chemical properties of the biochars, that is, pH, PZC, BET surface area measured by N_2, CEC, anion exchange capacity (AEC), and CHON contents, are summarized in Table 7.1. SEM images and XPS spectra were analyzed using a JSM 600F (JEOL, Japan) and a K-alpha system (Thermo Scientific, Waltham, MA) analyzer to investigate the biochar surface morphology and surface functional groups. Figures 7.1 and 7.2 show the SEM images and XPS spectra of biochars. SEM images in Figure 7.1. revealed that all biochars have comblike porous structures though shapes are slightly different. According to BET surface area measurement, mean pore sizes for WC, BS, and RS biochars are 13.7, 10.8, and 8.71 Å, respectively.

According to XPS spectra in Figure 7.2, C=O and C-O single bonding are dominants in biochars, indicating that oxygen-containing functional groups, such as hydroxyl and carboxyl functional groups, are dominant. Fourier transform Infrared spectroscopy analysis in previous studies also showed the development of the oxygen-containing functional groups [230].

Table 7.1. Properties of biochar used in the present study.

Types of black carbon	pH	PZC	BET S.A. (m^2/g)	AEC (meq/100 g)			CEC (meq/100 g)	Elemental contents (%)			
				pH 4	pH 6	pH 8		C	H	O	N
RS biochar	10.9	8.2	16.7	85.7	86.9	91.5	3.1	59.4	2.8	12.7	1.9
BS biochar	8.3	7.1	122.8	162.2	276.8	353.1	8.6	23.0	0.4	13.6	4.4
WC biochar	6.5	6.7	55.3	87.1	83.9	89.5	14.4	54.7	5.6	15.5	0.9

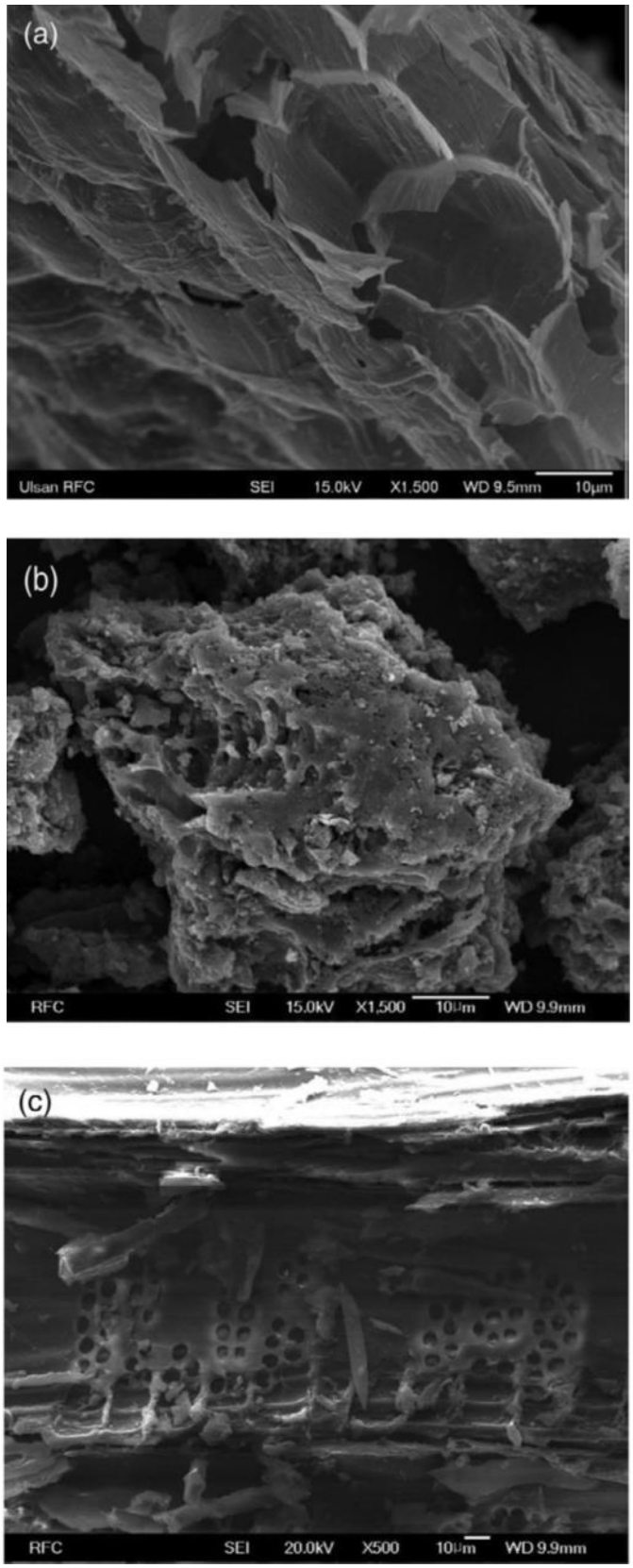

Figure 7.1. SEM images of (a) RS, (b) BS, and (c) WC biochars.

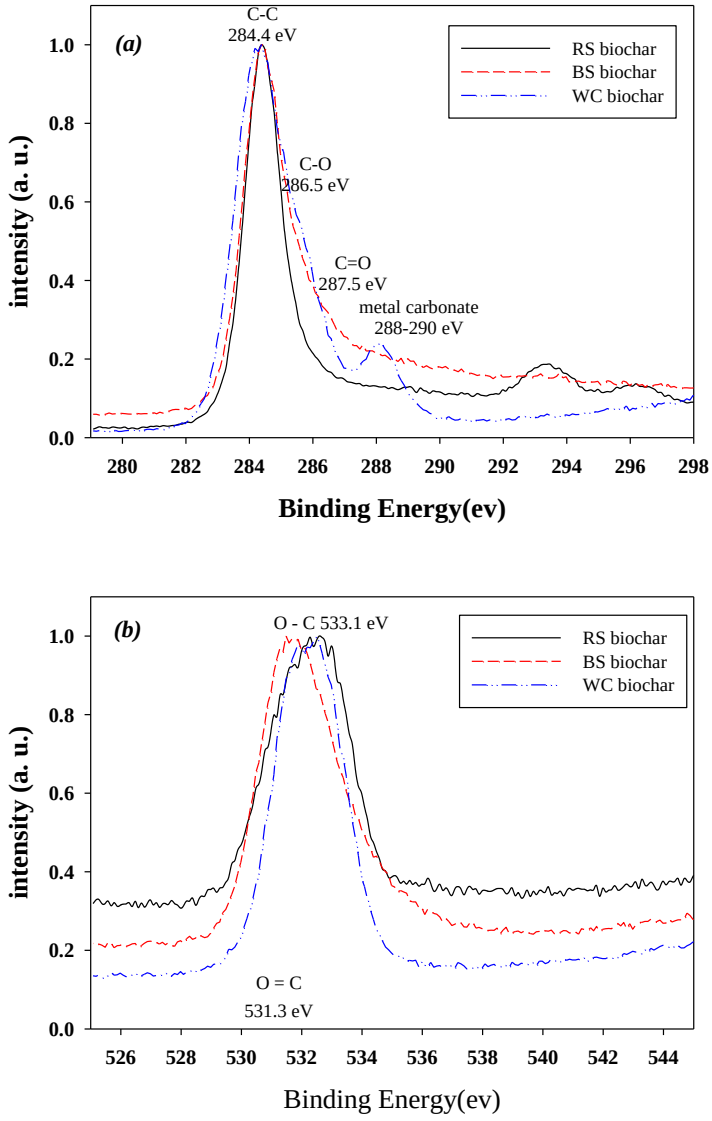

Figure 7.2. XPS spectra (a) C1s and (b) O1s of biochars used in the present study.

7.2.2. Batch experiments

Batch sorption experiments were performed using a 40 ml amber vial containing 20 ml of solution and biochar (0.05~5 g) at 25 ± 2 ℃. After sealing with screw caps with PTFE-silicon septa, duplicate vials were shaken by an orbital shaker at 180 rpm throughout the experiment, except during sampling. Preliminary experiments indicated that the sorption of nitro explosives, phenols, and metals to biochar reached equilibrium after 24 hr. Initial concentrations of nitro explosives, phenols, and metals were 5~80, 20~800, and 10~950 mg/L, respectively. For the metal sorption experiments, the initial pH was adjusted to 5~5.5 to prevent possible precipitation and maintain the initial concentration. After equilibrium was reached, aliquots were withdrawn using glass syringes and immediately passed through a 0.025 μm cellulose membrane filter (Millipore, MA) to determine nitro explosives, phenols, and metals. A set of control vials was established under identical conditions but without biochar to determine the possible loss of contaminants due to sorption to the inner surface of the vial. The adsorption amount of pollutants was calculated while taking into account the loss of pollutants in batch experiments.

7.2.3. Synthesis of biochar-mortar composites

Biochar–mortar composites were prepared via a slightly modified method following ASTM C109, the standard test method for compressive strength of hydraulic cement mortars (Using 50 mm cube specimens). Commercial ordinary portland cement (OPC) and a mixture of general sand and granite-weathered soil/sand (4:6 wt/wt) were used as cement and aggregate. The fineness module of the aggregate is 2.68. The standard blends of mortar, water to cement, and cement to aggregate weight ratios were 0.485:1 and 1:2.75, respectively. Furthermore, the specific gravity of cement, biochar, and aggregate was 3.15, 0.21, and 2.54, respectively. A portion of the cement (3 wt%, 5 wt%, 10 wt%, or 20 wt% of the initial cement weight) was

replaced with WC or RS biochar and mixed with the cement, aggregate, and water to synthesize the biochar–mortar composites. Mortar specimens (50 mm^3) were fabricated following the ASTM C109 method to determine compressive strength using a universal testing machine (MT-200S, Samyeon Tech., Daegu, South Korea). Curing periods were set to 3 days, 7 days, and 28 days. Mortar flowability was evaluated by following the ASTM C1437 method to determine mortar consistency. Thermal conductivity was determined following the ASTM E1461 method (Standard Test Method for Thermal Diffusivity by the Flash Method). Properties of mortar and biochar–mortar composites are summarized in Table 7.2. The pH and PZC of the biochar-mortar composite were 11.7~12.1, similar to that of mortar. By increasing the amount of biochar, carbon contents in the biochar–mortar composites accordingly increased. SEM images of mortar and biochar–mortar composites after 28 days of curing period are also summarized in Figure 7.3. Due to relatively low biochar contents (3~10%) in the biochar–mortar composites, crystalline and needle-shaped mortar structures in SEM images were not significantly changed. SEM-energy dispersive x-ray spectroscopy (EDX) analysis indicated that carbon contents of exposed surface gradually increased as the amount of biochar increased, consistent with carbon contents in Table 7.2.

Table 7.2. Properties of biochar–mortar composites.

				Elemental contents (wt%)			
		pH	PZC	C	H	O	N
Mortar		11.9	11.5	0.89	0.60	6.42	0.01
RS biochar-mortar composites	3% biochar	12.0	11.8	1.08	0.38	5.39	0.02
	5% biochar	12.1	11.8	1.35	0.37	6.01	0.03
	10% biochar	12.1	11.7	2.41	0.43	6.55	0.03
WC biochar-mortar composites	3% biochar	11.9	11.8	1.14	0.43	6.09	0.02
	5% biochar	12.1	11.8	1.84	0.44	7.23	0.03
	10% biochar	12.1	11.7	1.87	0.51	7.97	0.05

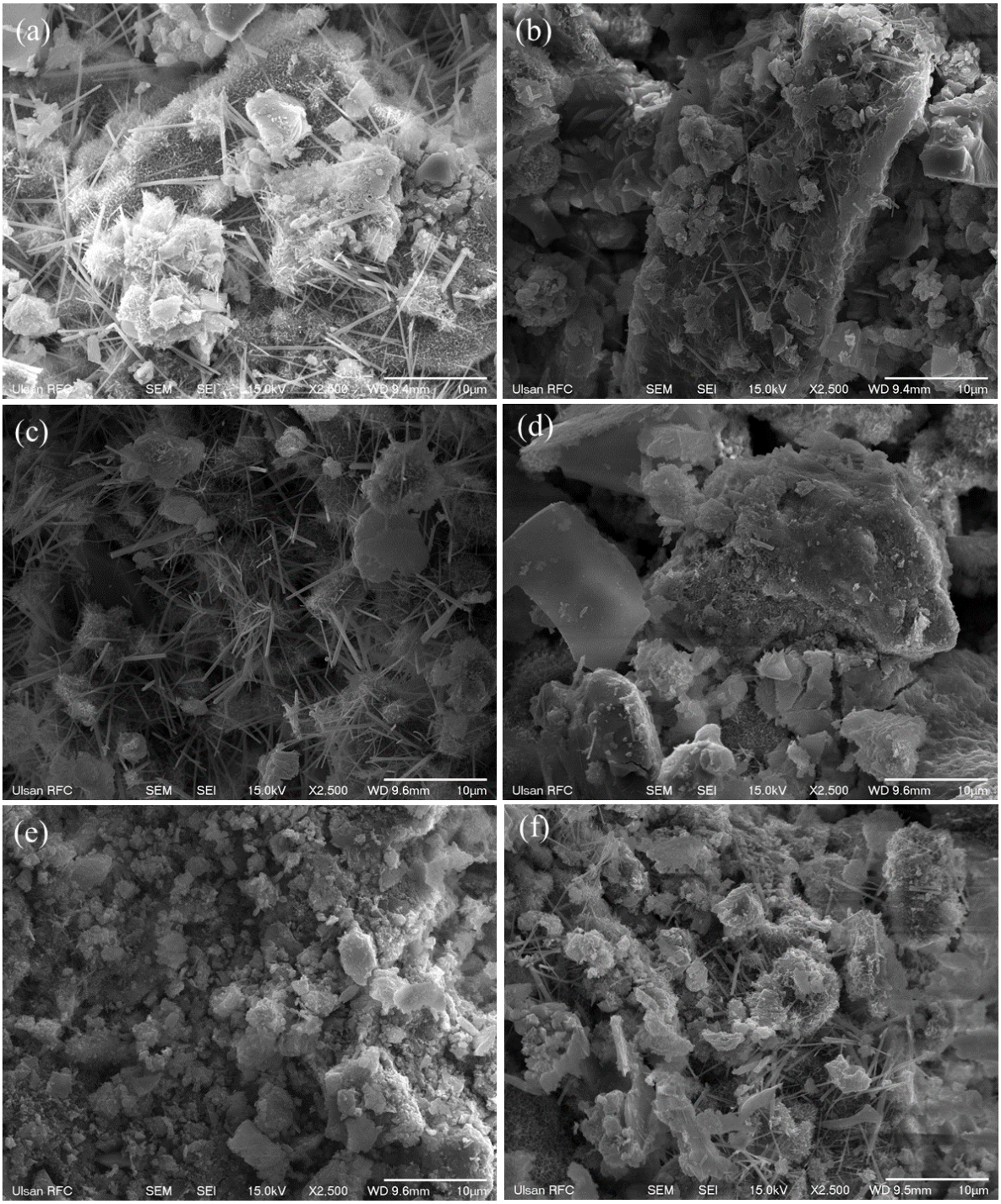

Figure 7.3. SEM images of biochar-mortar composites (a) Mortar only, (b) 3% RS biochar, and (c) 5% RS biochar, (d) 10% RS biochar, (e) 3% WC biochar, and (f) 5% WC biochar.

7.2.4. Chemical analysis

Phenol, DNT, TNT, RDX, and DCP were analyzed using a Dionex Ultimate® 3,000 HPLC (Sunnyvale, CA) equipped with a Dionex Acclaim® 120 guard column (4.3 mm×10 mm) and an Acclaim® 120 C-18 column (4.6 mm×250 mm, 5 μm). The analytical methods and conditions for quantifying contaminants are described in detail elsewhere [230], [318]. Pb concentration was determined by an atomic absorption spectrophotometer (AAS, 5100 ZL, Perkin Elmer, Waltham, MA) equipped with a graphite furnace. Concentrations of chromate (CrO_4^{2-}) and selenate (SeO_4^{2-}) were determined by Dionex ICS-1000 Ion Chromatography equipped with an Ionpac AS 22 column (4 mm×250 mm, Dionex, Sunnyvale, CA), and AG 22 guard column (4 mm×50 mm), and an AERS 500 suppressor (4 mm, 40 mA). A mixture of sodium carbonate (0.48 mM) and sodium bicarbonate (1.0 mM) was used as an eluent at a 1.5 ml/min flow rate. The injection volume was 125 μL, and the retention times for chromate and selenate were 20.7 min and 10.2 min, respectively. A calibration plot was performed for quantification purposes within the range of experimental concentrations used (coefficient of determination [R^2] greater than 0.99). Analytical duplicates, standards, and blank samples were used for quality control of the data.

Benzene and toluene were selected as compounds to determine the sorption capacity of biochar-mortar composites for volatile toxic contaminants. Biochar–mortar composites were crushed and ground to particles less than 0.85 mm (20 mesh). In a gas-tight syringe (A-2 series, VICI, Baton Rouge, FL), predetermined amounts of gas-phase compounds were put into 250 ml amber vials, including the biochar–mortar particles (5 g or 10 g). Then, the vials were sealed using Teflon® septa and screw-tight caps. After equilibrium was reached, gaseous samples were collected through the Mininert® valve using an airtight syringe. Benzene and toluene concentrations were measured using a gas chromatograph (GC, Agilent 7890B, Santa Clara, CA) equipped with a flame ionization detector (FID). A TCLP test was performed to confirm

the toxicity of the biochar mortar composite. The experiment was conducted according to the EPA Method 1311. The Microtox® bioassay test was conducted to confirm the results of the TCLP test. Procedures for the TCLP and Microtox® bioassay tests were described in detail in a previous paper [322].

7.3. Results and discussion

7.3.1. Sorption capacity of commercial biochars for various contaminants

Compared with the RS biochar synthesized in a laboratory, the commercial WC biochar had different characteristics. The PZC and pH were acidic (6.7 and 6.5, respectively) (Table 7.1), suggesting that the sorption of charged compounds to WC biochar may differ from that of RS biochar. WC biochar had a higher CEC (14.4 meq/100 g) and somewhat high BET surface area (55.3 m^2/g), favorable for cationic metal sorption. Due to a low pyrolysis temperature (400 ℃), the hydrogen and oxygen contents in WC biochar were also higher than those of RS biochar (Table 7.1), consistent with the XPS spectra shown in Figure 7.2. Compared with RS and WC biochar, BS biochar had a much higher BET surface area (122.8 m^2/g) and AEC (162.2~353.1 m^2/g), indicating favorable sorption of anionic compounds.

Compared with RS biochar, the sorption of nitro explosives by WC and BS biochar did not show a typical trend (Figure 7.4). According to Langmuir sorption isotherm models, BS biochar showed the highest maximum sorption capacity for TNT and RDX, 14.1 and 3.8 mg/g, respectively. WC biochar showed the lowest sorption capacity (7.5 and 0.9 mg/g for TNT and RDX, respectively). On the other hand, the sorption of DNT was lowest with BS biochar (4.2 mg/g), and the sorption of DNT to WC biochar (9.8 mg/g) was as high as that to RS biochar (10.2 mg/g).

The sorption mechanisms of DCP and phenol to biochar are somewhat different. It has been reported that the sorption of chlorophenols is affected by deprotonation of compounds,

surface charge, and hydrophobicity of biochar according to solution pH [123], [319]. As shown in Figure 7.4., WC and BS biochars are more favorable for the sorption of less deprotonated DCP due to the low pH of the biochars and low pK_a of DCP (7.90). According to Langmuir sorption isotherm models, the maximum sorption capacities of DCP for WC and BS biochars were 34.1 and 36.9 mg/g, respectively. The hydrophobicity of DCP is a function of pH [320], [321]. According to Nowosielski and Fein (1998) [320], log K_{ow} values of halogenated-phenols could be determined by the following equation:

$$\log K_{ow}(pH) - \log K_{ow}(n) - 2.9/\left(10^{(-1.4-pka+pH)} + 1\right) \quad \text{..... (1)}$$

Log K_{ow} (pH) is the log K_{ow} at the pH value of interest, and log K_{ow}(n) is the log K_{ow} of the neutral species. Thus, the estimated log K_{ow} of DCP at equilibrium pH (10.9, 8.3, and 6.5 as shown in Table 7.1) was 3.1, 0.56, and 0.30 for RS, BS, and WC biochars, respectively. The maximum sorption capacities of DCP to WC and BS biochars were significantly higher than that of RS biochar, indicating that hydrophobicity was not responsible for the sorption of DCP. Instead, the repulsive force arising from the deprotonation of DCP and the negative surface charge at equilibrium pH (10.9) accounted for the low sorption capacity of RS biochar for DCP. Similarly, the sorption of phenol was also affected by pH and surface charge. At equilibrium pH (8.3), less deprotonation of phenol (pK_a = 9.95) (compared with RS biochar) and the slightly negatively charged surface of BS biochar may facilitate the sorption of phenol, which showed a 3.3 mg/g maximum sorption capacity (Figure 7.4). Due to low log K_{ow} (−1.44) of phenol at equilibrium pH (6.5) according to the above estimation method (Nowosielski and Fein, 1998), extremely low deprotonation of phenol was not favorable for the sorption of phenol to WC biochar. The repulsive force between deprotonated phenol and the powerfully negatively charged surface of RS biochar also inhibited the sorption of phenol. The maximum sorption

capacities of WC and RS biochars are only 1.5 and 1.4 mg/g, respectively (Figure 7.5).

Sorption of cationic and anionic metals to biochar also showed a significant effect on pH. Regardless of BET surface area and CEC, RS biochar showed the highest sorption capacity for Pb (118 mg/g), according to Langmuir sorption isotherm models (Figure 7.6a). Though WC biochar had the highest CEC (14.4 meq/100 g) (Table 7.1), the capacity for Pb sorption was the lowest (8.6 mg/g), suggesting that ion exchange was not significantly involved. Instead, it appears that the biochar sorption capacity for Pb is correlated with equilibrium pH (Table 7.1 and Figure 7.6a), suggesting that surface precipitation at the biochar surface at elevated pH may be responsible. Similarly, RS biochar had the highest sorption capacities of chromate and selenate, 13.9 and 8.1 mg/g, respectively (Figure 7.6b and c). WC biochar had the lowest sorption capacity for chromate and selenate (0.2 and 2.0 mg/g, respectively). Considering PZC and equilibrium pH, the net surface charge of WC biochar was positive (Table 7.1). However, the sorption of chromate and selenate to WC biochar was by far less than that to RS and BS biochars.

Conversely, the sorption of chromate and selenate to the negatively charged surface of RS biochar is relatively significant, suggesting that electrostatic attraction may not be the driving force for the sorption of chromate and selenate. Elevated equilibrium pH is likely related to the sorption of chromate and selenate. Ligand exchange with hydroxyl functional groups on the biochar surface or co-precipitation with metal hydroxides at elevated pH may be responsible for the sorption of chromate and selenate. Overall, the performance of commercial WC biochar for the sorptive removal of contaminants from the water was not as good as that of RS biochar. The sorption capacity of WC biochar was competitive only for DNT and DCP, probably due to the high carbon contents and low equilibrium pH, respectively. The competitiveness in the sorption performance of BS biochar was limited for nitro explosives and phenols. For the sorption of cationic and anionic metals, WC and BS biochars did not show good performance.

On the other hand, RS biochar synthesized in a laboratory was a better sorbent to control the amount of cationic and anionic metals in water.

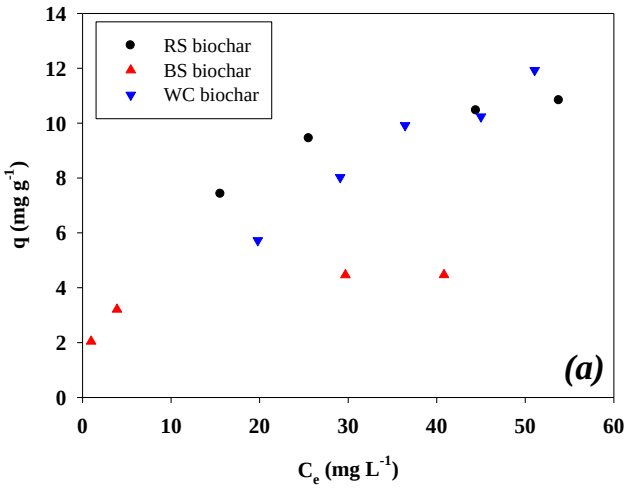

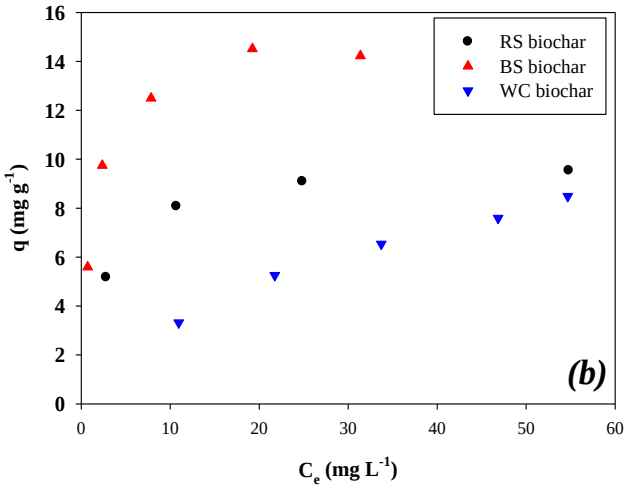

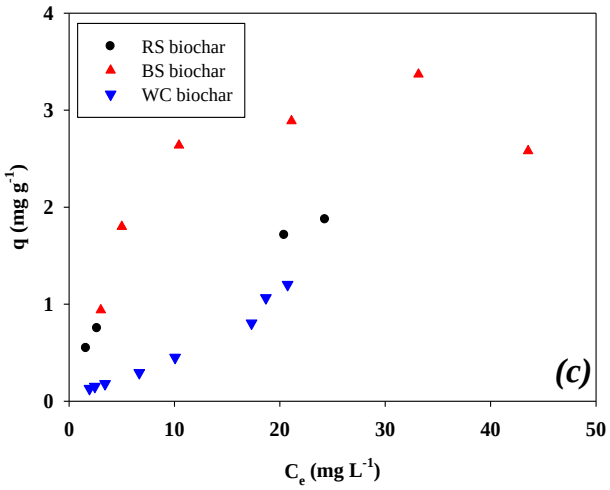

Figure 7.4. Sorption of (a) DNT, (b) TNT, and (c) RDX with RS, BS, and WC biochars.

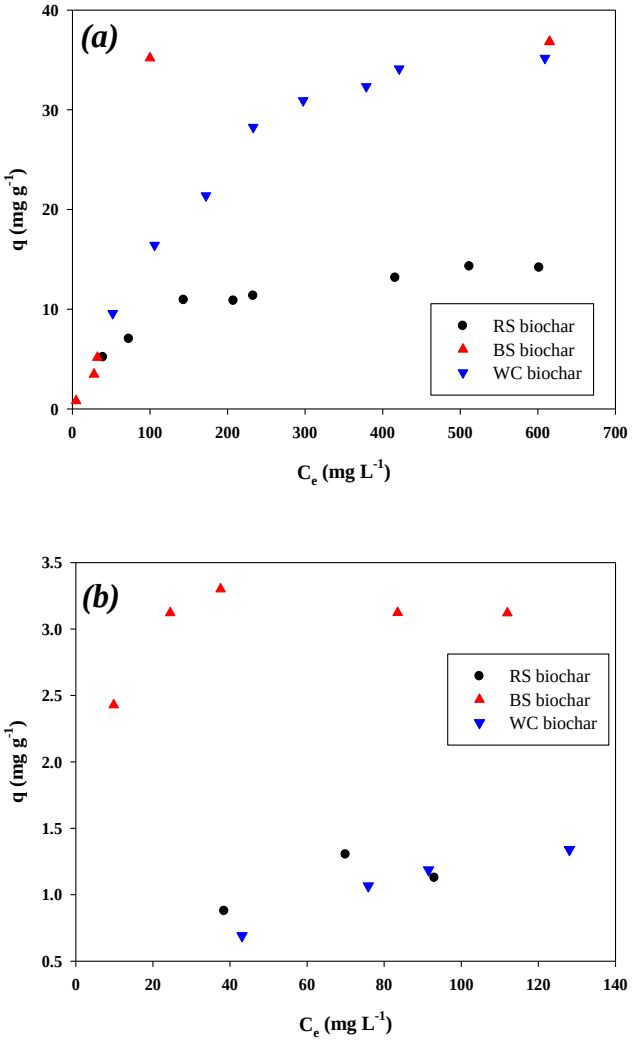

Figure 7.5. Sorption of (a) DCP and (b) phenols with RS, BS, and WC biochars.

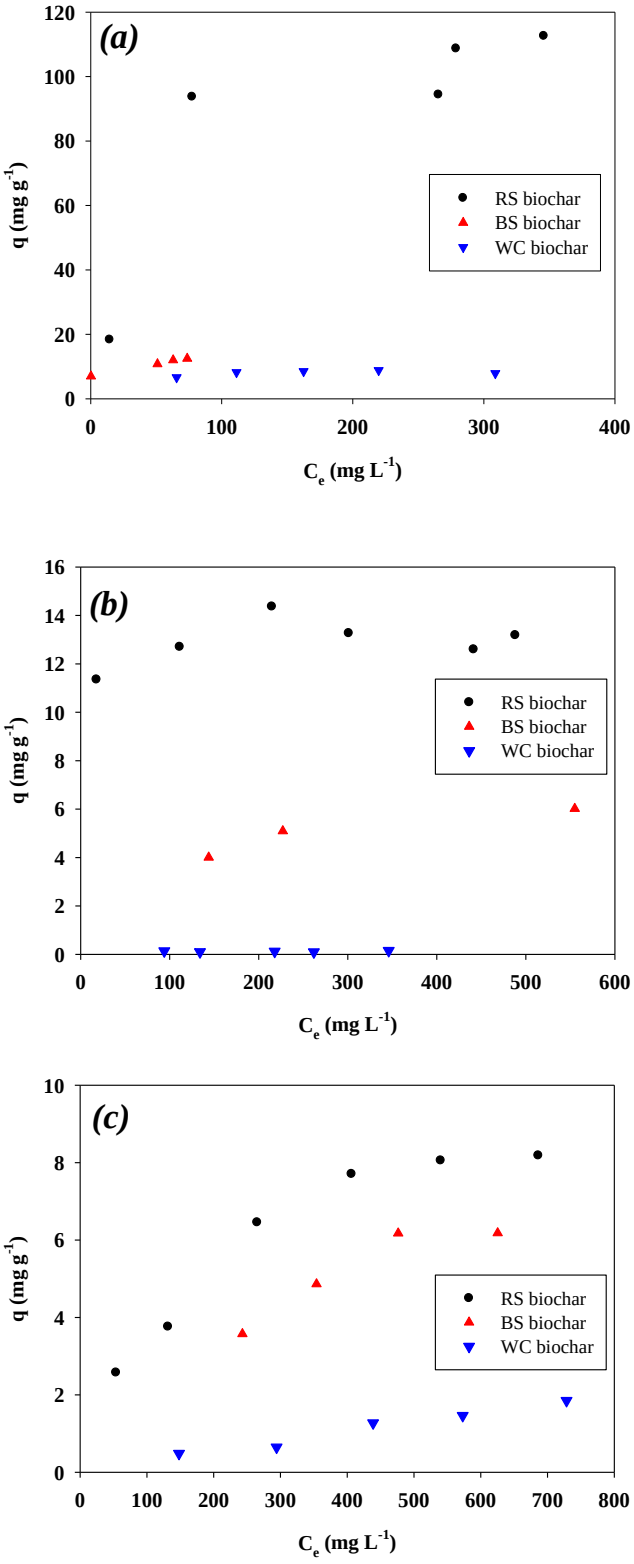

Figure 7.6. Sorption of (a) Pb, (b) CrO_4^{2-}, and (c) SeO_4^{2-} with RS, BS, and WC biochars.

7.3.2. Carbon sequestration with biochar-mortar composites

Carbon sequestration within construction material was examined by synthesizing biochar–mortar composites with WC and RS biochars. Regardless of biochar type, the PZC and pH of the biochar–mortar composites were close to those of the original mortar. By increasing the biochar percentage, the carbon content was slightly increased. However, other elements were not significantly changed due to their low contents in the biochar (Table 7.2). The mortar flowability of the biochar–mortar composites is summarized in Table 7.3. Compared to the control mortar without biochar, the biochar–mortar composites had lower flowability, probably due to the high water-holding capacity of biochar (1.82 mL/g and 1.64 mL/g for RS and WC biochars, respectively). Compared with the initial cone diameter (100 mm), 10% biochar in mortar resulted in a loss of flowability, suggesting that biochar content needs to be less than 10% for construction purposes. Biochar addition also decreased the compressive strength of mortar. As the curing period increased, the compressive strength gradually increased. Compared to the control mortar without biochar, a 3% addition of WC biochar to mortar showed 97% and 94% of the compressive strength in 7 days and 28 days, respectively (Figure 7.7). On the other hand, a 5% addition of WC biochar significantly decreased compressive strength, resulting in 59% of the compressive strength of the control mortar without biochar. For RS biochar, a 5% addition did not result in a decrease in compressive strength. Moreover, a 5% biochar addition slightly increased the compressive strength, resulting in 104% and 109%, respectively, of the control compressive strength after 7 days and 28 days. The advantage of adding RS biochar to mortar in terms of increasing compressive strength remains further examined. The thermal conductivity of the biochar–mortar composites did not show conclusive trends (Table 7.4). It is likely that an addition of 5% biochar slightly decreased thermal conductivity from 0.372 ± 0.054 W/m·K to 0.354 ± 0.067 W/m·K. Increasing biochar percentage to 10% may decrease thermal conductivity to 0.325 ±

0.012 W/m·K. However, considering errors, the effect of biochar on thermal conductivity may not be significant. The average value of biochar–mortar composites was 0.350 W/m·K, similar to gypsum. Overall, these results suggest that RS biochar may be more favorable for carbon sequestration without changing mortar properties. Thermal conductivity was not significantly changed with 5% biochar. Therefore, 5% biochar may be a critical threshold to maintain mortar properties for carbon sequestration.

Assuming the complete oxidation of carbon to CO_2 was $C + O_2 \rightarrow CO_2$, the CO_2 uptake as a form of biochar in the unit mass of biochar–mortar composites were calculated. According to the molar ratio in the stoichiometric reaction, 1 g of carbon can be fully converted to 3.67 g of CO_2. When 5% of RS and WC biochar was added to mortar, by subtracting the carbon content in mortar, carbon contents of the biochar–mortar composites due to the addition of biochar were 0.46% and 0.95%, respectively. Therefore, once 1 kg of biochar–mortar composites were made with the addition of 5% of RS or WC biochar, 16.9 or 34.9 g of CO_2 could be stored as a form of biochar in the biochar–mortar composites.

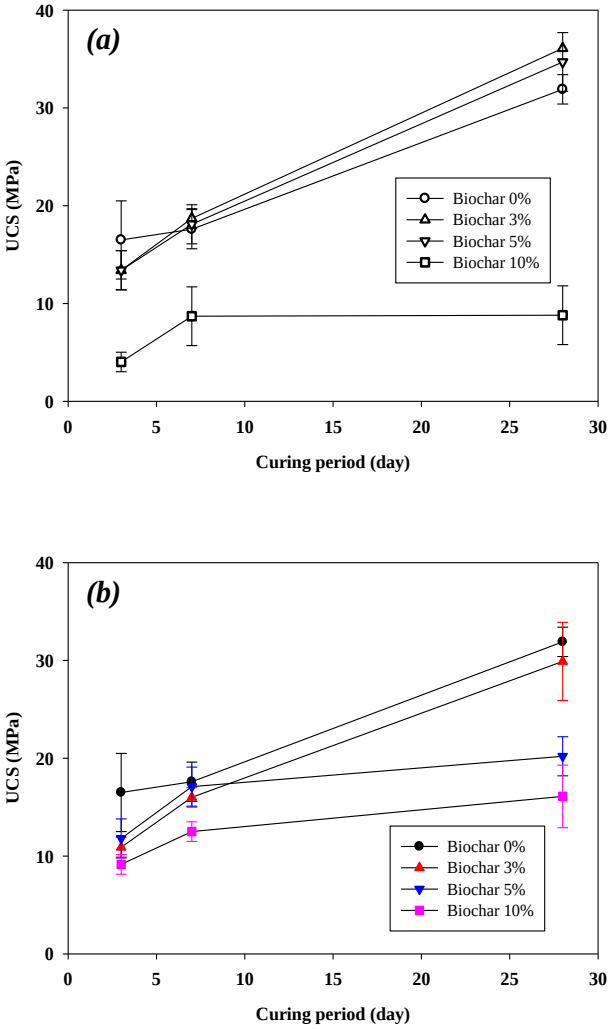

Figure 7.7. Compressive strength of biochar–mortar composites (a) RS biochar and (b) WC biochar at various curing periods.

Table 7.3. Mortar flowability of biochar–mortar composites (unit: mm, initial cone diameter: 100 mm).

Biochar content (%)	RS biochar-mortar composites	WC biochar-mortar composites
0	170	170
3	135	140
5	120	120
10	100	100

Table 7.4. Thermal conductivity of WC biochar–mortar composites.

Biochar content (%)	Thermal conductivity (W/m·K)
0	0.372 ± 0.054
5	0.354 ± 0.067
10	0.325 ± 0.012

Table 7.5. Concentrations (mg/L) of inorganic constituents in TCLP tests of biochar-mortar composites.

		Se	Ba	Cr	Cd	Pb	As	Ag	Hg
Regulatory level		1.0	100	5.0	1.0	5.0	5.0	5.0	0.2
RS biochar		0.04	0.49	-*	-	-	-	-	-
WC biochar		0.05	0.22	-	-	-	-	-	-
Mortar		0.05	0.38	0.14	-	-	-	-	-
RS biochar-mortar composites	3% biochar	0.05	0.46	0.12	-	-	-	-	-
	5% biochar	0.05	0.54	0.11	-	-	-	-	-
	10% biochar	0.04	0.40	0.10	-	-	-	-	-
WC biochar-mortar composites	3% biochar	0.04	0.41	0.08	-	-	-	-	-
	5% biochar	0.04	0.57	0.02	-	-	-	-	-
	10% biochar	0.04	0.58	0.04	-	-	-	-	-

* Not determined.

7.3.3. Environmental properties of biochar-mortar composites

Sick building syndrome is a severe and increasing concern for residents in condominium complexes in newly developed areas in South Korea. Benzene and toluene are well-known volatile contaminants that contribute to this syndrome. The results of benzene and toluene sorption to the biochar–mortar composites are summarized in Figure 7.8. In the presence of control mortar without biochar, only 9~10% of the benzene and toluene in the gas phase were removed. As biochar was added, the removal of benzene and toluene gradually increased regardless of biochar type. With 5% and 10% biochar addition, approximately 30% and 40% of the benzene and toluene were removed, respectively, suggesting that biochar may enhance the removal of benzene and toluene from the atmosphere. Due to high surface area and carbon content, it may be favorable for biochar–mortar composites to adsorb gas-phase contaminants in indoor environments. A TCLP test was performed to confirm toxicity in biochar-mortar composites. The leachate's total organic carbon (TOC) concentration after the TCLP procedure was less than 0.05 mg/L. Thus, organic compounds in a TCLP regulation list were excluded. The levels of inorganic constituents found via TCLP testing are summarized in Table 7.5. Concentrations of TCLP contaminant inorganic components (Se, Ba, Cr, Cd, Pb, As, Ag, and Hg) in the two biochar, mortar, and biochar–mortar composites (regardless of biochar content) were significantly lower than the regulatory level (Table 7.5.). This indicates that the compound is not hazardous. This indicates that the compound is not hazardous. Results from the Microtox® bioassay of the biochar, mortar, and biochar–mortar composites showed no decrease in the luminescence of Vibrio fischeri, indicating that there was no toxic effect of biochar–mortar composites on luminous bacteria. These results suggest that using biochar– mortar composites as construction materials may be a safe option to reduce sick building syndrome without exerting harmful effects on living creatures in indoor environments.

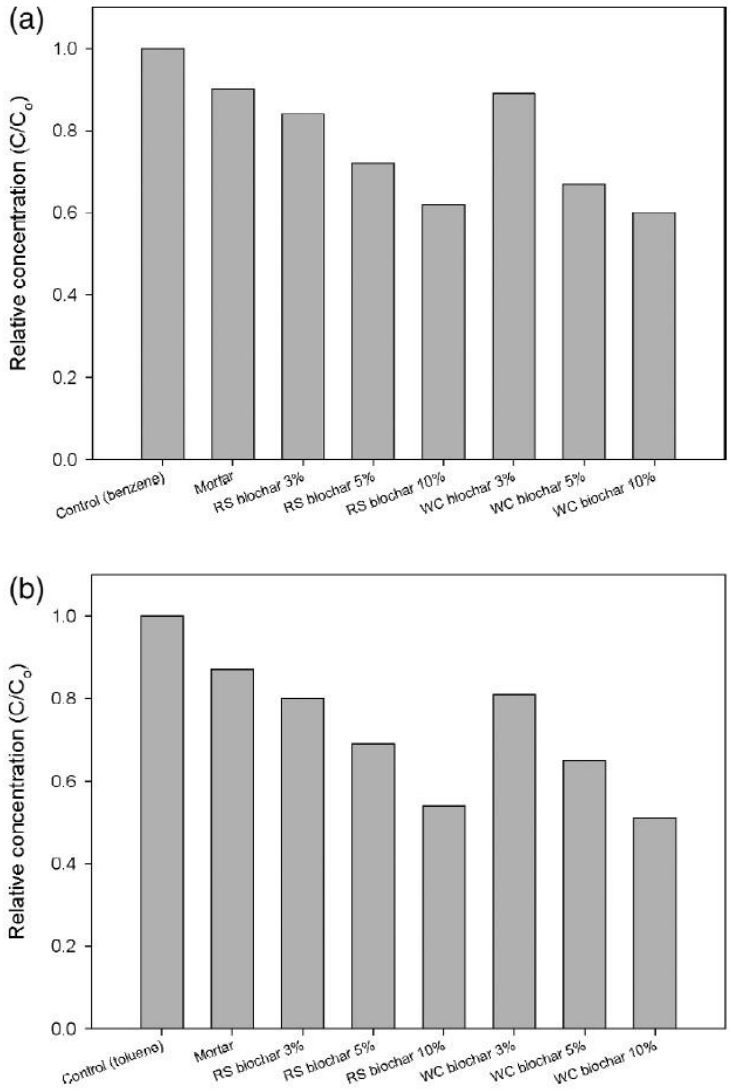

Figure 7.8. Removal of (a) benzene and (b) toluene from the atmosphere by biochar–mortar composites. The initial concentrations of benzene and toluene were 48.7~50.1 and 51.5~55.4 ppm, respectively.

7.4. Conclusions

In this study, the performance of commercially available biochars in carbon sequestration and sorptive removal of contaminants was evaluated. This study showed that the performance of commercial WC biochar and BS biochar as a sorbent was limited for some specific types of contaminants, as determined by sorption mechanisms. The sorption capacity of WC biochar was competitive only for DNT and DCP. The competitiveness of BS biochars in sorption performance was limited for nitro explosives and phenols. In an analysis of potential carbon sequestration with biochar–mortar composites, the construction properties of biochar–mortar composites were improved or unchanged with the addition of WC or RS biochar to mortar. The optimal biochar content level was 3–5% of the initial cement content in mortar. By increasing the biochar percentage in the mortar, removal of benzene and toluene from the atmosphere was enhanced, which means biochar–mortar composites may be beneficial in preventing sick building syndrome. According to the TCLP tests and Microtox®bioassay, the biochar–mortar composites did not show any toxicity.

The results suggest that carbon sequestration in the form of biochar– mortar composites may be a promising approach for mitigating CO_2 release without disturbing the engineering properties of the mortar. The effects of biochar on thermal conductivity and the sorption mechanisms of benzene and toluene to biochar–mortar composites need to be further examined.

Chapter 8. Conclusions

In this study, after synthesizing biomass into biochar through pyrolysis, we intend to study various application methods to increase the value of biochar. To this end, we further investigated the performance of biochar as a catalyst and an adsorbent through a series of batch experiments. Afterward, biochar mortars were fabricated and examined for their potential as building materials for carbon sequestration.

Experimental results showed that biochar has a porous structure and a high surface area, favorable features for removing nitro explosives and toxic cationic metals. Compared with GAC, biochar is an effective sorbent for removing Cd, Cu, Pb, and Zn from contaminated water. Compared with graphite and GAC, some biochars can also effectively sorb nitro explosives. Correlation analysis showed that nitro explosives' sorption capacity is related to BET surface area and carbon content. It was found that the sorption capacity of biochar for cationic toxic metals is significantly affected by pH, CEC, O:C, and H:C. XPS and blocking experiments unveil that surface functional groups are responsible for the sorption of cationic metals to biochar. On the other hand, carbon contents account for the sorption of nitro explosives, possibly through π–π EDA interaction and hydrophobic sorption.

In the case of halogenated phenol, triclosan, and ibuprofen removal confirmed that BS biochar was effective due to its high surface area compared to other biochars. The sorption of compounds to biochar relies on the compound's hydrophobicity, the surface area of biochar, and solution pH. Electrostatic interactions (mostly repulsion) and hydrophobic sorption are the main mechanisms to explain the sorption of the compounds to biochar. The sorption was not affected by ionic strength, whereas it was changed by dissolved humic acid. These results suggest that specific conditions may be required to remove ionizable organic compounds from water and soil using biochar. The involvement of other possible mechanisms, such as π-π EDA interactions and hydrogen bonding, remains to be determined.

In the case of Fe(0)-biochar using an iron-containing material, TNT, RDX, DBP, and DFP were rapidly removed. Fe(0)-biochar reduced contaminants in the water to create a reduced product. XANES and XPS analysis showed that even if Fe(0) was pyrolyzed together with rice straw, it did not change the redox properties of Fe(0). Surface blocking experiments showed that surface functional groups might also be an electron transfer mediator in reducing sorbed molecules with Fe(0)-biochar.

It was confirmed that the presence of polymer also improved the properties of biochar when pyrolyzed with biomass waste. Increasing carbon content and the development of surface functional groups significantly enhanced the sorption capacity of DNT and Pb on polymer/RS-derived biochar. However, the addition of polymer did not change the catalytic role of the biochar. These results suggest that the aromatic structure and surface functional groups of biochar may influence the catalytic properties.

Finally, we evaluated the performance of commercially available biochars for atmospheric carbon sequestration and contaminant adsorption removal. The results showed that the performance of commercial WC biochar and BS biochar as a sorbent was limited for some specific types of contaminants, as determined by sorption mechanisms. The sorption capacity of WC biochar was competitive only for DNT and DCP. The BS biochars in sorption were limited for nitro explosives and phenol removal. In an analysis of potential carbon sequestration with biochar–mortar composites, the construction properties of biochar–mortar composites were improved or unchanged with the addition of WC or RS biochar to mortar. The optimal biochar content level was 3–5% of the initial cement content in mortar. Removal of benzene and toluene from the atmosphere was improved by increasing the biochar ratio in the mortar, and the biochar-mortar composite was not toxic according to the TCLP test and Microtox® bioassay. This means that biochar-mortar composites may help prevent sick house syndrome.

Biochar suggests that it could be an attractive and alternative option for environmental

improvement for various organic pollutants and cationic metals, including nitro explosives and halogenated-phenol pharmaceuticals, through sorption and immobilization. However, biochar may contain toxic substances during manufacturing because of the significant influence of raw materials, so careful management is required to apply it to soil and water. The novel Fe(0)-biochar is a promising active strategy material as a catalyst to sorb and transform redox-sensitive contaminants for long-term remedial action on contaminated soils and sediments. Polymer/RS-derived biochar using polymer improved the properties of existing biochar and improved the adsorption capacity of DNT and Pb. Carbon sequestration in the form of biochar-mortar composites as one of the biochar utilization options suggests that it may be a promising approach to mitigate CO_2 emissions without compromising the engineering properties of the mortar.

References

[1] Dyer, G. 2011. “Climate wars the fight for survival as the world overheats”, Oxford: Oneworld, UK.

[2] Myeong S.J. 2018. “Impact of climate change-related natural disasters on rice production in South Korea”, J. Korean Soc. Hazard Mitig., 18(7):53-60.

[3] Myeong, S.J. 2014. “Agriculture under UNFCCC and Its policy implications”, J. Clim., 5(4):313-321.

[4] Hong, Y.C. 2008. “Climate change and human health”, J. Korean. Med. Assoc, 51(8):765-769.

[5] Lee, S.I., Kim, G.Y., Gwon, H.S., Lee, J.S., Choi, E.J., and Shin, J.D. 2020. “Effects of different nitrogen fertilizer and biochar applications on CO_2 and N_2O emissions from upland soil in the closed chamber”, Korean J. Soil Sci. Fert., 53(4):431-445.

[6] Fuss, S., Canadell, J.G., Peters, G.P., Tavoni, M., Andrew, R.M., Ciais, P., Jackson, R.B., Jones, C.D., Kraxner, F., Nakicenovic, N., Quéré, C.L., Raupach, M.R., Sharifi, A., Smith, P., and Yamagata, Y. 2014. “Betting on negative emissions”, Nature, 4:850-853.

[7] Lehmann, J. 2007. “A Handful of Carbon”, Nature, 447, 143-144.

[8] Marchetti, C. 1977, “On geoengineering and the CO_2 problem”, Climatic Change, 1:59-68.

[9] Lehmann, J., Gaunt, J., and Rondon, M. 2006. “Biochar sequestration in terrestrial ecosystems -a review”, Mitig. Adapt. Strateg. Glob. Chang, 11:403-427.

[10] IPCC. 2000. "Emission scenarios", Cambridge University Press, UK. 570.

[11] Batjes, N.H. 1998. “Mitigation of atmospheric CO_2 concentrations by increased carbon sequestration in the soil”, Biol. Fertil. Soils, 27(3):230~235.

[12] Izaurralde, R.C., Rosenberg, N.J., and Lai, L. 2001. “Mitigation of climatic change by soil carbon sequestration: issues of science, monitoring, and degraded lands” Adv. Agron., 70:1~75.

[13] Scholes, R.J., and Noble, I.R. 2001. "Storing carbon on land", Science, 294(5544):1012-1013.

[14] Schlesinger, W.H. 1990. “Evidence from chronosequence studies for a low carbon-storage potential of soils”, Nature, 348:232-234.

[15] Richter, D.D., Markewitz, D., Trumbore S.E., and Wells, C.G. 1999. “Rapid accumulation and turnover of soil carbon in a re-establishing forest”, Nature, 400:56-58.

[16] Post, W.M., and Kwon, K.C. 2000. “Soil carbon sequestration and land-use change: processes and potential”, Glob Chang Biol, 6:317-327.

[17] Schlesinger, W.H., and Lchter, J. 2001. “Limited carbon storage in soil and litter of experimental forest plots under increased atmospheric CO_2”, Nature, 411(6836):466~469.

[18] Lehmann J., and Joseph S. 2009. "Biochar for the environmental management", Science and technology. Earthscan, Washington, DC.

[19] Basu, P. 2013. “Biomass gasification, pyrolysis, and torrefaction: practical design and theory", 2nd ed, Academic Press, USA.

[20] Park, J.J. 2019. “Experimental study on the characteristics of slow pyrolysis and vapor

phase reactions for biomass particles", Ph.D. Dissertation, Sungkyunkwan University, Seoul, Korea.

[21] Atkinson, C.J., Fitzgerald, J.D., and Hipps, N.A. 2010. "Potential mechanisms for achieving agricultural benefits from biochar application to temperate soils: a review", Plant. Soil, 337:1~18.

[22] Werner, C., Kiese, R., and Butterbach-Bahl, K. 2007. "Soil-atmosphere exchange of N_2O, CH_4, and CO_2 and controlling environmental factors for tropical rain forest sites in western Kenya", J. Geophys. Res, 112:1-15.

[23] Choi, I.W., Seo, D.C., Kang, S.W., Lee, S.G., Seo, Y.J., Heo, J.S., and Cho, J.S. 2013. "Adsorption characteristics of heavy metals using sesame waste biochar", Korean J. Soil. Sci. Fert, 46(1):8-15.

[24] Chen, B., Chen, Z., and Lv, S. 2011a. "A novel magnetic biochar efficiently sorbs organic pollutants and phosphate", Bioresour. Technol, 102:716-723.

[25] Inyang, M., Gao, B., Yao, Y., Xue, Y., Zimmerman A.R., Pullammanappallil, P., and Cao, X. 2012. "Removal heavy metals from aqueous solution by biochars derived from anaerobically digested biomass", Bioresour. Technol, 110:50-56.

[26] Kung, C.C., Zhang, N. 2015. "Renewable energy from pyrolysis using crops and agricultural residuals: an economic and environmental evaluation", Energy part 2, 90:1532-1544.

[27] Verheijen, F., Jeffery, S., Bastos, A.C., Velde der van, M., and Diafas, I. 2010. "Biochar application to soils - a critical scientific review of effects on soil properties, processes and functions", JRC Sci., Rep, European Commission. doi: 10.2788/472.

[28] Ahmad, M., Lee, S.S., Dou, X., Mohan, D., Sung, J.K., Yang, J.E., and Ok, Y.S. 2012. "Effects of pyrolysis temperature on soybean stover-and peanut shell-derived biochar properties and TCE adsorption in water", Bioresour. Technol, 118:536-544.

[29] Kim, J.Y., Oh, S.Y., and Park, Y.K. 2020. “Overview of biochar production from preservative-treated wood with detailed analysis of biochar characteristics, heavy metals behaviors, and their ecotoxicity”, J. Hazard. Mater, 384:121356 https://doi.org/10.1016/j.jhazmat.2019.121356.

[30] Brassard, P., Godbout, S., Lévesque, V., Palacios, J.H., Raghavan, V., Ahmed, A., Hogue, R., Jeanne, T., and Verma, M. 2019. “Biochar for soil amendment”, char and carbon materials derived from biomass", 1st ed, Elsevier INC, Netherlands.

[31] Kumar, N.S., Shaikh, H.M., Asif, M., and Al-Ghurabi, E.H. 2021. “Engineered biochar from wood apple shell waste for high-efficient removal of toxic phenolic compounds in wastewater”, Nature, 11:2586 https://doi.org/10.1038/s41598-021-82277-2.

[32] Huang, P., Ge, C., Feng, D., Yu, H., Luo, J., Li, J., Strong, P.J., Sarmah, A.K., Bolan, N.S., and Wang, H. 2018a "Effects of metal ions and pH on ofloxacin sorption to cassava residue-derived biochar", Sci. Total. Environ, 616–617:1384–1391.

[33] Huang, S., Bao, J., Shan, M., Qin, H., Wang, H., Yu, X., Chen, J., and Xu, Q. 2018b. "Dynamic changes of polychlorinated biphenyls (PCBs) degradation and adsorption to biochar as affected by soil organic carbon content", Chemosphere 211:120–127.

[34] Chi, N.T.L, Anto, S., Ahamed, T.S., Kumar, S.S., Shanmugam, S., Samuel, M.S.,

Mathimani, T., Brindhadevi, K., and Pugazhendhi, A. 2021. “A review on biochar production techniques and biochar-based catalyst for biofuel production from algae”, Fuel, 287:119411.

[35] Cao, X. Sun, S., and Sun, R. 2017. “Application of biochar-based catalysts in biomass upgrading: a review”, RSC adv, 7:48793-48805.

[36] Yuan, Y., Bolan, N., Prévoteau, A., Vithanage, M., Biswas, J. K., Ok, Y.S., and Wang, H. 2017. "Applications of biochar in redox-mediated reactions", Bioresour. Technol, 246:271-281.

[37] Brown, T.R., Wright, M.M., and Brown, R.C. 2011. “Estimating profitability of two biochar production scenarios: slow pyrolysis vs fast pyrolysis”, Biofuels. Bioprod. Bioref, 5:54－68.

[38] Marris, E. 2006. “Putting the carbon back: black is the new green”, Nature, 442(7103):624-626

[39] Woo, S.H. 2013. “Biochar for soil carbon sequestration”, Clean Technology, 19(3):201~211

[40] Transparency Market Research. 2017. “Biochar market (feedstock-woody biomass, agricultural waste, and animal manure; application-electricity generation, agriculture, and forestry) – global industry analysis, size, share, growth, trends, and forecast 2017–2025, https://www.transparencymarketresearch.com/report-toc/2863.

[41] Bridgwater, A.V., Meier, D., and Radlein, D. 1999. “An overview of fast pyrolysis of biomass”, Org. Geochem, 30(12):1479-1493.

[42] Mohan, D., Pittman Jr., C.U., and Steele, P.H. 2006. "Pyrolysis of wood/biomass for bio-oil: a critical review", Energy Fuels. 20:848–889.

[43] Antal, M.J., and Grønli, M. 2003. “The art, science, and technology of charcoal production”, Ind. Eng. Chem. Res. 42:1619-1640.

[44] Enders, A., Hanley, K., Whitman, T., Joseph, S., and Lehmann, J., 2012. “Characterization of biochars to evaluate recalcitrance and agronomic performance”, Bioresour. Technol, 114:644-653.

[45] Blasi, C.D., Signorelli, G., Russo, C.D., and Rea, G. 1999. “Product distribution from pyrolysis of wood and agricultural residues”, Ind. Eng. Chem. Res. 38:2216-2224.

[46] Chen, D., Zhou, J., and Zhang, Q. 2014. “Effects of heating rate on slow pyrolysis behavior, kinetic parameters and products properties of Moso bamboo”, Bioresour. Technol, 169:313-319.

[47] Xiao, R., Chen, X., Wang, F., and Yu, G. 2010. “Pyrolysis pretreatment of biomass for entrained-flow gasification”, Appl. Energy, 87:149-155.

[48] Phan, N.A., Ruy, C., Sharifi, V.N., and Swithenbank, J. 2008. “Characterization of slow pyrolysis products from segregated wastes for energy production”, J. Anal. Appl. Pyrolysis, 81(1):65-71.

[49] Ortiz, O.A., Martinez, N.D., Mengual, C.A., and Abally, P.M. 2007. “Optimal operation profit of a pilot rotary kiln for charcoal activation”, Lat. Am. Appl. Res, 37, 2007-2013.

[50] Ronsse F. 2013. "Commercial biochar production and its certification", Interreg.

Conference.

[51] Lehmann, J. 2007. "Bio-energy in the black", Front. Ecol. Environ. 5:381–387.

[52] Lian, F., Huang, F., Chen, W., Xing, B., and Zhu, L. 2011. “Sorption of apolar and polar organic contaminants by waste tire rubber and its chars in single-and bi-solute systems”, Environ. Pollut. 159:850-857.

[53] Huang, H., Wang, Y.X., Tang, J.C., Zhu, W.Y. 2014 "Properties of maize stalk biochar produced under different pyrolysis temperatures and its sorption capability to naphthalene”, Environ. Sci. 35(5):1884.

[54] Yuan, J.H., Xu, R.K., and Zhang, H. 2011. "The forms of alkalis in the biochar produced from crop residues at different temperatures", Bioresour. Technol. 102:3488–3497.

[55] Lehmann, J., and Joseph, S. 2015. "Biochar for the environmental management science, technology, and implementation", 2nd ed. Earthscan, New York .

[56] Bruun, E.W., Ambus, P., Egsgaard, H., and Hauggaard-nielsen, H. 2012. "Effects of slow and fast pyrolysis biochar on soil C and N turnover dynamics", Soil. Biol. Biochem. 46:73–79.

[57] Sadaka, S., and Boateng, A.A., 2009. “Pyrolysis and bio-oil”, agriculture and natural resources, University of Arkansas, U.S. Dept. of Agriculture and county governments cooperating, USA, 1-6.

[58] Silber, A., Levkovitch, I., and Graber E.R. 2010. “pH-dependent mineral release and surface properties of corn straw biochar: agronomic implications”, Environ. Sci. Technol. 44:9318-9323.

[59] Novak, J.M., Busscher, W.J., Laird, D.A., Ahmedna, M., Watts, D.W., and Niandou, M.A.S. 2009. "Impact of biochar amendment on fertility of a Southeastern coastal plain soil", Soil Sci. 174:105–112.

[60] Chintala, R., Mollinedo, J., Schumacher, T.E., Malo, D.D., Julson, J. 2014. "Effect of biochar on chemical properties of acidic soil", Arch. Agron. Soil. Sci, 60(3):393–404.

[61] Suliman, W., Harsh, J.B., Abulail, N.I., Fortuna, A., Dallmeyer, I., and Garcia-Perez, M. 2016. "Influence of feedstock source and pyrolysis temperature on biochar bulk and surface properties", Biomass Bioenergy 84:37–48.

[62] Li, H., Cao, Y., Zhang, D., and Pan, B. 2018. "pH-dependent K_{ow} provides new insights into understanding the adsorption mechanism of ionizable organic chemicals on carbonaceous materials", Sci. Total. Environ, 618:269–275.

[63] Bansal, R.C., Donnet, J.B., and Stoeckli, F. 1988 "Active carbon", Marcel Dekker, New York, 158.

[64] Al-Wabel, M.I., Al-Omran, A., El-Nagger, A.H., Nadeem, M., and Usman, A.R. 2013. "Pyrolysis temperature-induced changes in characteristics and chemical composition of biochar produced from Conocarpus wastes", Bioresour. Technol, 131(3):374–379.

[65] Brown, R.A., Kercher, A.K., Nguyen, T.H., Nagle, D.C., and Ball, W.P. 2006. "Production and characterization of synthetic wood chars for use as surrogates for natural sorbents", Org. Geochem, 37(3):321–333.

[66] Anton-Herrero, R., Garciadelgado, C., Alonsoizquierdo, M., Garciarodriguez, G., Cuevas,

J., and Eymar, E. 2018. "Comparative adsorption of tetracyclines on biochars and stevensite: looking for the most effective adsorbent", Appl. Clay. Sci, 160:162–172.

[67] Gul, S., Whalen, J.K., Thomas, B.W., Sachdeva, V., and Hongyuan, D. 2015. "Physico-chemical properties and microbial responses in biochar-amended soils: mechanisms and future directions", Agric. Ecosyst. Environ, 206(1):46–59.

[68] Wang, H. 2015. "Removal of Pb(II), Cu(II), and Cd(II) from aqueous solutions by biochar derived from $KMnO_4$ treated hickory wood", Bioresour. Technol, 197(9):356–362.

[69] Lee, J.W., Kidder, M., Evans, B.R. 2010. "Characterization of biochars produced from corn stovers for soil amendment", Environ. Sci. Technol, 44(20):7970–7974.

[70] Clough, T.J., and Condron, L.M. 2010. "Biochar and the nitrogen cycle: introduction", J. Environ. Qual, 39:1218–1223.

[71] Kalinke, C., Oliveira, P.R., Oliveira, G.A., Mangrich, A.S., Marcolino-Jr, L.H., Bergamini, M.F. 2017. "Activated biochar: preparation, characterization and electroanalytical application in an alternative strategy of nickel determination", Anal. Chim. Acta, 983:103–111.

[72] Suliman, W., Harsh, J.B., Fortuna, A., Garcia-Perez, M., Abulail, N.I. 2017. "Quantitative effects of biochar oxidation and pyrolysis temperature on the transport of pathogenic and nonpathogenic Escherichia coli in biochar-amended sand columns", Environ. Sci. Technol, 51:5071–5081.

[73] Shinogia, Y., and Kanri, Y. 2003. "Pyrolysis of plant, animal and human waste: physical and chemical characterization of the pyrolytic products", Bioresour. Technol, 90:241–247.

[74] Moreno-Castilla, C. 2004. "Adsorption of organic molecules from aqueous solutions on carbon materials", Carbon, 42:83–94.

[75] Kinney, T.J., Masiello, C.A., Dugan, B., Hockaday, W.C., Dean, M.R., Zygourakis, K., and Barnes, R.T. 2012. "Hydrologic properties of biochars produced at different temperatures", Biomass Bioenergy, 41:34–43.

[76] Hammes, K., Torn, M.S., Lapenas, A.G., and Schmidt, M.W.I. 2008. "Centennial black carbon turnover observed in a Russian steppe soil", Biogeosciences, 5(5):1339–1350.

[77] Leng, L.J., Huang, H.J., Li, H., Li, J., and Zhou, W.G. 2019. "Biochar stability assessment methods: a review", Sci. Total. Environ, 647:210–222.

[78] Sun, X., Han, X.G., Ping, F., Zhang, L., Zhang, K.S., Chen, M., and Wu, W.X. 2018. "Effect of rice straw biochar on nitrous oxide emissions from paddy soils under elevated CO_2 and temperature", Sci. Total. Environ, 628:629–1009.

[79] Schmidt, H.P. 2012. 55 uses of biochar, Ithaka-journal, 286-289.

[80] Zwieten, L.V., Kimber, S., Morris, S., Chan, K.Y., Downie, A., Rust, J., Joseph, S., and Cowie, A. 2010. "Effects of biochar from slow pyrolysis of papermill waste on agronomic performance and soil fertility", Plant. Soil, 327(1/2):235–246.

[81] Steiner, C., Glaser, B., Teixeira, W.G., Lehmann, J., Blum, W.E.H., and Zech, W. 2008. "Nitrogen retention and plant uptake on a highly weathered central Amazonian ferralsol amended with compost and charcoal", J. Plant. Nutr. Soil. Sci, 171(6):893–899.

[82] Glaser, B., Lehmann, J., and Zech, W. 2002. "Ameliorating physical and chemical properties of highly weathered soils in the tropics with charcoal—a review", Biol. Fertil. Soils, 35(4):219–230.

[83] Benjamin, M.C.F., Stefano, M.L.M., Monica, G., Mark, S., and Johnson, S.W. 2019. "Lyon improving agricultural water use efficiency with biochar-a synthesis of biochar effects on water storage and fluxes across scales", Sci. Total. Environ, 657:853–862.

[84] Masulili, A., Utomo, W.H., and Syechfani, M.S. 2010. "Rice husk biochar for rice-based cropping system in acid soil 1. The characteristics of rice husk biochar and its influence on the properties of acid sulfate soils and rice growth in west Kalimantan, Indonesia", J. Agric. Sci. 2(1):39–47.

[85] Muhammad, S., Lukas, V.Z., Saqib, B., Aneela, Y., Avelino, N., Muhammad, A.C., Kashif, A.K., Umeed, A., Muhammad, S.R., Mirza, A.M., and Ronggui, H. 2018. "A concise review of biochar application to agricultural soils to improve soil conditions and fight pollution", J. Environ. Manag, 228:429–440.

[86] Kavitha, B., Reddy, P.V.L., Kim, B.J., Lee, S.S., Pandey, S.K., and Kim, K.H. 2018. "Benefits and limitations of biochar amendment in agricultural soils: a review", J. Environ. Manag, 227:146–154.

[87] Chen, W., Meng, J., Han, X., Lan, Y., and Zhang, W. 2019. “Past, present, and future of biochar”, Biochar, 1:75-87.

[88] Luo, Y., Durenkamp, M., De Nobili, M., Lin, Q., Devonshire, B.J., and Brookes, P.C. 2013. "Microbial biomass growth, following incorporation of biochars produced at 350 °C or 700 °C, in a silty-clay loam soil of high and low pH", Soil. Biol. Biochem,

57:513-523.

[89] Jeffery, S., Verheijen, F.G., Van Der Velde, M., and Bastos, A.C. 2011. "A quantitative review of the effects of biochar application to soils on crop productivity using meta-analysis", Agric. Ecosyst. Environ, 144(1):175-187.

[90] Cao, Y., and Pawłowski, A. 2013. "Life cycle assessment of two emerging sewage sludge-to-energy systems: evaluating energy and greenhouse gas emissions implications", Bioresour. Technol, 127:81–91.

[91] Zimmerman, A.R., Gao, B., Ahn, M.Y. 2011. "Positive and negative carbon mineralization priming effects among a variety of biochar-amended soils", Soil. Biol. Biochem, 43:1169–1179.

[92] Jia, J., Li, B., Chen, Z., Xie, Z., and Xiong, Z. 2012. "Effects of biochar application on vegetable production and emissions of N_2O and CH_4", Soil. Sci. Plant. Nutr, 58(4):503–509.

[93] Cayuela, M.L., Van Zwieten, L., Singh, B.P., Jeffery, S., Roig, A., and Sánchez-Monedero, M.A. 2014. "Biochar's role in mitigating soil nitrous oxide emissions: a review and meta-analysis", Agric. Ecosyst. Environ, 191:5–16.

[94] Shaheen, S.M., Niazi, N.K., Hassan, N.E.E., Bibi, I., Wang, H., Tsang, D.C.W., Ok, Y.S., Bolan, N., and Rinklebe, J. 2019. "Wood-based biochar for the removal of potentially toxic elements in water and wastewater: a critical review", Int. Mater. Rev, 64(4):216–247.

[95] Yang, X., Wan, Y., Zheng, Y., He, F., Yu, Z., Huang, J., Wang, H., Ok, Y.S., Jiang, Y., and Gao, B. 2019. "Surface functional groups of carbon-based adsorbents and their roles

in the removal of heavy metals from aqueous solutions: a critical review", Chem. Eng. J, 366:608–621.

[96] Xia, S., Song, Z., Jeyakumar, P., Bolan, N., and Wang, H. 2019. “Characteristics and applications of biochar for remediating Cr(VI)-contaminated soils and wastewater”, Environ Geochem Health, 42:1543-1567

[97] Bogusz, A., Nowak, K., Stefaniuk, M., Dobrowolski, R., and Oleszczuk, P. 2017. "Synthesis of biochar from residues after biogas production with respect to cadmium and nickel removal from wastewater", J. Environ. Manag, 201:268–276.

[98] He, L., Fan, S., Müller, K., Wang, H., Che, L., Xu, S., Song, Z., Yuan, G., Rinklebe, J., Tsang, D.C.W., Ok, Y.S., and Bolan, N. 2018. "Comparative analysis biochar and compost-induced degradation of di-(2-ethylhexyl) phthalate in soils", Sci. Total. Environ, 625:987–993.

[99] Chen, Y., Jiang, Z., Wu, D., Wang, H., Li, J., Bi, M., and Zhang, Y. 2019. "Development of a novel bio-organic fertilizer for the removal of atrazine in soil", J. Environ. Manag, 233:553–560.

[100] Czernik, S., and Bridgwater, A.V. 2004. "Overview of applications of biomass fast pyrolysis oil", Energy Fuels. 18:590–598.

[101] Abdullah, H., and Wu, H. 2009. “Biochar as a fuel: 1. properties and grindability of biochars produced from the pyrolysis of mallee wood under slow-heating conditions”, Energy Fuels, 23(8):4174-4181.

[102] Wijayanta, A.T., Alam, M.S., Nakaso, K., Fukai, J., Kunitomo, K., and Shimizu, M. 2014. "Combustibility of biochar injected into the raceway of a blast furnace", Fuel.

Process. Technol, 117:53–59.

[103] Jiang, K.M., Cheng, C.G., Ran, M., Lu, Y.G., and Wu, Q.L. 2018. "Preparation of a biochar with a high calorific value from chestnut shells", New. Carbon. Mater, 33(2):183–187.

[104] Fagbohungbe. M.O., Herbert, B.M. J., Hurst, L., Ibeto, C.N., Li, H., Usmani, S.Q., and Semple., K.T. 2017. “The challenges of anaerobic digestion and the role of biochar in optimizing anaerobic digestion”, Waste Manage, 61:236-249.

[105] Kumar, A., Kumar, A., Sharma, G., Naushad, M., Stadler, F.J., Ghfar, A.A., Dhiman, P., and Saini, R.V. 2017. "Sustainable nano-hybrids of magnetic biochar supported g-C_3N_4/$FeVO_4$ for solar-powered degradation of noxious pollutants-synergism of adsorption, photocatalysis & photo-ozonation", J. Clean. Prod, 165:431–451.

[106] Qiu, Y., Xiao, X., Cheng, H., Zhou, Z., and Sheng, G.D. 2009. "Influence of environmental factors on pesticide sorption by black carbon: pH and model dissolved organic matter", Environ. Sci. Technol, 43:4973–4978.

[107] Keiluweit, M., Nico, P.S., Johnson, M.G., and Kleber, M. 2010. "Dynamic molecular structure of plant biomass-derived black carbon (biochar)", Environ. Sci. Technol, 44:1247–1253.

[108] Dong, X., Ma, L.Q., and Li, Y. 2011. "Characteristics and mechanisms of hexavalent chromium removal by biochar from sugar beet tailing", J. Hazard. Mater, 190:909–915.

[109] Agrafioti, E., Kalderis, D., and Diamadopoulos, E. 2014. "Arsenic and chromium removal from water using biochars derived from rice husk, organic solid wastes and

sewage sludge", J. Environ. Manage, 133:309–314.

[110] Igalavithana, A.D., Mandal, S., Niazi, N.K., Vithanage, M., Parikh, S.J., Mukome, F.N., Rizwan, M., Oleszczuk, P., Al-Wabel, M., Bolan, N., and Tsang, D.C. 2017. "Advances and future directions of biochar characterization methods and applications", Crit. Rev. Environ. Sci. Technol, 47(23):2275–2330.

[111] Ambaye, T.G., Vaccari, M., Hullebusch, E.D.V., Amrane, A., and Rtimi, S. 2020. "Mechanisms and adsorption capacities of biochar for the removal of organic and inorganic pollutants from industrial wastewater", Inter. J. Environ. Sci & Tech, 1-22.

[112] Rizwan, M., Ali, S., Qayyum, M.F., Ibrahim, M., Rehman, M.Z., Abbas, T., and Ok, Y.S. 2016. "Mechanisms of biochar-mediated alleviation of toxicity of trace elements in plants: a critical review", Environ. Sci. Pollut. Res, 23:2230–2248.

[113] Ali, S., Rizwan, M., Qayyum, M.F., Ok, Y.S., Ibrahim, M., Riaz, M., Arif, M.S., Hafeez, F., Al-Wabel, M.I., and Shahzad, A.N. 2017. "Biochar soil amendment on alleviation of drought and salt stress in plants: a critical review", Environ. Sci. Pollut. R, 24:12700–12712.

[114] Trakal, L., Veselská, V., Šafařík, I., Vítková, M., Číhalová, S., and Komárek, M. 2016. "Lead and cadmium sorption mechanisms on magnetically modified biochars", Biores. Technol, 203:318–324.

[115] Puga, A.P., Abreu, C.A., Melo, L.C.A., and Beesley, L. 2016. "Biochar application to a contaminated soil reduces the availability and plant uptake of zinc, lead & cadmium", J. Environ. Manag, 159:86–93.

[116] Mohan, D., and Pittman Jr, C.U. 2007. "Arsenic removal from water/wastewater using adsorbents-a critical review", J. Hazard. Mater, 142:1–53.

[117] Liu, Z., and Zhang, F.S. 2009. "Removal of lead from water using biochars prepared from hydrothermal liquefaction of biomass", J. Hazard. Mater, 167:933–939.

[118] Cao, X., Ma, L., Gao, B., and Harris, W. 2009. "Dairy-manure derived biochar effectively sorbs lead and atrazine", Environ. Sci. Technol. 43:3285–3291.

[119] Zhang, H., Wang, Z., Li, R., Guo, J., Li, Y., Zhu, J., and Xie, X. 2017. "TiO_2 supported on reed straw biochar as an adsorptive and photocatalytic composite for the efficient degradation of sulfamethoxazole in aqueous matrices", Chemosphere, 185:351-365.

[120] Zhang, X., Wang, H., He, L., Lu, K. Sarmah, A., Li, J., Bolan, N.B., Pei, J., Huang, H. 2013a. "Using biochar for remediation of soils contaminated with heavy metals and organic pollutants", Environ. Sci. Pollut. Res, 20:8472–8483.

[121] Zhang, W., Mao, S., Chen, H., Huang, L., and Qiu, R. 2013b. "Pb(II) and Cr(VI) sorption by biochars pyrolyzed from the municipal wastewater sludge under different heating conditions", Bioresour. Technol, 147:545–552.

[122] Sun. K., Ro, K., Guo, M., Novak, J., Mashayekhi, H., and Xing, B. 2011. "Sorption of bisphenol A, 17α-ethinyl estradiol and phenanthrene on thermally and hydrothermally produced biochars", Bioresour. Technol, 102:5757–5763.

[123] Ahmad, M., Rajapaksha, A.U., Lim, J.E., Zhang, M., Bolan, N., Mohan, D., Vithanage, M., Lee S.S., and Ok, Y.S. 2014. "Biochar as a sorbent for contaminant management in soil and water: a review", Chemosphere. 99:19–33.

[124] Zheng, H., Wang, Z., Zhao, J., Herbert, S., and Xing, B. 2013. "Sorption of antibiotic sulfamethoxazole varies with biochars produced at different temperatures", Environ. Pollut, 181:60–67.

[125] Spokas, K.A., 2010. "Review of the stability of biochar in soils: predictability of O:C molar ratios", Carbon Manage. 1:289–303.

[126] Sun, Y., Gao, B., Yao, Y., Fang, J., Zhang, M., Zhou, Y., Chen, H., and Yang, L. 2014. "Effects of feedstock type, production method, and pyrolysis temperature on biochar and hydrochar properties", Chem. Eng. J, 240:574–578.

[127] Zhu, D., and Pignatello, J.J. 2005. "Characterization of aromatic compound sorptive interactions with black carbon (charcoal) assisted by graphite as a model", Environ. Sci. Technol. 39:2033–2041.

[128] Li, J.M., Cao, L.R., Yuan, Y., Wang, R.P., Wen, Y.Z., and Man, J.Y. 2018. "Comparative study for microcystin-LR sorption onto biochars produced from various plant- and animal-wastes at different pyrolysis temperatures: influencing mechanisms of biochar properties", Bioresour. Technol, 247:794–803.

[129] Chen, X., Chen, G., Chen, L., Chen, Y., Lehmann, J., McBride, M.B., and Hay, A.G. 2011b. "Adsorption of copper and zinc by biochars produced from pyrolysis of hardwood and corn straw in aqueous solution", Bioresour. Technol, 102:8877–8884. https ://doi.org/10.1016/j.biort ech.2011.06.078

[130] Wang, X., Guo, Z., Hu, Z., and Zhang, J. 2020. “Recent advances in biochar application for water and wastewater treatment: a review”, PeerJ, 8:e9164.

[131] Liu, D. Ding, Z. Ali, E.F., Kheir, A.M.S, Eissa, M.A., and Ibrahim, O.H.M. 2021.

"Biochar and compost enhance soil quality and growth of roselle (hibiscus sabdariffa L.) under saline conditions", Nature, 11:1.

[132] Woolf, D., Amonette, J.E., Street-Perrott, F.A., Lehmann, J., and Joseph, S. 2010. "Sustainable biochar to mitigate global climate change", Curr. Sci, 1:1–9.

[133] Cha, J.S., Park, S.H., Jung, S.C., Ryu, C.K, Jeon, J.K., Shin, M.C., and Park, Y.K. 2016. "Production and utilization of biochar: a review", J. Ind. Eng. Chem, 40:1-15.

[134] Kambo, H.S., and Dutta, A. 2015. "A comparative review of biochar and hydrochar in terms of production, physico-chemical properties, and applications", Renew. Sust. Energ. Rev, 45:359-378.

[135] Rajapaksha, A.U., Chen, S.S., Tsang, D.C.W., Zhang, M., Vithanage, M., Mandal, S., Gao, B., Bolan, N.S., and Ok, Y.S. 2016, "Engineered/designer biochar for contaminant removal/immobilization from soil and water: potential and implication of biochar modification", Chemosphere, 148:276-291.

[136] Bartholomew, C.H., Farrauto, R.J. 2005. "Fundamentals of industrial catalytic processes", 2nd Edition, John Wiley & Sons, USA, New York.

[137] Lin, Y.C., and Huber, G.W. 2009. "The critical role of heterogeneous catalysis in lignocellulosic biomass conversion", Energy Environ. Sci, 2:68-80.

[138] Su, Y., Fan, B., Wang, L., Liu, Y., Huang, B., Fu, M., Chen, L., and Ye, D. 2013. "MnOx supported on carbon nanotubes by different methods for the SCR of NO with NH_3", Catal. Today, 201:115-121.

[139] Johnson, L., Thielemans, W., and Walsh, D.A. 2011. "Synthesis of carbon-supported Pt

nanoparticle electrocatalysts using nanocrystalline cellulose as reducing agent", Green Chem, 13:1686.

[140] Ma, M., Dai, Y., Zou, J. L., Wang, L., Pan, K., and Fu, H. G. 2014. "Synthesis of iron oxide/partly graphitized carbon composites as a high-efficiency and low-cost cathode catalyst for microbial fuel cells", ACS Appl. Mater. Interfaces, 6:13438-13447.

[141] Chen, T., Li, D. Jiang, H., and Xiong, C. 2015. "High-performance Pd nanoalloy on functionalized activated carbon for the hydrogenation of nitroaromatic compounds", Chem. Eng. J, 259:161-169.

[142] Klinghoffer, N.B., Castaldi, M.J., and Nzihou, A. 2015. "Influence of char composition and inorganics on catalytic activity of char from biomass gasification", Fuel, 157:37-47.

[143] Perander, M., Demartini, N., Brink, A., Kramb, J., Karlströma, O., Hemming, J., Moilanen, J., Konttinen, J., and Hupa, M. 2015. "Catalytic effect of Ca and K on CO_2 gasification of spruce wood char", Fuel, 150:464-472.

[144] Liu, W.J., Jiang, H., and Yu, H.Q. 2015. "Development of biochar-based functional materials: toward a sustainable platform carbon material", Chem Rev 115(22):12251–12285.

[145] Sheng, Y., and Zhu, L. 2018. "Biochar alters microbial community and carbon sequestration potential across different soil pH", Sci. Total. Environ., 622-623:1391-1399.

[146] Blanco-Canqui, H., 2017. "Biochar and soil physical properties", Soil Sci. Soc. Am. J,

81(4):687–711.

[147] El-Naggar, A., Awad, Y.M., Tang, X.Y., Liu, C., Niazi, N.K., Jien, S.H., Tsang, D.C.W., Song, H., Yong, S.O., and Sang, S.L., 2018. "Biochar influences soil carbon pools and facilitates interactions with soil: a field investigation", Land. Degrad.Dev, 29:2162-2171.

[148] Lamb, M.C., Sorensen, R.B., Butts, C.L. 2018. “Crop response to biochar under differing irrigation levels in the southeastern USA”, J. Crop Improv, 32 (3):305-317.

[149] Liu, Q., Zhang, Y., Liu, B., Amonette, J.E., Lin, Z., Liu, G., Ambus, P., and Xie, Z. 2018. "How does biochar influence soil N cycle? a meta-analysis", Plant Soil, 426 (15):1-15.

[150] Shi, R.Y., Li, J.Y., Jiang, J., Kamran, M.A., Xu, R.K., and Qian, W. 2018. "Incorporation of corn straw biochar inhibited the re-acidification of four acidic soils derived from different parent materials. Environ. Sci. Pollut. Res. 25:9662–9672.

[151] Wang, Y., Liu, Y., Liu, R., Zhang, A., Yang, S., Liu, H., Yang, Z., and Yang, Z. 2017. "Biochar amendment reduces paddy soil nitrogen leaching but increases net global warming potential in Ningxia irrigation, China”, Sci. Rep, 7:1592–1602.

[152] Bashir, S., Hussain, Q., Akmal, M., Riaz, M., Hu, H., Ijaz, S.S., Iqbal, M., Abro, S., Mehmood, S., and Ahmad, M. 2017. "Sugarcane bagasse-derived biochar reduces the cadmium and chromium bioavailability to mash bean and enhances the microbial activity in contaminated soil", J. Soils Sediments, 18:3-4.

[153] Martin, S.M., Kookana, R.S., Van Zwieten, L., and Krull, E. 2012. "Marked changes in herbicide sorption–desorption upon ageing of biochars in soil", J. Hazard. Mater,

231:70–78.

[154] Lorenz, K., and Lal, R. 2005. "The depth distribution of soil organic carbon in relation to land use and management and the potential of carbon sequestration in subsoil horizons", Adv. Agron. 88:35–66.

[155] Sohi, S.P., Krull, E., Lopez-Capel, E., and Bol, R. 2010. “Chapter 2 - a review of biochar and its use and function in soil”, Adv. Agron., 105:47-82.

[156] Ciais, P., Wattenbach, M., Vuichard, N., Smith, P., Piao, S. L., Don, A., Luyssaert, S., Janssens, I.A., Bondeau, A., Dechow, R., Leip, A., Smith, P. C., Beer, C., Van DerWerf, G. R., Gervois, S., Van-Oost, K., Tomelleri, E., Freibauer, A., Schulze, and E.D., CARBOEUROPE, Synthesis Team. 2010. "The european carbon balance. part 2: croplands", Glob. Change Biol. 16, 1409–1428.

[157] Oguntunde, P.G., Fosu, M., Ajayi, A.E., van de Giesen, N. 2004. "Effects of charcoal production on maize yield, chemical properties and texture of soil", Biol. Fertil. Soils, 39:295–299.

[158] Blackwell, P., Riethmuller, G., and Collins, M. 2009. "Biochar application to soil", Earthscan, London, UK, pp. 207–226.

[159] Liu, X., Zhang, A., Ji, C., Joseph, S., Bian, R., Li, L., Pan, G., and Paz-Ferreiro, J. 2013. "Biochar’s effect on crop productivity and the dependence on experimental conditions—a meta-analysis of literature data", Plant Soil, 373:583–594.

[160] Yamato, M., Okimori, Y., Wibowo, I.F., Anshori, F., and Ogawa, M. 2006. "Effects of the application of charred bark of Acacia mangium on the yield of maize, cowpea and peanut, and soil chemical properties in South Sumatra, Indonesia", Soil Sci. Plant

Nutr, 52:489–495.

[161] Manya`, J.J. 2012. "Pyrolysis for biochar purposes: a review to establish current knowledge gaps and research needs", Environ. Sci. Technol, 46:7939–7954.

[162] Spokas, K.A., Cantrell, K.B., Novak, J.M., Archer, D.W., Ippolito, J.A., Collins, H.P., Boateng, A.A., Lima, I.M., Lamb, M.C., McAloon, A.J., Lentz, R.D., and Nichols, K.A. 2012. "Biochar: a synthesis of its agronomic impact beyond carbon sequestration", J. Environ. Qual, 41:973–989.

[163] Lehmann, J., da Silva, J.P., Steiner, C., Nehls, T., Zech, W., and Glaser, B. 2003. "Nutrient availability and leaching in an archaeological anthrosol and a ferralsol of the central Amazon basin: fertilizer, manure and charcoal amendments", Plant Soil, 249:343–357.

[164] Biederman, L.A., and Harpole, W.S. 2013. "Biochar and its effects on plant productivity and nutrient cycling: a meta-analysis", GCB-Bioenerg, 5:202–214.

[165] Busscher, W.J., Novak, J.M., Evans, D.E., Watts, D.W., Niandou, M.A.S., and Ahmedna, M. 2010. "Influence of pecan biochar on physical properties of a Norfolk loamy sand", Soil Sci, 175:10–14.

[166] Ameloot, N., Graber, E.R., Verheijen, F.G.A., and De Neve, S. 2013. "Interactions between biochar stability and soil organisms: review and research needs", Eur. J. Soil. Sci, 64:379–390.

[167] Lehmann, J., Rillig, M.C., Thies, J., Masiello, C.A., Hockaday, W.C., and Crowley, D.

2011. "Biochar effects on soil biota—a review", Soil Biol. Biochem. 43:1812–1836.

[168] Glaser, B. 2007, "Prehistorically modified soils of central Amazonia: a model for sustainable agriculture in the twenty-first century", Phil. Trans. R. Soc. B, 362:187–196.

[169] Brewer, C.E., Schmidt-Rohr, K., Satrio, J.A., and Brown, R.C. 2009. "Characterization of biochar from fast pyrolysis and gasification systems", Environ. Prog. Sus. Energ, 28:386–396.

[170] Mao, J.D., Johnson, R.L., Lehmann, J., Olk, D.C., Neves, E.G., and Thompson, M.L. 2012. "Abundant and stable char residues in soils: implications for soil fertility and carbon sequestration", Environ. Sci. Technol, 46:9571–9576.

[171] Lorenz, K., and Lal, R. 2014. “Biochar application to soil for climate change mitigation by soil organic carbon sequestration”, J. Plant. Nutr. Soil. Sci, 177:651-670.

[172] Solomon, D., Lehmann, J., Wang, J., Kinyangi, J., Heymann, K., Lu, Y., Wirick, S., and Jacobsen, C. 2012. “Micro- and nano-environments of C sequestration in soil: A multi-elemental STXM–NEXAFSassessment of black C and organomineral associations”, Environ. Sci. Technol, 438:372–388.

[173] Roberts, K.G., Gloy, B.A., Joseph, S., Scott, N.R., and Lehmann, J., 2010. "Life cycle assessment of biochar systems: estimating the energetic, economic, and climate change potential", Environ. Sci. Technol, 44:827-833.

[174] Kuzyakov, Y., Subbotina, I., Chen, H., Bogomolova, I., and Xu, X. 2009. "Black carbon decomposition and incorporation into soil microbial biomass estimated by 14C labeling", Soil Biol. Biochem, 41:210–219.

[175] Cheng, C.H., Lehmann, J., and Engelhard, M.H. 2008. "Natural oxidation of black carbon in soils: changes in molecular form and surface charge along a climosequence", Geochim. Cosmochim. Acta, 72:1598–1610.

[176] Qambrani, N.A., Rahman, M.M., Won, S.G., S, S.M., and Ra, C.S. 2017. "Biochar properties and eco-friendly applications for climate change mitigation, waste management, and wastewater treatment: a review", Renew. Sust. Energ. Rev., 79:255-273.

[177] Shafie, S.T., Salleh, M.A.M., Hang, L.L., Rahman, M.M., and Abdul Karim Ghani, W.A.W. 2012. "Effect of pyrolysis temperature on the biochart nutrient and water retention capacity", J Environ Eng (New York), 1(6):323-337.

[178] Watson, R.T., Noble, I.R., Bolin, B., and Dokken, D.J. 2000. "Land use, land-use change, and forestry. in intergovernmental panel on climatic change special report", Cambridge University Press, UK. 875.

[179] Liu, Y., Yang, M., Wu, Y., Wang, H., Chen, Y., and Wu, W. 2011. "Reducing CH_4 and CO_2 emissions from waterlogged paddy soil with biochar", J. Soil. Sediment, 11(6):930–9.

[180] Feng, Y., Xu, Y., Yu, Y., Xie, Z., and Lin, X. 2012. "Mechanisms of biochar decreasing methane emission from Chinese paddy soils", Soil. Biol. Biochem, 46:80–88.

[181] Spokas, K.A., Koskinen, W.C., Baker, J.M., and Reicosky, D.C. 2009. "Impacts of woodchip biochar additions on greenhouse gas production and sorption/degradation of two herbicides in a Minnesota soil", Chemosphere, 77(4):574–581.

[182] Yanai, Y., Toyota, K., and Okazaki, M. 2007. "Effects of charcoal addition on N_2O

emissions from soil resulting from rewetting air-dried soil in short-term laboratory experiments", Soil. Sci. Plant. Nutr, 53(2):181–188.

[183] Taghizadeh-Toosi A, Clough, T.J., Condron, L.M., Sherlock, R.R., Anderson, C.R., and Craigie, R.A. 2011. "Biochar incorporation into pasture soil suppresses in situ nitrous oxide emissions from ruminant urine patches", J. Environ. Qual, 40(2):468–476.

[184] Singh B.P., Hatton, B.J., Singh, B., Cowie, A.L., and Kathuria, A. 2010. "Influence of biochars on nitrous oxide emission and nitrogen leaching from two contrasting soils", J. Environ. Qual, 39(4):1224–1235.

[185] Bruun, E.W., Müller-Stöver, D., Hauggaard-Nielsen, P.A.H. 2011. “Application of biochar to soil and N_2O emissions: potential effects of blending fast-pyrolysis biochar with anaerobically digested slurry”, Eur. J. Soil. Sci, 62(4):581-589.

[186] Zhang A, Cui, L., Pan, G., Li, L., Hussain, Q., Zhang, X., Zheng, J., and Crowley, D. 2010. "Effect of biochar amendment on yield and methane and nitrous oxide emissions from a rice paddy from Tai Lake plain, China", Agric. Ecosyst. Environ, 139(4):469–475.

[187] Castaldi, S., Riondino, M., Baronti, S., Esposito, F.R., Marzaioli, R., Rutigliano, F.A., Vaccari, F.P., and Miglietta, F. 2011. "Impact of biochar application to a Mediterranean wheat crop on soil microbial activity and greenhouse gas fluxes", Chemosphere, 85(9):1464–1471.

[188] Dell, R.M., and Rand, D.A.J. 2001. “Energy storage-a key technology for global energy sustainability”, J. Power. Sour, 100:2-17.

[189] Linares, N., Silvestre-Albero, A.M., Serrano, E., Silvestre-Albero, J., and Garcia-Martinez, J. 2014. “Mesoporous materials for clean energy technologies”, Chem. Soc. Rev, 43:7681-7717.

[190] Lee, H.W., Kim, Y.M., Kim, S.D., Ryu, C.K., Park, S.H., and Park, Y.K. 2018. “Review of the use of activated biochar for energy and environmental applications”, Carbon Letters, 26:1-10.

[191] Chun, Y., Sheng, G., Chiou, C.T., and Xing, B. 2004. "Compositions and sorptive properties of crop residue-derived chars", Environ. Sci. Technol. 38:4649–4655.

[192] Chen, B., Zhou, D., and Zhu, L. 2008. "Transitional adsorption and partition of nonpolar and polar aromatic contaminants by biochar of pine needles with different pyrolytic temperatures", Environ. Sci. Technol. 42:5137–5143.

[193] Yang, Y., and Sheng, G. 2003. "Enhanced pesticide sorption by soils containing particulate matter-from crop residue burns", Environ. Sci. Technol, 37:3635–3639.

[194] Yang, Y., Chun, Y., Sheng, G., and Huang, M. 2004. "pH-dependence of pesticide adsorption by wheat-residue-derived black carbon", Langmuir, 20:6736–6741.

[195] Sheng, G., Yang, Y., Huang, M., and Yang, K. 2005. "Influence of pH on pesticide sorption by soil containing wheat residue-derived char", Environ. Pollut. 134:457–463.

[196] Sander, M., and Pignatello, J.J. 2005. "Characterization of charcoal adsorption sites for aromatic compounds: Insights drawn from single-solute and bi-solute competitive experiments", Environ. Sci. Technol. 39:1606–1615.

[197] Rio, S., C. Faur-Brasquet, L. Le Coq, and P. Le Cloirec. 2005. "Structure characterization and adsorption properties of pyrolyzed sewage sludge", Environ. Sci. Technol. 39:4249–4257.

[198] Jindarom, C., Meeyoo, V., Kitiyanan, B., Rirksomboon, T., and Rangsunvigit, P. 2007. "Surface characterization and dye adsorptive capacities of char obtained from pyrolysis/gasification of sewage sludge", Chem. Eng. J. 133:239–246.

[199] Loganathan, V.A., Feng, Y., Sheng, G.D., and Clement, T.P. 2009. "Crop residue derived char influences sorption, desorption, and bioavailability of atrazine in soils", Soil Sci. Soc. Am. J. 73:967–974.

[200] Zhou, Z., D. Shi, Y. Qiu, and D. Sheng. 2010. "Sorptive domains of pine chars as probed by benzene and nitrobenzene", Environ. Pollut. 158:201–206.

[201] Yakkala, K., Yu, M.R., Yang, J.K., and Chang, Y.Y. 2013. "Adsorption of TNT and RDX contaminants by ambrosia trifida l.var. trifida derived biochar", Res. J. Chem. Environ. 17:62–71.

[202] Seredych, M., and Badosz, T.J. 2006. "Removal of copper on composite sewage sludge/industrial sludge-based adsorbents: The role of surface chemistry", J. Colloid. Interface. Sci, 302:379–388.

[203] Machida, M., Mochimaru, T. and Tatsumoto, H. 2006. "Lead(II) adsorption onto the graphene layer of carbonaceous materials in aqueous solution", Carbon 44:2681–2688.

[204] Mohan, D., Pittman, Jr, C.U., Bricka, M., Smith, F., Yancey, B., Mohammad, J., Steele, P.H., Alexandre-Franco, M.F., Gómez-Serrano, V., and Gong, H. 2007. "Sorption of

arsenic, cadmium, and lead by chars produced from fast pyrolysis of wood and bark during bio-oil production", J. Colloid Interface Sci. 310:57–73.

[205] Lima, I.M., Boateng, A.A., and Klasson, K.T. 2009. "Pyrolysis of broiler manure: char and product gas characterization", Ind. Eng. Chem. Res. 48:1292–1297.

[206] Uchimiya, M., Lima, I.M., Klasson, K.T., Chang, S., Wartelle, L.H., and Rodgers, J.E. 2010. "Immobilization of heavy metal ions (Cu(II), Cd(II), Ni(II), and Pb(II)) by broiler litter-derived biochars in water and soil", J. Agric. Food Chem. 58:5538–5544.

[207] Uchimiya, M., Chang, S., and Klasson, K.T. 2011. "Screening biochars for heavy metal retention in soil: role of oxygen functional groups", J. Hazard. Mater. 190:432–441.

[208] Uchimiya, M., Wartelle, L.H., Klasson, K.T., Fortier, C.A., and Lima, I.M. 2011. "Influence of pyrolysis temperature on biochar property and function as a heavy metal sorbent in soil", J. Agric. Food Chem. 59:2501–2510.

[209] Lu, H., Zhang, W., Yang, Y., Huang, X., Wang, S., and Qiu, R. 2012. "Relative distribution of Pb^{2+} sorption mechanisms by sludge-derived biochar", Water Res. 46:854–862.

[210] Borchard, N., Prost, K., Kautz, T., Moeller, A., and Siemens., J. 2011. "Sorption of copper (II) and sulphate to different biochars before and after composting with farmyard manure", Eur. J. Soil Sci. 63:399–409.

[211] Peng, F., He, P.W., Luo, Y., Lu, X., Liang, Y., and Fu, J. 2012. "Adsorption of phosphate by biomass char deriving from fast pyrolysis of biomass waste", Clean Soil Air Water 40:493–498.

[212] Song, W., and Guo, M. 2012. “Quality variation of poultry litter biochar generated at different pyrolysis temperatures”, J. Anal. Appl. Pyrolysis 94:138–145.

[213] Rump, H.H., and Krist, H. 1988. “Laboratory manual for the examination of water, wastewater and soil”, VCH, New York.

[214] Hesse, P.R. 1971. “A textbook of soil chemical analysis”, John Murry, London, United Kingdom.

[215] Faria, P., J. Órfão, and M. Pereira., 2004. “Adsorption of anionic and cationic dyes on activated carbons with different surface chemistries”, Water Res, 38:2043–2052.

[216] Gardea-Torresdey, J.L., Becker-Hapak, M.K., Hosea, J.M., and Darnall, D.W. 1990. “Effect of chemical modification of algal carboxyl groups on metal ion binding”, Environ. Sci. Technol. 24:1372–1378.

[217] Chen, J.P., and L. Yang. 2006. “Study of a heavy metal biosorption onto raw and chemically modified Sargassum sp. via spectroscopic and modeling analysis", Langmuir 22:8906–8914.

[218] Oh, S.Y., Chiu, P.C., and Cha, D.K. 2008. "Reductive transformation of 2,4,6-trinitrotoluene, hexahydro-1,3,5-trinitro-1,3,5-triazine, and nitroglycerin by pyrite and magnetite", J. Hazard. Mater. 158:652–655.

[219] Oh, S.Y., Son, J.G. and Chiu, P.C. 2013. "Biochar-mediated reductive transformation of nitro herbicides and explosives", Environ. Toxicol. Chem. 32:501–508.

[220] Sparks, D.L. 2002. "Environmental soil chemistry", 2nd ed. Academic Press, New York.

[221] Yinon, J., and Zitrin, S. 1993. "Modern methods and applications in analysis of

explosives", John Wiley & Sons, New York.

[222] Sohi, S., Loez-Capel, E., Krull, E., and Bol, R. 2009. "Biochar's role in soil and climate change: a review of research needs", CSIRO Land and Water Science Report 05/09, SCIRO.

[223] Major, J., Lehmann, J., Rondon, M., and Goodale, C. 2010. "Fate of soil-applied black carbon: downward migration leaching and soil respiration", Glob Chang Biol. 16:1366–1379.

[224] Pattanayak, J., Mondal, K., Mathew, S., and Lalvani, S.B. 2000. "A parametric evaluation of the removal of As(V) and As(III) by carbon-based adsorbent", Carbon. 38:589–596.

[225] Oh, S. Y., and Yoon, M.K. 2013. "Biochar for treating acid mine drainage", Environ Eng Sci. 30:589–593.

[226] Uchimiya, M., Klasson, K.T., Wartelle, L.H., and Lima, I.M. 2011b. "Influence of soil properties on heavy metal sequestration by biochar amendment: 1. copper sorption isotherm and the release of cations", Chemosphere 82:1431–1437.

[227] Mui E.L.K., Cheung W.H., Valix, M., and McKay, G. 2010. "Dye adsorption onto char from bamboo", J. Hazard Mater. 177:1001–1005.

[228] Wang, S., Ma, Q., and Zhu, Z.H. 2009. "Characteristics of unburned carbons and their application for humic acid removal from water", Fuel Process. Technol, 90:375–380.

[229] Kasozi, G.N., Zimmerman, A.R., Nkedi-Kizza, P., and Gao, B. 2010. "Catechol and

humic acid sorption onto a range of laboratory-produced black carbons (biochars)", Environ. Sci. Technol. 44:6189–6195.

[230] Oh, S.Y., and Seo, Y.D. 2014. "Sorptive removal of nitro explosives and metals using biochar", J. Environ. Qual, 43:1663–1671.

[231] Wang, J.P., Chen, Y.Z., Feng, H.M., Zhang, S.J., and Yu, H.Q. 2007. "Removal of 2,4-dichlorophenol from aqueous solution by static-air-activated carbon fibers", J. Colloid. Interface. Sci, 313:80–85.

[232] Liu, Q.S., Zheng, T., Wang, P., Jiang, J.P., and Li, N. 2010. "Adsorption isotherm, kinetic and mechanism studies of some substituted phenols on activated carbon fibers", Chem. Eng. J, 157:348–356.

[233] Hamdaoui, O., and Naffrechoux, E. 2007. "Modeling of adsorption isotherms of phenol and chlorophenols onto granular activated carbon. Part 1. two-parameters models and equations allowing determination of thermodynamic parameters", J. Hazard. Mater, 147:381–394.

[234] Yang, K., Wu, W., Jing, Q., and Zhu, L. 2008. "Aqueous adsorption of aniline, phenol, and their substitutes by multi-walled carbon nanotubes", Environ. Sci. Technol, 42:7931–7936.

[235] Ni, J., Pignatello, J.J., and Xing, B. 2011. "Adsorption of aromatic carboxylate ions to black carbon (biochar) is accompanied by proton exchange with water", Environ. Sci. Technol, 45:9240–9248.

[236] Li, X., Pignatello, J.J., Wang, Y., and Xing, B. 2013 "New insight into adsorption mechanism of ionizable compounds on carbon nanotubes", Environ. Sci. Technol,

47:8334–8341.

[237] Hansch, C., Leo, A., and Hoekman, D. 1995. "Exploring QSAR: Volume 2: hydrophobic, electronic, and steric constants (hydrophobic, electronic & steric constants)", American Chemical Society. Washington, DC

[238] Stringer, R., and Johnston, P. 2001. "Chlorine and the environment: an overview of the chlorine industry", Kluwer Academic Pub. Dordrecht.

[239] Kuramochi, H., Maeda, K., and Kawamoto, K. 2004. "Water solubility and partitioning behavior of brominated phenols", Environ. Toxicol. Chem. 23:1386–1393.

[240] Mackay, D., Shin, W.Y., Ma, K.C., and Lee, S.C. 2006. "Handbook of physical-chemical properties and environmental fate of organic chemicals", 2nd ed, Taylor & Francis, Boca Raton.

[241] Behera, S.K., Oh, S.Y., and Park, H.S. 2010. "Sorption of triclosan onto activated carbon, kaolinite and montmorillonite: effects of pH, ionic strength, and humic acid", J. Hazard Mater. 179:684–691.

[242] Behera, S.K., Oh, S.Y., Park, H.S. 2012. "Sorptive removal of ibuprofen from water using selected soil minerals and activated carbon", Int. J. Environ. Sci. Technol. 9:85–94.

[243] Pignatello, J.J., Kwon, S., and Lu, Y. 2006. "Effect of natural organic substance and adsorptive properties of environmental black carbon (char): attenuation of surface activity by humic and fulvic acids", Environ. Sci. Technol, 40:7757–7763.

[244] Ahmad, M., Lee, S.S., Rajapaksha, A.U., Vithanage, M., Zhang, M., Cho, J.S., Lee, S.E., and Ok S.Y. 2013. “Trichloroethylene adsorption b pine needle biochars produced

at various pyrolysis temperatures", Bioresour. Technol. 143:615-622.

[245] Lattao, C., Cao, X., Mao, J., Schmidt-Rohr, K., and Pignatello, J.J. 2014. "Influence of molecular structure and adsorbent properties on sorption of organic compounds to a temperature series of wood char", Environ. Sci. Technol, 48:4790–4798.

[246] Fellet, G., Marchiol, L., Vedove, D., and Peressotti, A. 2011. "Application of biochar on mine tailings: effects and perspectives", Chemosphere, 83:1262-1267.

[247] Moon, D.H., Park, J.W., Chang, Y.Y., Ok, Y.S., Lee, S.S., Ahmad, M., Koutsopytos, A., Park, J. H., and Baek, K. 2013. "Immobilization of lead in contaminated firing range soil using biochar", Environ. Sci. Pollut. Res, 20:8464–8471.

[248] Mohan, D., Sarswat, A., Ok, Y.S., and Pittman Jr, C.U. 2014. "Organic and inorganic contaminants removal from water with biochar, a renewable, low cost and sustainable adsorbent--a critical review", Bioresour. Technol. 160:191–202.

[249] Ludwig, R.D., Su, C., Lee, T.R., Wilkin, R.T., Acree, S.D., Ross, R.R., and Keeley, A. 2007. "In situ chemical reduction of Cr(VI) in groundwater using a combination of ferrous sulfate and sodium dithionite: a field investigation", Environ. Sci. Technol, 41:5299–5305.

[250] Heijman, C.G., Grieder, E., Holliger C., and Schwarzenbach, R.P. 1995. "Reduction of nitroaromatic compounds coupled to microbial iron reduction in laboratory aquifer columns", Environ. Sci. Technol. 29:775–783.

[251] Oh, S.Y., Cha, D.K., and Chiu, P.C. 2002. "Graphite-mediated reduction of 2,4-dinitrotoluene with elemental iron" Environ. Sci. Technol, 36:2178–2184.

[252] Hoch, L.B., Mack, E.J., Hydutsky, B.W., Hershman, J.M., Skluzacek, J.M., and Mallouk, T.E. 2008. "Carbothermal synthesis of carbon-supported nanoscale zero-valent iron particles for the remediation of hexavalent chromium", Environ. Sci. Technol. 42:2600–2605.

[253] Choi, H., Agarwal, S., and Al-Abeed, S.R. 2009. "Adsorption and simultaneous dechlorination of PCBs on GAC/Fe/Pd: mechanistic aspects and reactive capping barrier concept", Environ. Sci. Technol. 43:488–493.

[254] Sunkara, B., Zhan, J., He, J., McPherson, G.L., Piringer, G., and John, V.T. 2010. "Nanoscale zero-valent iron supported on uniform carbon microspheres for the in-situ remediation of chlorinated hydrocarbons", ACS Appl. Mater. Interfaces. 2:2854–2862.

[255] Tseng, H.H., Su J.G., and Liang, C. 2011. "Synthesis of granular activated carbon/zero-valent iron composites for simultaneous adsorption/dechlorination of trichloroethylene", J. Hazard. Mater, 192:500–506.

[256] Chang, C., Lian, F., and Zhu, L. 2011. "Simultaneous adsorption and degradation of γ-HCH by nZVI/Cu bimetallic nanoparticles with activated carbon support", Environ. Pollut. 159:2507–2514.

[257] Zhuang, Y., Ahn, S., Seyfferth, A.L., Masue-Slowey, Y., Fendorf, S., and Luthy, R.G. 2011. "Dehalogenation of polybrominated diphenyl ethers and polychlorinated biphenyl by bimetallic, impregnated, and nanoscale zero-valent iron", Environ. Sci. Technol, 45:4896–4903.

[258] Su, Y.F., Cheng, Y.L., and Shih, Y.H. 2013. "Removal of trichloroethylene by zerovalent

iron/activated carbon derived from agricultural wastes", J. Environ. Manage, 129:361–366.

[259] Wu, X., Yang, Q., Xu, D., Zhong, Y., Luo, K., Li, X., Chen H., and Zeng, G. 2013. "Simultaneous adsorption/reduction of bromate by nanoscale zero-valent iron supported on modified activated carbon", Ind. Eng. Chem. Res, 52:12574–12581.

[260] Devi, P., and Saroha A.K. 2014. "Synthesis of the magnetic biochar composites for use as an adsorbent for the removal of pentachlorophenol from the effluent", Bioresour. Technol. 169:525–531.

[261] Oh, S.Y., Seo, Y.D., and Ryu, K.S. 2016. "Reductive removal of 2,4-dinitrotoluene and 2,4-dichlorophenol with zero-valent iron-included biochar", Bioresour. Technol, 216:1014–1021.

[262] Yamashita, T., and Hayes, P. 2008. "Analysis of XPS spectra of Fe^{2+} and Fe^{3+} ions in oxide materials", Appl. Surf. Sci. 254:2441–2449

[264] Summers, W.R. 1990. "Characterization of formaldehyde and formaldehyde-releasing preservatives by combined reversed-phase cation-exchange high-performance liquid chromatography with post-column derivatization using nash's reagent", Anal. Chem. 62:1397–1402.

[263] Oh, S.Y., and Seo, Y.D. 2016a. "Sorption of halogenated-phenols and pharmaceuticals to biochar: affecting factors and mechanisms", Environ. Sci. Pollut. Res. 23:951–961.

[265] Oh, S.Y., Cha, D.K. Kim, B.J., and Chiu, P. C. 2005. "Reductive Transformation of hexahydro1,3,5-trinitro-1,3,5-triazine (RDX), octahydro-1,3,5,7-tetranitro-1,3,5,7-tetrazocine (HMX), and methylenedinitramine (MDNA) with elemental iron",

Environ. Toxicol. Chem, 24:2812–2819.

[266] Shih, Y.H., and Tai, Y.T. 2010. "Reaction of decabrominated diphenyl ether by zerovalent iron nanoparticles", Chemosphere. 78:1200–1206.

[267] Keum, Y.S., and Li, Q.X. 2005. "Reductive debromination of polybrominated diphenyl ethers by zero-valent iron", Environ. Sci. Technol, 39:2280–2286.

[268] Lin, C.H., Shih, Y.H., and MacFarlane, J. 2015. "Amphiphilic compounds enhance the dechlorination of pentachlorophenol with Ni/Fe bimetallic nanoparticles", Chem. Eng. J, 262:59–67.

[269] Shih, Y.H., Chen, M.Y., Su, Y.F., and Tso, C.P. 2016. "Concurrent oxidation and reduction of pentachlorophenol by bimetallic zero-valent Pd/Fe nanoparticles in an oxic water", J. Hazard.Mater, 301:416–423.

[270] Weber, E.J. 1996. "Iron-mediated reductive transformations: investigation of reaction mechanism", Environ. Sci. Technol, 30:716.

[271] Yoon, J. Muhammad, S., Jang, D., Sivakumar, N., Kim, J., Jang, W.H., Lee, W.H., Park, Y.U., Kang, K., and Yoon, W.S. 2013. "Study on structure and electrochemical properties of carbon-coated monoclinic $Li_3V_2(PO_4)_3$ using synchrotron-based in situ X-ray diffraction and absorption", J. Alloys. Compd, 569:76–81.

[272] Odziemkowski, M.S., Schuhmacher, T.T., Gillham, R.W., and Reardon, E.J. 1998. "Mechanism of oxide film formation on iron in simulating groundwater solutions: Raman spectroscopic studies", Corros. Sci, 40:371–389.

[273] Masiello, C.A., Gallagher, M.E., Randerson, J.T., Deco, R.M., and Chadwick, O.A. 2008.

“Evaluating two experimental approaches for measuring ecosystem carbon oxidation state and oxidative ratio”, J. Geophys. Res.: biogeosci, 113:G03010, https://doi.org/10.1029/2007JG000534.

[274] Kemper, J.M., Ammar, E., and Mitch, W.A. 2008. "Abiotic Degradation of Hexahydro-1,3,5-trinitro-1,3,5-triazine in the Presence of Hydrogen Sulfide and Black Carbon", Environ. Sci. Technol, 42:2118–2123.

[275] Yu, X., Gong, W., Liu, X., Shi, L., Han, X., and Bao, H. 2011. "The use of carbon black to catalyze the reduction of nitro-benzenes by sulfides", J. Hazard. Mater, 198:340–346.

[276] Xu, W., Pignatello J.J., and Mitch, W.A. 2013. "Role of black carbon electrical conductivity in mediating hexahydro-1,3,5-trinitro-1,3,5-triazine (RDX) transformation on carbon surfaces by sulfides", Environ. Sci. Technol, 47:7129–7136.

[277] Goeringe, S., Tacconi, N.R.de., and Chenthamarakshan, C.R. 2001. "Redox characterization of furnace carbon black surfaces", Carbon. 39:515–522.

[278] Men´endez, J.A., Xia, B., Phillips, and Radovic, L.R. 1997. "On the modification and characterization of chemical surface properties of activated carbon: microcalorimetric, electrochemical, and thermal desorption probes", Langmuir. 13:3414–3421.

[279] Mao, J.D., Johnson, R.L., Lehmann, J., Olk, D.C., Neves, E.G., Thompson, M.L., and Schmidt-Rohr, K. 2012. "Abundant and stable char residues in soils: implications for soil fertility and carbon sequestration", Environ. Sci. Technol, 46:9571–9576.

[280] Abnisa, F., Wan Daud, W.M.A., and Sahu, J.N. 2014. "Pyrolysis of mixtures of palm shell and polystyrene: an optional method to produce a high-grade of pyrolysis oil", Environ. Prog. Sustain. 33:1026–1033.

[281] Hovart, N., and Ng, F.T.T. 1999. "Tertiary polymer recycling: study of polyethylene thermolysis as a first step to synthetic diesel fuel", Fuel. 78:459–470.

[282] Murugan, S., Ramaswamy, M.C., and Nagarajan, G. 2008. "The use of tyre pyrolysis oil in diesel engines", Waste Manage, 28:743–2749.

[283] Ates, F., Miskolcczi, N., and Borsodi, N., 2013. "Comparison of real waste (MSW and MPW) pyrolysis in batch reactor over different catalysts. Part 1: product yields, gas and pyrolysis oil", Bioresour. Technol. 133:443–454.

[284] Muhammad, C., Onwudili, J.A., and Williams, P.T. 2015. "Thermal degradation of real-world waste plastics and simulated mixed plastics in a two-stage pyrolysis–catalysis reactor for fuel production", Energy Fuels, 29:2601–2609.

[285] United Nations Environment Programme (UNEP), 2009. "Converting waste agricultural biomass into a resource", UNEP division of technology, industry and economics, international environmental technology centre, Osaka/Shiga, Japan.

[286] Sannita, E., Aliakbarian, B., Casazza, A.A., Perego, P., and Busca, G. 2012. "Mediumtemperature conversion of biomass and wastes into liquid products, a review", Renew. Sust. Energ. Rev. 16:6455–6475.

[287] Elliott, D.C. 2007. "Historical developments in hydroprocessing bio-oils", Energy Fuels. 21:1792–1815.

[288] Bridgwater, A.V. 2012. "Review of fast pyrolysis of biomass and product upgrading", Biomass Bioenergy. 38:68–94.

[289] Cheng, Y.T., Jae, J.H., Shi, J., Fan, W., and Huber, G.W. 2012. "Production of renewable energy aromatic compounds by catalytic pyrolysis of lignocellulosic biomass with bifunctional Ga/ZSM-5 catalysts", Angew. Chem. Int. Ed. 51:1387–1390.

[290] Liu, W.J., Tian, K., Jiang, H., Zhang, X.S., Ding, H.S., and Yu, H.Q. 2012. "Selectively improving the bio-oil quality by catalytic fast pyrolysis of heavy-metal-polluted biomass: take copper (Cu) as an example", Environ. Sci. Technol, 46:7849–7856.

[291] Bhattacharya, P., Steele, P.H., Hassan, E.B.M., Mitchell, B., Ingram, L., and Pittman Jr, C.U., 2009. "Wood/plastic co-pyrolysis in an augur reactor: chemical and physical analysis of the products", Fuel. 88:1251–1260.

[292] Paradela, F., Pinto, F., Gulyurtlu, I., Cabrita, I., and Lapa, N. 2009. "Study of the slow batch pyrolysis of mixtures of plastics, tyres and forestry biomass wastes", J. Anal. Appl. Pyrol, 85:392–398.

[293] Önal, E., Uzun, B.B., and Pütün, A.E. 2014. "Bio-oil production via co-pyrolysis of almond shell as biomass and high density polyethylene", Energy Convers. Manage, 78:704–710.

[294] Martínez, J.D., Veses, A., Mastral, A.M., Murillo, R., Navarro, M.V., Puy, N., Artigues, A., Bartrolí, J., and García, T. 2014. "Co-pyrolysis of biomass with waste tyres: upgrading of liquid bio-fuel", Fuel Process. Technol, 119:263–271.

[295] Dorado, C., Mullen, C.A., and Boateng, A.A. 2014. "H-ZSM5 catalyzed co-pyrolysis of biomass and plastics", ACS Sustainable Chem. Eng. 2:301–311.

[296] Brebu, M., Ucar, S., Vasile, C., and Yanik, J. 2010. "Co-pyrolysis of pine scone with synthetic polymers", Fuel. 89:1911–1918.

[297] Sajdak, M., and Muzyka, R. 2014. "Use of plastic waste as a fuel in the co-pyrolysis of biomass. Part 1: the effect of the addition of plastic waste on the process and products", J. Anal. Appl. Pyrolysis, 107:267–275.

[298] Xue, Y., Zhou, S., Brown, R.C., Kelkar, A., and Bai, X. 2015. "Fast pyrolysis of biomass and waste plastic in a fluidized bed reactor", Fuel, 156:40–46.

[299] Ko, K.H., Sahajwalla, V., and Rawal, A. 2014. "Specific molecular structure changes and radical evolution during biomass-polyethylene terephthalate co-pyrolysis detected by 13C and 1H solid-state NMR", Bioresour. Technol, 170:248–255.

[300] Suriapparao, D.V., Ojha, D.K., Ray, T., and Vinu, R. 2014. "Kinetic analysis of co-pyrolysis of cellulose and polypropylene", J. Therm. Anal. Calorim, 117:1441–1451.

[301] Bernardo, M., Lapa, N., Goncalves, M., Mendes, B., Pinto, F., Fonseca, I., and Lopes, H. 2012. "Physico-chemical properties of chars obtained in the co-pyrolysis of waste mixtures", J. Hazard. Mater, 219–220:196–202.

[302] Oh, S.Y., and Seo, Y.D. 2015. "Factors affecting sorption of nitro explosives to biochar: pyrolysis temperature, surface treatment, competition, and dissolved metals", J. Environ. Qual, 44:833–840.

[303] Oh, S.Y., Son, J.G., Hur, S.H., Chung, J.S., and Chiu, P.C. 2013a. "Black carbon-mediated reduction of 2,4-dinitrotoluene by dithiothreitol", J. Environ. Qual, 42:815–821.

[304] Beesley, L., Moreno-Jiménez, E., Gomez-Eyles, J.L., Harris, E., Robinson, B., and Sizmur, T.A. 2011. “A review of biochar’s potential role in the remediation, revegetation and restoration of contaminated soils”, Environ Pollut, 59:3269-3282.

[305] Tan, X., Liu, Y., Zeng, G., Wang, X., Hu, X., Gu. Y., and Yang, Z. 2015. "Application of biochar for the removal of pollutants from aqueous solutions", Chemosphere, 125:70-85.

[306] Lian, F., and Xing, B. 2017. "Black carbon (biochar) in water/soil environments: molecular structure, sorption, stability, and potential risk", Environ Sci. Tech, 51:13517-13532.

[307] Xiong, X., Yu, I.K.M., Cao, L., Tsang, D.C.W., Zhang, S. and Ok, Y.S. 2017. "A review of biochar-based catalysts for chemical synthesis, biofuel production, and pollution control", Bioresour Technol. 246:254-270.

[308] Ogawa, M., and Okimori, Y. 2010. "Pioneering works in biochar research, Japan", Aust J Soil Res, 48:489-500.

[309] Schmidt, H.P., and Wilson, K. 2019. "The 55 uses of biochar", Biochar J, 2014;2014. www.biochar-journal.org/en/ct/2.

[310] Pieplow, H. 2019. "Biochar in South Korea: experiences from every day", Biochar J, 2014. www.biochar-journal.org/en/ct/35.

[311] Worrell, E., Price, L., Martin, N., Hendriks, C., and Meida, L.O. 2001. "Carbon dioxide emission from the global cement industry", Annu Rev Energy Environ, 26:303-329.

[312] Habert, G., and Roussel, N. 2009. "Study of two mix-design strategies to reach carbon

mitigation objectives", Cem Concr. Compos. 31:397-402.

[313] Turner, L.K., and Collins, F.G. 2013. "Carbon dioxide equivalent (CO_2-e) emissions: a comparison between geopolymer and OPC cement concrete", Constr. Build. Mater., 43:125-130.

[314] Yang, K.H., Jung, Y.B., Cho, M.S., and Tae, S.H. 2015. "Effect of supplementary cementitious materials on reduction of CO_2 emissions from concrete", J Clean Prod, 103:774-783.

[315] Schmidt, H.P. 2019. "The use of biochar as building material", Biochar J, 2014;2014. www.biochar-journal.org/en/ct/3.

[316] Gupta, S., Kua, H.W., and Cynthia, S.Y.T. 2017. "Use of biochar-coated polypropylene fibers for carbon sequestration and physical improvement of mortar", Cem. Concr. Compos, 83:171-187.

[317] Gupta, S., Kua, H.W., and Low, C.Y. 2018. 'Use of biochar as carbon sequestration additive in cement mortar", Cem. Concr. Compos, 87:110-129.

[318] Oh, S.Y., and Seo, Y.D. 2016b. "Polymer/biomass-derived biochar for use as a sorbent and electron transfer mediator in environmental applications", Bioresour. Technol, 218:77-83.

[319] Oh, S.Y., and Seo, Y.D. 2019 "Factors affecting the sorption of halogenated-phenols onto polymer/biomass-derived biochar: effects of pH, hydrophobicity, and deprotonation", J. Environ. Manage, 232:145-152.

[320] Nowosielski, B.E., and Fein, J.B. 1998. "Experimental study of octanol-water partition

coefficients for 2,4,6-trichlorophenol and pentachlorophenol: derivation of an empirical model of chlorophenol partitioning behavior", Appl Geochem, 13:893-904.

[321] Wightman, P.G., and Fein, J.B. 1999. "Experimental study of 2,4,6 trichlorophenol and pentachlorophenol solubilities in aqueous solutions: derivation of a speciation-based chlorophenol solubility model", Appl Geochem, 14:319-331.

[322] Oh, S.Y., Yoon, H.S., Jeong, T.Y., Kim S.D., and Kim, D.W. 2016b. "Reduction and persulfate oxidation of nitro explosives in contaminated soils using Fe-bearing materials", Environ Sci: Processes Impacts. 18:863-871

[323] Barcelo, L., Kline, J., Walenta, G., and Gartner, E. 2014. "Cement and carbon emissions", Mater Struct. 47:1055-1065.

[324] International Energy Agency (IEA). 2016. "CO_2 Emission from Fuel Combustion"

[325] Zhu, D.Q., Kwon, S., and Pignatello, J.J., 2005. "Adsorption of single-ring organic compounds to wood charcoals prepared under different thermochemical conditions", Environ. Sci. Technol, 39:3990–3998.

[326] Mukherjee, A., Zimmerman, A.R., and Harris, W. 2011. "Surface chemistry variations among a series of laboratory-produced biochars", Geoderma, 163:247–255.

[327] Rumpel, C., and Ko¨gel-Knabner, I. 2011. "Deep soil organic matter-a key but poorly understood component of terrestrial C cycle", Plant Soil, 338:143–158.

[328] Oh, S.Y., and Chiu, P.C. 2009. "Graphite- and soot-mediated reduction of 2,4-dinitrotoluene and hexahydro-1,3,5-trinitro-1,3,5-triazine", Environ. Sci. Technol.

43:6983–6988.

[329] Qiu, Y., Zheng, Z., Zhou, Z., and Sheng, G.D. 2009. "Effectiveness and mechanisms of dye adsorption on a straw-based biochar", Bioresour. Technol, 100:5348–5351.

[330] Zwieten, L.V., Singh, B.P., Joseph, S.D., and Kimber, S. 2009. “Biochar and emission of non-CO_2 greenhouse gases from soil”, Biochar for environmental management science and technology (227-249), Earthscan, Gateshead, UK.

[331] UC Davis Biochar Database [Web site], (2022, Jan 03), http://biochar.ucdavis.edu/.

[332] Ulusal, A., Varol, E.A., Bruckman, V.J., and Uzun B.B. 2021. “ Opportunity for sustainable biomass valorization to produce biochar for improving soil characteristics”, Biomass Convers. Biorefin, 11:1041-1051.

[333] Dai, Y., Zheng, H., Jiang, Z., and Xing B. 2020. “Combined effects of biochar properties and soil conditions on plant growth: A meta-analysis”, Sci. Total Environ, 713:136635, https://doi.org/10.1016/j.scitotenv.2020.136635.

[334] Glaser, B., Haumaier, L., Guggenberger, G., and Zech, W. 2001. “The Terra Preta phenomenon – a model for sustainable agriculture in the humid tropics”, Sci. Nat, 88(1):37-41.

국문요약

본 연구에서는 biomass를 열분해를 통해 biochar로 합성한 후 흡착제, 환원제, 촉매제 및 건축자재 등 건축 및 환경 분야에 복합소재로 활용하고자 연구하였다. 오염물질 저감 능력 파악을 위해 biochar를 사용하여 nitro-explosives와 금속 오염물질을 제거하기 위해 회분식 실험을 진행하였다. 다양한 biomass를 이용하여 제조된 biochar는 다공성 구조와 높은 표면적을 지니고 있어 GAC와 비교하였을 때 Cd, Cu, Pb 및 Zn 와 같은 금속을 제거하는 흡착제로서 경쟁력이 있었다. 일부 biochar는 물에서 nitro-explosives를 효과적으로 제거하였다.

오염물질 제거를 위한 biochar의 최대 흡착능력 및 특성 사이의 상관관계를 고찰한 결과 독성 금속에 대한 biochar의 흡착능력은 양이온교환용량 (CEC)과 관련이 깊었다. XPS, FT-IR 분석 결과 표면 작용기가 biochar 표면에서 독성 금속 흡착에 영향을 주고 있었다. 그리고 nitro-explosives의 경우에는 탄소 함량에 비례하는 것을 보여주어 π–π EDA 작용에 의해 nitro-explosives가 biochar에 흡착되고 있음을 설명하고 있었다.

Biochar의 흡착제로의 평가를 위해 9가지 할로겐화 페놀 (DCP, DBP, DFP, 4CP, 2CP, 4BP, 2BP, 4FP, 2FP)와 두가지 의약품 (triclosan and ibuprofen)을 오염물질로 사용하여 회분식 실험을 실시하였다. 낙엽, 볏짚, 옥수수 줄기, 커피 찌꺼기 및 bio-solid를 이용하여

합성한 biochar와 GAC와 비교하였을 때 대부분 물에서 할로겐화 페놀류 및 의약품을 효과적으로 제거하지 못하였다. 이는 biochar 시스템상에서의 pH의 증가와 페놀의 deprotonation이 흡착능력을 낮추는 원인으로 파악된다. 이후 오염물질의 pH를 4 또는 7로 유지하였을 때, biochar의 흡착능력이 증가하였다. 흡착제와 흡착된 물질의 특성을 고려하였을 때 할로겐화 페놀에 대한 biochar의 흡착능력은 비표면적과 탄소함량 그리고 오염물질의 소수성과 관련이 있다. 의약품의 경우, 흡착제의 PZC 및 pH, 의약품의 deprotonation에 따라 GAC, graphite 및 biochar의 흡착능력에 영향을 주었으며, biochar 제조시의 열분해 온도는 할로겐화 페놀 및 의약품 흡착능력에 큰 영향을 미치지 않았다.

Fe(0)와 RS biomass를 동시 열분해 합성하여 Fe(0)-included biochar (Fe(0)-biochar)를 제조하였다. Nitro-explosives (TNT 및 RDX) 및 할로겐화 페놀 (DBP 및 DFP) 제거는 biochar의 첨가로 인해 흡착능력이 증가하였다. 흡착된 오염물질은 환원되었으며, 이는 Fe(0)-biochar 내부의 Fe(0)가 환원제로서의 역할을 했음을 나타내고 있다. Fe(0)와 직접 비교하였을 때, Fe(0)-biochar에 의한 환원변환이 향상되었으며 이는 Fe(0)-biochar의 biochar가 전자전달 매개체로 작용되어 반응 속도를 증가시켰다. 추가 실험을 통해 biochar의 표면작용기가 전자전달의 촉매적 특성 향상에 관여하고 있었다.

Polymer 및 RS biomass을 동시 열분해 합성하여 제조된 polymer/RS-derived biochar

의 경우, 탄소함량, CEC, BET S.A., 및 pH의 값이 RS biochar와 비교하였을 때 증가하였다. 탄소 함량이 증가한 결과 DNT 흡착능력이 향상되었다. 그리고 높은 pH 와 증가된 CEC의 값을 통해 Pb 흡착능력도 증가하였다. DTT에 의한 DNT 환원 실험 진행 결과 RS 및 polymer/RS-derived biochar의 촉매로서 성능은 크게 차이 나지 않았다.

국내에서 대량으로 확보할 수 있는 wood chip 과 BS biochar 그리고 RS biochar를 사용해 흡착능력을 분석하였고 건축 및 환경분야 응용을 위하여 biochar 특성에 따라 제조된 biochar-mortar의 탄소 격리 능력에 대해서도 평가하였다. Biochar-mortar는 3~5 v%의 biochar가 함유되었을 때 유동성, 압축강도 및 열전도를 포함한 mortar의 공학적 특성을 크게 변화시키지 않았다. 또한, biochar-mortar 내 biochar 함량이 증가함에 공기 중 benzene 및 toluene 농도가 감소하였다. 이는 biochar가 mortar에 포함된다면 대기중 휘발성 독성 오염물질을 제거하는 데 유리할 것으로 보였다. TCLP 및 Micotox®bioassay 실험 결과 biochar-mortar의 독성이 존재하지 않음을 보여주고 있다. 이러한 결과는 biochar와 biochar 기반 복합재료가 경쟁력이 있으며 오염물질에 대한 흡착제, 촉매 및 환원제만이 아니라 탄소저감을 위한 방안으로도 효과적으로 사용될 수 있다. 결과적으로 biochar의 다양한 가치향상 방법은 CO_2 저감을 위한 탄소격리 방안으로서 유망한 옵션이 될 수 있다.